METER-WAVELENGTH OBSERVATIONS OF PULSARS USING VERY-LONG-BASELINE INTERFEROMETRY

N. R. VANDENBERG

JULY 1974

ASTROMONY PROGRAM

UNIVERSITY OF MARYLAND

COLLEGE PARK, MARYLAND

GODDARD SPACE FLIGHT CENTER

GREENBELT, MARYLAND

APPROVAL SHEET

Title of Thesis: Meter-wavelength observations of pulsars
using very-long-baseline interferometry

Name of Candidate: Nancy Ruth Vandenberg
Doctor of Philosophy, 1974

Thesis and Abstract Approved: *Wm. C. Erickson*

                                William C. Erickson
                                Professor
                                Department of Physics & Astronomy

Date Approved: *17 July 1974*

VITA

Name: Nancy R. Vandenberg

Permanent Address: 1087 Sylvan Drive
                        Benton Harbor, Michigan 49022

Degree and date to be conferred: Ph.D.   August, 1974

Date of birth: July 18, 1946

Place of birth: Ann Arbor, Michigan

Secondary education: St. Mary Academy, Monroe, Michigan

Collegiate institutions	Dates	Degree	Date of degree
Mundelein College, Chicago	1963-67	B.S.	June, 1967
Columbia University (Goddard Institute)	summer 1967	--	--
Georgetown University	1967-68	--	--
University of Maryland	1968-1974	Ph.D.	August, 1974

Major: Physics

Minor: Mathematics

Publications: see next pages

Positions held:
    Programmer - Western Electric Co. (Chicago), summer 1966.
    Programmer - Whirlpool Corp. (Benton Harbor), summer 1967.
    NASA Trainee - Georgetown University, 1967-8.
    NDEA Fellow - University of Maryland, 1968-71.
    Research assistant - University of Maryland (working at Goddard
                        Space Flight Center), 1969-1974

Professional society memberships:
    American Astronomical Society
    Royal Astronomical Society

PUBLICATIONS

N. R. Vandenberg, T. A. Clark, W. C. Erickson, G. M. Resch, J. J. Broderick, R. R. Payne, S. H. Knowles, A. B. Youmans, "VLBI observations of the Crab nebula pulsar," Ap.J. 180, L27 (1973).

H. F. Hinteregger, G. W. Catuna, C. C. Counselman, P. A. Ergas, R. W. King, C. A. Knight, D. S. Robertson, A. E. E. Rogers, I. I. Shapiro, A. R. Whitney, T. A. Clark, L. K. Hutton, G. E. Marandino, R. A. Perley, G. M. Resch, N. R. Vandenberg, "Cygnus X-3 radio source: Lower limit on size and upper limit on distance," Nature Phys. Sci. 240, 159 (1972).

N. R. Vandenberg, W. C. Erickson, G. M. Resch, T. A. Clark, J. J. Broderick, "VLBI observations of the Crab nebula pulsar," BAAS 4, 320 (1972).

J. C. Novaco, N. R. Vandenberg, "A model of the local region of the Galaxy," BAAS 4, 318 (1972).

G. E. Marandino, G. M. Resch, N. R. Vandenberg, T. A. Clark, H. F. Hinteregger, C. A. Knight, D. S. Robertson, A. E. E. Rogers, I. I. Shapiro, A. R. Whitney, R. M. Goldstein, D. J. Spitzmesser, "Further observations of brightness variation in the small scale structure of 3C273 and 3C279," BAAS 4, 315 (1972).

D. S. Robertson, C. A. Knight, A. E. E. Rogers, I. I. Shapiro, A. R. Whitney, T. A. Clark, G. E. Marandino, N. R. Vandenberg, R. M. Goldstein, "Measurements of the gravitational deflection of radio waves," BAAS 3, 474 (1971).

A. R. Whitney, I. I. Shapiro, A. E. E. Rogers, D. S. Robertson, C. A. Knight, T. A. Clark, G. E. Marandino, N. R. Vandenberg, R. M. Goldstein, "High-accuracy determinations of 3C273-3C279 position difference from long-baseline interferometer fringe phase measurements," BAAS 3, 465 (1971).

C. A. Knight, D. S. Robertson, I. I. Snapiro, A. R. Whitney, A. E. E. Rogers, T. A. Clark, G. E. Marandino, N. R. Vandenberg, R. M. Goldstein, "Observations with the Haystack-Goldstone interferometer of phase scintillations due to the solar corona," BAAS 3, 447 (1971).

C. A. Knight, A. E. E. Rogers, I. I. Shapiro, A. R. Whitney, T. A. Clark, R. M. Goldstein, G. E. Marandino, N. R. Vandenberg, "Detection of double-source structure in the nucleus of the quasi-stellar radio source 3C279," BAAS 3, 416 (1971).

T. A. Clark, R. M. Goldstein, H. F. Hinteregger, C. A. Knight, G. E. Marandino, D. S. Robertson, A. E. E. Rogers, I. I. Shapiro, D. J. Spitzmesser, N. R. Vandenberg, A. R. Whitney, "Variations in the fine structure of the quasars 3C279 and 3C273," BAAS 3, 383 (1971).

A. R. Whitney, I. I. Shapiro, A. E. E. Rogers, D. S. Robertson, C. A. Knight, T. A. Clark, R. M. Goldstein, G. E. Marandino, N. R. Vandenberg, "Quasars revisited: Rapid time variations observed via very-long-baseline interferometry," Science $\underline{173}$, 225 (1971).

C. A. Knight, D. S. Robertson, A. E. E. Rogers, I. I. Shapiro, A. R. Whitney, T. A. Clark, R. M. Goldstein, G. E. Marandino, N. R. Vandenberg, "Quasars: Millisecond-of-arc structure revealed by very-long-baseline interferometry," Science $\underline{172}$, 52 (1971).

T. A. Clark, B. Donn, W. M. Jackson, W. T. Sullivan, N. R. Vandenberg, "Search for microwave H_2O emission in comet Bennett (1969i)," A.J. $\underline{76}$, 614 (1971) and BAAS $\underline{3}$, 281 (1971).

ABSTRACT

Title of thesis: Meter-wavelength observations of pulsars
                  using very-long-baseline interferometry

Nancy Ruth Vandenberg, Doctor of Philosophy, 1974

Thesis directed by: Professor William C. Erickson

This thesis presents the results of an investigation of the angular structure imposed on pulsar radiation due to scattering in the interstellar medium. The technique of very-long-baseline interferometry (VLBI) was used to obtain the necessary high angular resolution (~0.1 arcsec). The interferometers formed by the Arecibo (305 m), NRAO (92 m), and Sugar Grove (46 m) telescopes were used at radio frequencies of 196, 111, and 74 MHz during seven separate observing sessions between 1971 November and 1973 February. The observations were concentrated on the Crab nebula pulsar (PSR 0531+21), and several strong, low-dispersion pulsars were also observed.

A crude visibility function for the Crab nebular pulsar was obtained during a 144-MHz VLBI experiment in 1971 March. The visibility function is consistent with a Gaussian brightness distribution having a half-power diameter of 0.05 ± 0.03 arcsec. Since only a small range of points in the (u,v) plane was sampled in the later experiments, the fringe visibilities were also interpreted in terms of a Gaussian model, yielding half-power diameters of 0.03 ± 0.01, 0.07 ± 0.01, and 0.18 ± 0.01 arcsec at 196, 111, and 74 MHz, respectively. A Gaussian distribution supports the view that the apparent angular sizes are caused by multipath scattering in the interstellar medium. The apparent sizes obtained at all four frequencies scale as

wavelength to the power 2.0 ± 0.4, supporting theoretical scattering laws which predict a wavelength-squared scaling. At 74 MHz the measured size agrees with that derived from an independent interplanetary scintillation experiment. The angular sizes were not observed to vary during the entire observing period.

The technique of differential fringe phase was used to show that the pulsar and the "compact source" in the Crab nebula are conincident to within 0.001 arcsec which corresponds to ~2 a.u. at the distance to the nebula. The total time-averaged flux from the compact source was also obtained. The fluxes measured at 74 MHz (105 Jy) and 111 MHz (40 Jy) lie on the extrapolation from higher radio frequencies of the spectrum of the pulsing flux, and the 196-MHz flux (8 Jy) agrees with the pulsar's flux. Variations in the total flux of up to 25% were observed.

The data were also analyzed to yield the Fourier components of the Crab nebula pulsar's pulse shape by coherently de-dispersing the signal. To obtain the correlated pulse profile, the components (including the n=0 harmonic) were added in a Fourier sum. At 196 MHz the reconstructed pulse shape is identical with the single-telescope profiles observed at Arecibo. The 111-MHz pulse profile contains both pulsing and non-pulsing components, each of which contributes approximately equally to the total flux. The reconstructed pulse shape agrees with the single-telescope pulse profile observed at Arecibo. No pulsing component was detected at 74 MHz.

The ratio of pulsing to total flux (I_p/I_T) at 111 MHz was found to vary over the one and one-half years of observing. During the winter of 1971-2 there was more pulsing than steady power $(I_p/I_T \sim 0.6)$ whereas in the winter 1972-3 the steady power was the dominant component $(I_p/I_T \sim 0.4)$.,

The fringe visibility of the time-averaged pulsing flux and of each Fourier component is the same as that of the total flux. Both the pulse shapes and ratios of I_p/I_T are similar for the unresolved and partially resolved fluxes. These statements show that there is no dependence of fringe visibility on pulse phase. This fact, and the observed combination of temporal and angular broadening, rule out scattering theories which employ a simple single-screen model of the interstellar medium. A two-screen model in which one screen is in the Crab nebula improves the agreement, but the model is still not consistent with all aspects of the observations. A new model is proposed in which the temporal broadening is dominated by scattering in the small filament which lies in the nebula in front of the pulsar, while the extended interstellar medium causes the angular broadening. This model explains the otherwise-discordant angular and temporal effects.

Apparent angular sizes were also measured, at 111 MHz only, for four other pulsars: PSR 0834+06, 0950+08, 1133+16, and 1919+21. Each pulsar is only slightly resolved, but within the experimental uncertainty the apparent sizes of these pulsars and of the Crab nebula pulsar are consistent with the scattering size scaling as the square root of distance (or dispersion measure).

METER-WAVELENGTH OBSERVATIONS OF PULSARS

USING VERY-LONG-BASELINE INTERFEROMETRY

by

Nancy Ruth Vandenberg

Dissertation submitted to the Faculty of the Graduate School
of the University of Maryland in partial fulfillment
of the requirements for the degree of
Doctor of Philosophy
1974

TABLE OF CONTENTS

x

LIST OF FIGURES

LIST OF TABLES

LIST OF SYMBOLS AND ABBREVIATIONS

Symbol	Definition	First used or defined on page
a	characteristic scale size of irregularities	102
b	baseline length	55
A_n	amplitude of the nth Fourier component	23
D	dispersion	24
E	average pulse energy	29
F	pulse repetition rate	23
G	dispersion time delay	24
I_P	pulsing flux	22
I_{PR}	partially resolved pulsing flux	46
I_S	steady, or non-pulsing, flux	22
I_{SR}	partially resolved steady flux	46
I_T	total flux (observed on short baseline)	22
I_{TR}	partially resolved total flux (observed on long baseline)	46
IPS	interplanetary scintillations	1
ℓ_ϕ	distance over which one radian of phase shift occurs	98
L	distance of observer from scattering screen	86
m_P	polarization of pulsing flux	76
m_T	polarization of total flux	63
n	index number for Fourier components	23
n_e	volume density of electrons	99
Δn_e	rms electron density fluctuation	102
N	column density of electrons	99
pdf	probability density function	87

CHAPTER I

INTRODUCTION AND PURPOSE OF THESIS

Pulsars have provided theoretical astronomers with objects which exist
in a physical state previously only postulated. They offer a passive astro-
physical laboratory for the study of highly condensed matter, extreme mag-
netic fields, and high energy plasmas. Observational radio astronomers
have also been provided with a new phenomenon: pulsars are essentially
point sources. But pulsars are not only point sources, they are also
sources which very elegantly turn themselves off periodically to allow
observers, without ever moving their telescopes, to make calibration runs
and off-source measurements.

Many of the spectral, temporal, and spatial features which have been
observed in the radio radiation from pulsars are due to scattering in the
media through which the radiation has passed. Narrow-band structure in
the frequency domain has been studied by Rickett (1970), Huguenin et al.
(1969), Ewing et al. (1970), and Lang (1971a). Temporal variations of
the flux density (due to drifting diffraction patterns) have also been
studied by several observers: Lang and Rickett (1970), Galt and Lyne
(1972), Rickett and Lang (1973), and Slee et al. (1974). To investigate
the angular structure imposed on the radiation Galt et al. (1970) and
Vandenberg et al. (1973) used the technique of very-long-baseline inter-
ferometry (VLBI). The method of interplanetary scintillations (IPS) has
been used by Cronyn (1970a), Zeissig and Lovelace (1972), and Armstrong
et al. (1973) to study the angular structure. Also, the Crab nebula pulsar
was studied by many observers, e.g. Bell and Hewish (1967), via IPS long
before it was known to be a pulsar.

1

The project described in this thesis exploited the VLBI technique to achieve the high spatial resolution (~0.1 arcsec) necessary to study the angular structure in the radiation from pulsars. This resolution is obtainable only with VLBI and IPS and has added another dimension to the understanding of pulsars and the propagation media. This project represents the first application of the VLBI technique to pulsars after the early observations by the Canadian VLBI group (Galt et al. 1970).

A. Interstellar scattering and interferometric observations of pulsars

This section describes the phenomena associated with a simple thin screen model for interstellar scattering. The VLBI experiments described in the next chapters provide tests of this model's predictions. The agreement of observations with the model is discussed in Chapter V.

With an interferometer we can measure the total time-averaged power from a pulsar and obtain a certain amount of correlated flux. From the pulsing power we may also obtain what we call a "correlated pulse profile." The correlated profile might be expected to appear quite different from that observed with a single telescope for the reasons discussed below.

1. Scattering. The most important effect on the pulse profile is the fact of scattering of the pulsar's radiation in the interstellar medium. Assume for simplicity that the density irregularities which are responsible for the scattering are distributed uniformly along the line of sight to the pulsar. For many purposes we can then represent the interstellar medium simply as a thin phase-changing screen (figure I-1). Two effects of the scattering should be seen. First, the radiation from the pulsar will be received from a angular extent θ_s which is much larger than the intrinsic size of the source ψ. Second, since the radiation which is

received from the edges of the
scattering cone has travelled a
longer path than the radiation
which comes straight through
unscattered, a narrow pulse
emitted at the pulsar (as in
figure I-2a) will be broader when

Figure I-1. Thin screen
scattering configuration.

it is received at the earth. As the time delay, τ, approaches (figure I-2b)
and exceeds (figure I-2c) the pulse period, P, the pulse shape broadens and

a baseline of continuous flux
is added to the profile.
Eventually an average con-
tinuum value of the flux is
reached. This phenomenon was
first proposed by Cronyn (1970b)
as an explanation for the ap-

Figure I-2. Schematic pulse
trains for various time delays.

parent decrease in the amount of pulsing flux which was observed from the
Crab nebula pulsar at low frequencies. The amount of broadening is
wavelength-dependent such that at longer wavelengths the average time
delay and scattering angle both increase.

2. Interferometric observations. Now if we observe the pulsar with
an interferometer which has a fringe spacing on the order of the scatter-
ing size θ_s, we would partially resolve the apparent source and could then
estimate its angular size. Cohen and Cronyn (1974) point out that in order
to observe an apparent angular size of θ_s rather than ψ, we must also use
a bandwidth greater than $1/\tau$ or a time constant longer than the character-
istic time for the drifting diffraction pattern. Either of these two

conditions insures that the rays arriving from various directions within the scattering cone are incoherent.

The pulse profile which the interferometer observes would originate from the central area of the scattering disk where the radiation has not travelled as long a distance as in the outer parts. Therefore the pulse profile observed with an interferometer which partially resolves the scattering disk should be narrower than that observed with a single telescope.

Another way of considering this phenomenon is to note that the apparent angular size of the source increases as the pulse progresses. At the start of a pulse, the radiation comes from a point source; at a later phase in the pulse period the radiation arrives from an annulus around the center; finally near the end of the period the radiation comes from near the edges of the scattering cone and we observe a large source. This changing apparent source size means that the fringe visibility, γ, should decrease as a function of pulse phase, and that the pulse from a partially resolved source should appear to be narrower than that from an unresolved source.

Figure I-3 is a schematic drawing of an unresolved broad pulse and a partially resolved pulse (a), and the fringe visibility as a function of pulse phase (b). Using an interferometer with very high resolution and high sensitivity the unscattered pulse shape could presumably be observed. The visibility function for pulsar radiation is discussed in more detail by Cronyn (1974).

Figure I-3. Pulse shapes (a) and fringe visibility function (b).

Another cause for an expected difference between the correlated pulse profile and the single-telescope profile is due to the pulse baseline or zero level. Single-telescope observers usually choose a baseline level at the minimum of the pulse profile, thus assuming that the pulsar actually "turns off" between pulses. If the pulse profile has both pulsing and non-pulsing power (which may be due to scattering, as described above, or to the intrinsic radiation pattern of the pulsar) then this method ignores the continuous source. With single-telescope observations, a procedure using on- and off-source measurements would be required to detect the continuous component. However such an observation would require high sensitivity because most pulsars are weak sources and any underlying continuous component would be still weaker and more difficult to detect.

With an interferometer, however, the large-scale structure of the sky background is washed out. The pulsar has a small angular size and its radiation, including both non-pulsing and pulsing components, will be correlated over a long baseline. Hence the level of zero correlated power is the true zero level of the pulsar's power.

In the case of the Crab nebula pulsar, the nebula makes single-telescope observations even more difficult. A long-baseline interferometer has the unique advantage of suppressing the strong radiation from the spatially large nebula and giving the ability to observe only the small compact source which is the pulsar.

B.   Summary of thesis and thesis work

This thesis is concerned with low-frequency (100- to 200-MHz) VLBI observations of several strong pulsars, concentrating on the Crab nebula pulsar. The observed angular structure is interpreted in terms of a model

in which the scattering of the Crab nebula pulsar's radiation occurs in both the nebula and the interstellar medium. The experimental techniques, from data-taking through processing to calibration, are described in chapter II; attention is focused on the peculiarities presented by pulsars as sources observed with an interferometer. The next two chapters discuss the results of the Crab nebula pulsar observations: first the average total flux (Chapter III), and then the pulse profiles and pulsing power (Chapter IV). Each of the various models of the Crab nebula and the interstellar medium which have been proposed to explain the observed phenomena is discussed in Chapter V. Comparisons are made between predictions of the models and the new results presented in this thesis. Chapter VI presents the results of observations of several other pulsars. Finally Chapter VII summarizes the results and presents suggestions for further work.

The series of experiments on which this thesis is based involved a multitude of people: figuratively, if not literally, a cast of thousands. This joint project involved people at the University of Maryland, Goddard Space Flight Center, Arecibo Observatory, and the Naval Research Laboratory. It is difficult to separate the tasks of individuals in a VLBI group, but I shall attempt to outline the areas in which I played an active role. Then, in the interest of coherence, the remainder of the thesis will not distinguish my separate work.

The original experiment was conceived by T. A. Clark, W. C. Erickson, and J. J. Broderick, and I entered the project after the first observations had been analyzed (Erickson et al. 1972). From then on I was involved in every aspect of the planning, observing, processing, and analysis operations.

During the thesis work, my "official" advisor was W. C. Erickson; my work was also directed by T. A. Clark who acted as my "unofficial" advisor.

During the course of the experiments a wide variety of objects was observed: pulsars, compact galaxies and quasars, and supernova remnants. The responsibility for detailed data analysis fell to one person for each of the three source categories. The observations of extragalactic objects were studied by G. M. Resch and the results of the analysis are presented in his thesis (Resch 1974). Observations of the supernova remnant Cassiopeia A were analyzed by L. K. Hutton (Hutton et al. 1974). The Crab nebula pulsar and the other pulsar observations were analyzed by me and the results are contained in this thesis.

For pulsar data I made extensive modifications to the main processing program (VLBI1) to include the ability to gate the correlation routine. This also required that the normalization scheme of the second processing program (VLBI2) be completely revamped which I also accomplished. I also made many additional program innovations which were not directly involved with pulsar observations because I had assumed responsibility for maintaining the software system for all of the VLBI data processing done at Goddard.

As an aid to scheduling observations for VLBI experiments, I wrote the PRESKED and SKED programs which are briefly described in Appendix A. These two programs are now used by several other VLBI groups. After observing priorities were agreed upon in group discussion, I did the major part of all the detailed scheduling for the experiments discussed in this thesis. I participated in setting up the equipment for every experiment, and, during the course of the seven observing sessions, I assisted in tape-hanging at each of the three telescopes.

Once the data tapes were returned to Goddard after the recording sessions, I took charge of the data processing operation for all but one of the experiments. This work involved sorting and pairing all of the data tapes, preparing jobs for the computers, and finally examining the output of VLBI1 and VLBI2 to decide if re-processing was necessary. For each experiment I also processed several runs to search for the proper clock settings. Normalization of the raw correlation coefficients and flux calibration schemes were agreed upon by the group in meetings and discussions in which I participated. Application of these schemes to the data was done by G. M. Resch and forms a part of his thesis.

Analysis of the pulsar data was done entirely by me with suggestions, advice, and discussion by the group. This thesis represents my study of the pulsar data.

C. Other research

Before my thesis work was begun, I participated in other VLBI projects including the many "Oktoberfest" relativity experiments and several other experiments in what is now called the "Quasar Patrol" project (Knight et al. 1971; Whitney et al.1971).

During the time that the low-frequency experiments were being done, I began a series of VLBI experiments at 2.3 GHz (13 cm) in order to measure accurate positions of pulsars relative to extragalactic sources. The collaborators were G. S. Downs and P. E. Reichley of the Jet Propulsion Laboratory, and T. A. Clark, W. C. Erickson, and myself. One purpose of the program was to compare positions measured with comparable accuracy using VLBI and pulse timing techniques in an attempt to resolve some discrepant measurements. Another purpose was to examine the positions derived from

experiments spaced several months apart for evidence of proper motion and/or parallax of pulsars. Manchester et al. (1974) have observed proper motion of PSR 1133+16 using pulse timing techniques.

Two observing sessions were held in 1972 using the Goldstone antenna and the NRAO 42-m telescope. The data were reduced and analyzed to determine fringe v'sibilities of various sources. The Vela pulsar, PSR 0833-45, is found to be partially resolved. Its measured angular size is presumably due to scattering along the line of sight through the Gum nebula and the rest of the interstellar medium. More accurate normalization factors are being derived to improve the estimate of fringe visibility. The data will also be analyzed to yield relative position measurements, which can hopefully be combined with the results of other interferometric studies of pulsars now in progress at CalTech and NRAO.

CHAPTER II

EXPERIMENTAL METHODS

A.   Description of experiments

Since 1970 there have been several meter-wavelength VLBI experiments

using a variety of baselines in the United States. Clark and Erickson

(1973) have summarized some of these experiments. Figure II-1 is a map

showing the baselines for the
experiments discussed in this
thesis and table II-1 lists
the dates, stations, obser-
ving frequencies, and reso-
lutions.

1.   Earliest experiments.

One early meter-wavelength VLBI
experiment (in 1970 January at

Figure II-1. U.S. map showing
baselines. Refer to table II-1
to identify stations.

121 MHz from Maryland Point to NRAO) provided the first low-frequency VLBI

data on the Crab nebula pulsar. The technique for obtaining the Fourier

components of a pulse shape was developed by W. C. Erickson and T. A. Clark

and was first used for these observations. The data have been analyzed and

published by Erickson et al. (1972).

Another meter-wavelength experiment (1971 March at 144 MHz between

Owens Valley, Vermilion River, and Sugar Grove) used one partly-steerable

and two fully-steerable telescopes which enabled extensive hour-angle cov-

erage of several sources. Figure II-2 shows the (u,v)-plane coverage (for

the Crab nebula) of these three baselines along with those of later experi-

ments. The pulsar's scattering disk was substantially resolved with the

10

Table II-1

Low-frequency VLBI experiments

Date	Freq (MHz)	Telescopes Name	Symbol*	Size(m)	Baseline Symbol*	Length(Mλ)	Fringe spacing (arcsec)
1970 Jan. 10-12	121.6	Maryland Point NRAO	M N	25 92	MN	0.092	2.2
1971 Mar. 9-14	144.3	Sugar Grove Vermilion River Owens Valley	S V O	46 36 40	SV SO VO	0.36 1.27 1.62	0.55 0.16 0.12
1971 Nov. 23-24 1971 Dec. 19-20 1972 Jan. 23-24	196.5 and 111.5	Arecibo NRAO Sugar Grove	A N S	305 92 46	AN AS NS	1.7 1.6 0.033	0.12 0.12 (196.5) 6
1972 Feb. 25-27 1972 Mar. 26-28					AN AS NS	0.94 0.93 0.019	0.20 0.20 (111.5) 10
1972 Dec. 4-9 1973 Feb. 23- Mar. 2	111.5 and 74.0				AN AS NS	0.62 0.62 0.022	0.30 0.30 (74.0) 15

*These symbols will be used throughout other tables.

longest baseline and the range of fringe visibilities gave some indication of the brightness distribution. The experiment demonstrated that interstellar scattering does occur and that meter-wavelength VLBI is technically feasible. However, since all sources except the Crab nebula pulsar were partially resolved with the longest baseline it was also shown that more sensitivity was necessary in future projects.

2. Latest experiments. With the results of the early experiments in mind, a multi-purpose meter-wavelength VLBI program was begun in late 1971 and spanned one and one-half years (see table II-1). There were five two- or three-day observing sessions monthly from 1971 November through 1972 March, and week-long sessions in 1971 December and 1973 February. The telescopes used were Arecibo (305 m), NRAO (92 m), and Sugar Grove (46 m). They form two long baselines (2550 km) and one short baseline (50 km).

a. Primary purpose of experiments. The original purpose of the monthly experiments was simply to monitor the apparent angular size of the Crab nebula pulsar and compare any observed changes to the variations in the pulse shape which were being observed at Arecibo. These pulse shape variations have been reported by Rankin and Counselman (1973). Comparisons between the size variations and the different pulse shapes could yield information on the location and dynamics of the scattering medium. The VLBI experiments were done simultaneously with the regular Crab nebula pulsar monitoring observations at Arecibo.

Another purpose of the experiments was to determine the wavelength dependence of interstellar scattering by observing several strong pulsars, especially the Crab nebula pulsar, at two frequencies, 196 and 111 MHz. In the later experiments, the observing frequency of 74 MHz was

Figure II-2. (u,v)-plane tracks for Crab nebula. Each track is labelled to indicate frequency and baseline. Symbols for each baseline are contained in table II-1.

added and 196 MHz was deleted because it turned out that interstellar scattering effects were not strong enough at the higher frequency. Various other aspects of the Crab nebula pulsar were also investigated. Enough Fourier components were detected to allow reconstruction of pulse shapes. Also of interest was the polarization of the pulsar at low frequencies

The Crab nebula pulsar was the primary source in all of the experiments, and in order to minimize ionospheric and interplanetary propagation effects the observations were scheduled in the winter when the Crab nebula is near the anti-solar direction.

b. Other sources. A large number of extragalactic sources suspected of having, or known to have, compact components were also part of the program. About 120 sources were observed at least once. Several of the stronger sources were also used for polarization and total power calibration observations. The intent was to obtain low-frequency spectral information on the compact components alone by resolving large structures such as halos. For many sources, the synchrotron self-absorbed region of the spectrum should occur near our observing frequencies. Another purpose of the extragalactic source observations was to compare the VLBI-observed angular sizes to those derived from interplanetary scintillation (IPS) techniques. The extragalactic sources will not be discussed further in this thesis except as calibration sources. The results of the observations are presented by Resch (1974).

In the 1972 December experiment, a selection of supernova remnants was observed in a search for compact sources such as the pulsar in the Crab nebula. No such sources were found, although fine structure similar to that seen at centimeter wavelengths was found in Cassiopeia A. The results of

these observations are reported by Hutton et al. (1974), and are not discussed in this thesis.

c. Scheduling considerations. Due to the limited hour-angle coverage of the moveable feeds of the NRAO and Arecibo telescopes, the amount of time a source was visible at all three stations was never more than about one hour. Figure II-2 showed the pitifully short (u,v) tracks for the Crab nebula on these three baselines. The primary sources (the Crab nebula pulsar, five strong pulsars, and four calibration sources) were observed during their entire period of mutual visibility every day. For the remainder of the extragalactic sources, at least two runs were scheduled on each of two different days. The redundancy was insurance against sporadic interference, tapes with excessive errors, and all the possible problems which plague us in the heat of battle. Scheduling programs and other preparation procedures are described in Appendix A.

There is as much data from each of the last two observing sessions as from the first five sessions combined. Also, changes in the characteristics of the Crab nebula pulsar did not occur during the first winter. Normalization and calibration procedures were improved between the two winters also. For these reasons, differences will often be noted between results of the two "sets" of experiments where the first set comprises the first five sessions in winter 1971-2 and the second set comprises the two sessions in winter 1972-3.

3. Recording system. For all of the low-frequency experiments the Mark I VLBI recording system was used. It has a 350-kHz bandwidth and records a clipped and sampled video signal on standard computer tapes; one tape holds three minutes of data. The data can be processed with either a general purpose computer or a special purpose processor such

as the one at Haystack Observatory. The system is described more completely
in Appendix A. Another recording system is used by many other VLBI groups.
It is known as the Mark II system (Clark 1973) and has a 2-MHz bandwidth.
The data is clipped and sampled and recorded on video tape. one tape lasts
from one to five hours. The data must be processed on special purpose pro-
cessors.

There were several reasons for choosing the Mark I system over the
Mark II system. The two major motivations were 1) the certainty that ac-
curate correlation amplitudes could be extracted from the raw data, and
2) the sophisticated software system available for data reduction. The
accuracy of the programs was recently tested by recording a partially-
correlated "man-made" signal on two recorders at the same site. Normal
process ng of the data produced correlation amplitudes within 5% of the
known fraction of correlated signal. This assured us that the recording
and processing operations do indeed enable us to recover the true signal.

The software system of the MIT/Goddard reduction programs has been
written with exhausting attention to detail (Whitney 1974; Hinteregger
1972). In particular, the phase is carefully tracked throughout the re-
duction so that the recovery of pulsar Fourier components is possible.
The ability to activate the correlation routine only when a pulsar was
"cn" was added to the programs in order to obtain increased sensitivity
on pulsar observations. None of these features was available with the Mark II
system at the time this project was begun, and in fact several approxi-
mations which make it impossible to do these types of data reduction were
built into the Mark II pre-processor.

The other reason for using Mark I was that the integration time and
bandwidth advantages of the Mark II system could not be exploited. At

frequencies between about 100 and 200 MHz there are numerous bands with interfering signals from radio and television stations. The Mark I bandwidth is just narrow enough to fit between most of the interference, but we probably could not have used the entire bandwidth of the Mark II system since this requires a clear band simultaneously at all the stations. Also at low frequencies phase fluctuations due to the ionosphere and interplanetary medium limit the coherent integration time to a few hundred seconds or less so that we could not have made longer coherent observations with the Mark II system.

B. Description of processing

1. Program VLBI1. The data tapes from all the experiments described in the previous section were carried or mailed to Goddard Space Flight Center and processed on the IBM 360/91 and 360/75 computers using the programs called VLBI1 and VLBI2. The function of each component of the interferometer and of the programs is shown in figure II-3. Details concerning the programs, the algorithms, approximations, and the theory of processing can be found in the theses of Whitney (1974) and Hinteregger (1972). The ideas and equations necessary to understand the basic processing and the Fourier component method are considered next.

a. Ephemeris data. A set of ephemeris data peculiar to the experiment being processed is provided to program VLBI1 (figure II-3 at location a). The data set contains such information as the position of each source observed, the locations of the telescopes, the total local oscillator frequencies, any instrumental time delays, and the individual stations' clock epochs. At low frequencies the effect of ionospheric refraction is often important, and it acts as an additional, but unknown,

Figure II-3. Block diagram of functions of recording systems and processing programs. Locations labelled (a) through (f) are referred to in the text of sections B-1 and B-2.

time delay. The a priori values of the parameters in the data set are as
accurate as possible, but small errors in these values or in instrumental
or propagation effects are not critical because the final program searches
for the maximum correlation over a range of values.

b. Phase. It is most important to understand what is meant by
phase throughout the processing programs: how is the a priori phase cal-
culated, how is the observed phase determined, and what information does
the residual phase contain?

The expression which is used to calculate the a priori phase is
derived in Appendix B and we will use the result:

$$\phi(t)_{calc} = \phi_o + f\Delta t_R + \Delta\omega_{LO} \Delta t_{LO} \quad . \qquad (II-1)$$

The first term, ϕ_o, is called the "fundamental phase" which is due to the
geometrical delay. The second term accounts for the phase due to the rate
of change of the geometrical delay as the earth rotates; the total fringe
rate is f and the phase is counted during the time elapsed, Δt_R, since a
reference time t_o. The last term includes any frequency offset between
the two local oscillators, $\Delta\omega_{LO}$; the phase is counted during the time
elapsed, Δt_{LO}, since the start of the oscillator at t_{LO}.

c. Correlation process. The observed correlation function,
which describes the fringes, is obtained by multiplying the bit streams
from two data tapes (figure II-3, at c) after shifting by the number of
bits corresponding to the total time delay (figure II-3, at b). Because
the time delay "resolution function" has a width $\sim(2\pi \times bandwidth)^{-1}$, a
range of ±3 bit delays centered on the nominal delay is used to define
the correlation function. Then the seven-point function is mixed with
"fake" fringes (figure II-3, at d) having the a priori calculated phase

of equation II-1. This process is called "fast fringe rotation" and is done to reduce the fringe frequency and time delay to small values which are more easily handled.

The phase, after mixing, is:

$$\phi_{obs} - \phi_{calc} = f_R \Delta t_R + \omega \tau_R \qquad \text{(II-2)}$$

where f_R = residual fringe rate,

τ_R = residual time delay,

ω = total local oscillator frequency.

The quantity $\omega \tau_R$ is also called the residual phase, ϕ_R, and it is made up of two terms:

$$\phi_R = \Delta \phi_o + \phi_{instr} \qquad \text{(II-3)}$$

where $\Delta \phi_o$ = residual fundamental phase,

ϕ_{instr} = instrumental phase.

The instrumental phase contains terms such as clock errors and instrumental time delays which change slowly or not at all with time. The unknown ionospheric delays also enter in this term. The instrumental phase is indeterminate since it also includes the absolute phase difference between the two local oscillators; it can be eliminated only by using differential measurements.

The correlation function is next averaged (figure II-3, at e) over 0.2 sec (one record) which restricts the residual fringe rate to ±2.5 Hz. The resulting complex correlation functions for the nominally 900 records in one run are written on an output tape (figure II-3, at f) along with all the ephemeris information relevant to the observation and many numbers calculated by the program. The fringe amplitudes and phases

will be manipulated and averaged by the next processing program to obtain
the best estimates of the fringe rate, time delay, fringe phase, and fringe
amplitude.

2. Program VLBI2. a. Residual parameters. The second processing
program is called VLBI2. It reads the ~900 complex correlation functions
into an array which represents the complex observable space. The data
array is Fourier transformed irto the (residual time-delay, residual fringe-
rate) domain; this array extends ± 4.5 μsec in the time-delay dimension and
± 2.5 Hz in the frequency dimension. The peak of the correlation function
is searched for in this plane, and the maximum is found at some value of
τ_R and f_R. The best-fit values of τ_R and f_R are determined by interpolation
using a finely-spaced Fourier transform around the preliminary value.

b. Fringe amplitude and phase. The seven points in each cor-
relation function are then averaged using the best-fitting value for τ_R
to adjust the phase across the bandpass. The resulting complex numbers
are the amplitudes and phases of the fringes for each record. The shortest
coherent integration time is one record (0.2 sec) and averages of fringe
amplitude and phase for various longer coherent integration times are also
calculated by the program. The choice of an appropriate integration time
is discussed in part C-3 of this chapter (page 40).

c. Uncertainties. The maximum fringe amplitude is not a single
point but rather an "island" surrounded by smaller islands which are the
noise and sidelobes of the response pattern. Figure II-4 is a schematic
drawing of this island. The shape of the pattern is approximately a sinc
function and the width, i.e. the extent of the island, is an indication
of how well the fringe amplitude and phase can be determined. For one
observation, the fringe rate can be estimated to an accuracy of at least

$(2\pi \times T \text{ sec})^{-1}$ where T is the

coherent integration time. For

a 180-sec average, the uncer-

tainty in fringe rate is

~1 m Hz. The time delay

can be determined to at

least $(2\pi \times 350 \text{ kHz})^{-1}$

~0.5 μsec. These esti-

Figure II-4. Correlation peak
in the (τ_R, f_R) plane.

mates can be improved if the signal to noise ratio is very high.

3. Pulsars: Fourier component method. This section discusses how

the response of the interferometer changes when the source is a pulsar

which has a characteristic time signature. Then the method used to re-

cover the Fourier components of the pulse shape is described. The approach

used in this section is different from that presented in the paper by

Erickson et al. (1972).

a. Pulsar intensity. We can specify the pulsar's intensity

as a function of time by

$$I_T(t) = I_S + I_P(t) \tag{II-4}$$

where $I_T(t)$ = total intensity,

I_S = steady or non-pulsing component of the total intensity,

$I_P(t)$ = intensity in the pulse train.

We can further represent the total intensity as a Fourier sum,

$$I_T(t) = \sum_{n=-\infty}^{\infty} A_n \exp 2\pi i (nF\Delta t_R + \phi_n) \tag{II-5}$$

where A_n = amplitude of the nth Fourier component of the pulse shape

[note that A_o includes I_S and is the time average of $I_T(t)$],

ϕ_n = phase of the nth Fourier component,

$F = 1/P$ = pulse repetition rate,

Δt_R = elapsed time since the reference time, t_o.

The various components of the total intensity are illustrated in figure II-5.

This is not a complete description of the source radiation however, because all pulsar radiation is dispersed in its passage through the interstellar medium. The

Figure II-5. Components of the total intensity of a pulsar.

effect of dispersion is to shift the pulse later in time by an amount depending on the frequency and in such a way that pulses arrive later at lower frequencies. To illustrate this, figure II-6 shows schematically some pulses in the (time, frequency) plane. The pulses sweep across a given passband at a rate $\Delta\omega/\Delta t$, which, over a small range of frequency, can be approximated as a constant,

Figure II-6. Dispersed pulses in the (time, frequency) plane.

$$\Delta\omega/\Delta t = -\omega \cdots D \cong -F/G \qquad (II-6)$$

where D = dispersion constant, measured as the difference in the time of

arrival of the same pulse at two frequencies,

1/G = spacing of the pulses in the frequency domain (G = $2FD/\omega^3$),

1/F = spacing of the pulses in the time domain (pulse period).

Since the entire pulse is delayed, the pulse <u>shape</u> is not changed and each

Fourier component is affected the same way. The time delay due to dis-

persion is

$$t_D = D\Delta(1/\omega^2) \qquad (II-7)$$

which can be represented as a phase shift of $-2\pi i n FD/\omega^2$. The expression

for the total flux including the effects of dispersion is

$$I_T(t) = \sum_{n=-\infty}^{\infty} A_n \exp 2\pi i(nF\Delta t_R + nG\omega + \phi_n) \quad . \quad (II-8)$$

   b.   Response of interferometer. The response of an interferom-

eter is the product of the source intensity and the fringe pattern,

$$R(t) = \left[I_S + I_p(t)\right] \times \exp 2\pi i\phi(t) \quad .$$

When $\phi(t)$ is given by equations II-2 and II-3 for the residual phase, we

have

$$R(t) = \sum_{n=-\infty}^{\infty} A_n \exp 2\pi i \left[(\Delta\phi_0 - nG\omega) + (f_R - nF)\Delta t_R + \phi_{instr} + \phi_n\right].$$

$$(II-9)$$

Notice that the residual fringe rate is given by $(f_R - nF)$. This means

that for a pulsar there are many sets of fringes, one for each value of

n, in contrast to only one peak for a steady source. The fringes are

separated from each other in fringe frequency by the pulse repetition rate

and their amplitudes are modulated by the amplitude of the nth Fourier

component, A_n. Also, since the pulsar is dispersed, there is a phase

change across the passband. This is shown in equation II-9 by the fact

that the residual fundamental phase is given by $(\Delta\phi_o - nG\omega)$. In the

transform domain a phase shift corresponds to a time delay, so that each

set of fringes occurs at a different delay. Figure II-7 shows the (τ_R, f_R)

plane for a dispersed pulsar
having F = 1 Hz and G = 1 μsec.
Appendix C shows pictorially
the various sets of fringes.

      c.   Recovery of A_n and ϕ_n.

To obtain the amplitude and phase of

the nth Fourier component, a time

delay of nG and a fringe rate off-

set of nF are inserted during pro-

Figure II-7. Multiple sets
of fringes for a dispersed
pulsar.

cessing so that the main response of the interferometer is centered on the

nth set of fringes in the (τ_R, f_R) plane. Since one processing pass through

VLBI1 covers an area in the (τ_R, f_R) plane of about 9 μsec by 5 Hz, all the

fringe islands which occur within this domain can be found by searching with

program VLBI2 at the appropriate locations. Additional processing passes

are required for fast and/or highly dispersed pulsars and for higher order

components (see the pictures in Appendix C).

    In practice, obtaining A_n and ϕ_n is done in the following way.

Returning to equation II-1 for the calculated phase, we set $\Delta\omega_{LO} = nF$,

insert an instrumental time delay $\tau_i = nG$, and specify t_{LO} as some UT near

the start of the tape. (The value of t_{LO} actually depends on the exact

manner in which time is referenced in the programs.) The calculated phase
we obtain is then:

$$\phi_{calc} = \phi_0 + f\Delta t_R + nF\Delta t_{LO} \quad . \qquad (II\text{-}10)$$

The observed phase of the nth Fourier component is:

$$\phi_u(t) = nF(t - t_n) \qquad (II\text{-}11)$$

where t_n is the time at which the sine wave of frequency nF has its maxi-
mum or epoch. The output of VLBI2 is the residual phase of the nth compo-
nent:

$$\phi_{nR} = \Delta\phi_0 + \phi_{instr} + nF(t_n - t_{LO}) \quad , \qquad (II\text{-}12)$$

and for n = 0 the residual phase is given by equation II-3.

Differential measurements between the residual phases for n = 0
and n ≠ 0 allow the instrumental phase and the residual fundamental phase
to be eliminated. The "differential residual phase" of the nth component
is

$$\Delta\phi_{nR} = \phi_{nR} - \phi_{OR}$$
$$= nF(t_n - t_{LO}) \quad . \qquad (II\text{-}13)$$

d. Pulse shape reconstruction. To reconstruct the pulse shape
the differential phases of equation II-13 and the corresponding amplitudes
are added in a Fourier sum. Since t_{LO} is known in UT, the residual phases
contain information on the epoch of each component with respect to UT, and
the reconstructed pulse contains information which can yield the pulse
time-of-arrival in UT.

The Fourier components are summed according to the equation

$$I_T(t) = \sum_{n=-\infty}^{\infty} A_n \exp 2\pi i(\Delta\phi_{nR} - nFt) \ . \qquad \text{(II-14)}$$

In practice, the number of Fourier components which were detected in the processing is finite so the sum is actually from $-N$ to $+N$ where N is variable but always less than 10. The function $I_T(t)$ is interpolated so that the resulting pulse shape is smooth, although it must be remembered that there are only $N + 1$ independent points in the pulse profile. For the computer program which reconstructs and plots a 100-point pulse, the sum is represented as

$$I_T(t_i) = \sum_{n=-N}^{+N} A_n \exp 2\pi i(\Delta\phi_{nR} - nt_i/100) \qquad \text{(II-15)}$$

where $i = 0$ to 99.

The pulse shape which results from this process is an average pulse shape unsmoothed by dispersion effects. This profile is equilvant to that which would result from single-telescope observations of the average pulse shape over three minutes having no dispersion and having the sensitivity of a 350-kHz bandwidth system.

e. Zero-baseline interferometer. Because there is frequency structure within the Mark I passband, we can also obtain information about the pulsing power by auto-correlation. The data is processed in the same way as for cross-correlation in that time-delay and fringe-rate offsets are applied, but only one tape is used. The Fourier components n = 1, 2, ... N are obtained. Because this is an auto-correlation process the n = 0 component has a correlation coefficient of unity and the amplitudes of the +n and -n components are identical and the phases have opposite signs. The pulse shape is reconstructed in the same manner as for the cross-correlation

profiles, the only exception being that an arbitrary-level n = 0 component

must be added to raise the baseline of the pulse. The components obtained

this way and the resulting profile are called "zero-baseline" components

and profiles. Usually the Arecibo Mark I data tape was used for the zero-

baseline processing because the sensitivity was the highest at this station.

4. Pulsars: gating method. a. Description of processing. From

pulsar VLBI data we can obtain either the Fourier components, as just de-

scribed, or the time-averaged power. The interval over which the average

power is measured can be restricted by "gating" the correlation routine so

that it operates only when the pulse is "on." This makes the process more

efficient since most pulsars are "off" more than 90% of the time.

The gate used with the VLBI1 correlation routine is not a true box-

car function but is actually "fuzzy." This is because 2 msec is the short-

est segment of data for which the correlation routine is called, and if a

pulse begins anywhere within that segment the correlation is done; simi-

larly, the trailing edge of the gate is only defined to within 2 msec.

The record length, 0.2 sec, is not commensurate with any pulse period so

that some pulses may straddle two records with the resulting loss of about

5 msec of data, the length of the inter-record gap. If the pulse width is

less than 5 msec, an entire pulse may be lost in the gap. These contin-

gencies are handled by the subroutine which opens and closes the gate

The observed correlation function is normalized by the actual amount of

data correlated so the duty cycle of the pulsar is automatically accounted

for in the correlation coefficient. The remainder of the processing is

the same as for a continuum source.

b. Epoch measurement. The time-of-arrival (epoch) of one pulse

must be known to an accuracy of about one millisecond so that the gate can

be placed properly over the pulse. Although it is possible to search for the correct epoch by placing the gate at different trial epochs until the maximum correlation is found, this is time-consuming and impractical.

To monitor the average pulse shape during the observing sessions, the IF signal was sent to a multi-channel signal averager which was triggered by a clock running at the pulse repetition frequency. The stored signal was displayed on an oscilloscope and a polaroid picture was taken to record the profile. The time at which the clock had been started was recorded so that the UT of the start of the trace was known. The epoch of the pulse could be read off the picture in units of percentage of the pulse period, giving the pulse epoch relative to UT. This time was recorded and later used in the processing program to calculate the time at which the gate should be opened.

Besides knowing the epoch of the pulse, another requirement for using the gating method is that there be only one pulse in the Mark I passband at any one time. This is the case for all of the low-dispersion pulsars we observed. However, the gating method as described above cannot be used for the Crab nebula pulsar because its dispersion measure is so high and period so short that several pulses (e.g. ~5 at 111 MHz) are present across the band simultaneously. If we had used the gating method for this pulsar, we would add up "on" and "off" signals when we integrate across the passband, which is what the method tries to avoid in the first place. For the Crab nebula pulsar, the pulsing power is recovered by de-dispersing the signal as described in the previous section.

c. Sensitivity and flux measurements. The intensity of pulsar radiation is expressed in a variety of ways. Pulsar spectra are usually presented as plots of log E vs. log ω where E is the "average pulse energy"

in units of $J\ m^{-2}\ Hz^{-1}$. This quantity is not dependent on the details of the pulse shape, it is simply a measure of the average received energy. The intensity is also given in terms of the "peak flux density," $S_p = E/\tau_e$, where w_e is the equivalent pulse profile width. Yet another quantity is the "equivalent continuum flux density," $S_c = E/P$, where P is the pulse period. S_c is the total time-averaged flux density, that is, the flux which the pulsar would have if it were smeared into a non-pulsing continuum source. By using the gating method we measure the flux density averaged over the gate width: $S_p = E/w_g$; nominally we set $w_g > w_e$ to include most of the pulse profile.

Gating increases the signal-to-noise ratio in the following way. If we do not gate, then we must detect a continuum source signal S_c in the presence of a noise level σ_c. With a gate, the integration time is decreased by a factor w_g/P, so the noise level is increased to $\sigma_p = \sigma_c\sqrt{P/w_g}$, but now the signal to be detected is larger, $S_p = S_c P/w_g$. Therefore, the signal-to-noise ratio is enhanced by a factor $\sqrt{P/w_g}$ if gating is used. Typically, $P/w_g \gtrsim 20$, so the signal-to-noise ratio improvement is at least a factor of 4.5 over the case where pulsars are treated as continuum sources.

We can recover the correlation coefficient of a single pulse provided that the pulse period is less than 0.2 sec, the shortest coherent integration time. The detection limit for single pulses is very high however because the integration time is only w_g.

d. Replication of fringes. In the previous section on the Fourier component method it was noted that for a pulsar there are many sets of fringes spaced by the pulse repetition frequency. For the Crab nebula pulsar $F \sim 30$ Hz so the fringes are well-separated from the ambiguities which occur due to sampling by the Mark I recording system. However,

for pulsars with F ~ 1 Hz the different sets of fringes are closely spaced in the fringe rate spectrum and they could be mistaken for the zero-order fringes if not properly taken into account. The search by program VLBI2 for fringes is restricted to the range $\pm F/2$ so that these ambiguities are avoided. Appendix C contains pictorial representations of a sample of data, and the corresponding fringe rate spectrum, to illustrate the replication.

C. Calibration procedures and correction factors

1. Flux scale. a. General method. All of the data from the seven experiments were normalized by the following general method. Since the correlation coefficient, ρ, is a fraction of the mean total system temperature it can be expressed as a temperature by multiplying by the mean temperature:

$$T_{corr} = \rho \sqrt{T_{sys1} \cdot T_{sys2}} \ . \qquad (II-16)$$

Measurements of each antenna's efficiency, e, expressed in Kelvins per Jansky, can then be used to convert the temperature to flux density:

$$S_{corr} = T_{corr}/\sqrt{e_1 e_2} \qquad (II-17)$$

For the 1971 March experiment at 144 MHz the correlation coefficients have not been converted to fluxes because little information on system parameters and total power records is available. However, because each telescope in this experiment had approximately the same sensitivity the correlation coefficients, in correlation units, can be intercompared between the three baselines.

The system configuration at each station varied greatly from one experiment to the next as improvements in receivers and observing techniques were gradually made. A discussion of some of the situations encountered in this learning process is contained in Appendix A.

b. First set of experiments. For the first set of experiments, system temperatures were estimated by adding together the known contributions to temperature:

$$T_{sys} = T_a(\text{source}) + T_{sky} + T_{receiver} \qquad (II-18)$$

At meter wavelengths, all but a handful of sources are weaker than the sky background so the source antenna temperature can usually be neglected. The sky background temperature was estimated by reading the contour level near the source position from the 178-MHz map of Turtle and Baldwin (1962) and scaling to our frequencies with a brightness temperature spectral index of -2.5. The random error in estimating the sky temperature is about 20%. The error also depends on frequency because the sky background becomes smoother at lower frequencies and it also forms a larger fraction of the total system temperature.

The receiver temperature was accurately measured at NRAO and Sugar Grove only in March 1972. For each station, the receivers were assumed to be similar enough each time that the 1972 March measurements were valid for every other month also. At Arecibo, the receiver system also was changed every experiment but here the temperature was measured each time, and these values were used. The receiver temperature has an uncertainty of about 20% due to these problems.

The total error in the system temperatures will be due to random errors in scaling the sky map for background temperature, and to a systematic

error from uncertainties in receiver temperature. Overall, the estimate
of the total system temperature for each station is probably accurate to
30%.

The dish efficiency of the 92-m NRAO telescope was carefully
measured at 111 and 196 MHz in 1972 March (Hutton 1972), and these curves
were adopted for all the previous experiments. The efficiency is a strong
function of hour angle, and the normalization from correlation units to
Janskys will thus be dependent on the hour angle of the source at NRAO.
At 111 and 196 MHz the efficiency is a monotonically decreasing function
of hour angle, but at 74 MHz the efficiency is a more complicated function.
The adopted curves for all frequencies are shown schematically in figure
II-8. At Arecibo, the vari-
ation of efficiency with hour
angle was not as severe as at
NRAO but the effects were
included. The efficiency
of the telescope at Sugar
Grove did not vary with
distance from zenith. The
feed systems at all three
stations were the same each
month so it was assumed that
the antenna efficiencies did not vary.

Figure II-8. Hour-angle dependence
of efficiency for NRAO 92-m telescope.

The total error in normalization from correla⁻'⁻ ι units to
Janskys for this set of experiments is estimated to b‹ ... ;u₁ 20%. Table
II-2 contains typical values of receiver temperature and efficiency;
table A-1 lists the individual values for each telescope and observing
session.

A special problem exists for the 1972 March experiment: the sensitivity of the Sugar Grove station was reduced to below its usual value by about a factor of three. The decrease in sensitivity appears to vary randomly during the experiment, however, making a correction factor difficult to compute. For this reason only the Arecibo-NRAO baseline flux measurements will be presented for this one experiment.

    c.   **Second set of experiments.** During the last set of experiments the system temperatures were measured for every run. This eliminates uncertainties due to estimating background temperatures but introduces reliance on a calibration noise source. The random error in one estimate of system temperature is about 10%. The curves for efficiency as a function of hour angle at NRAO and zenith angle at Arecibo were again measured by tracking a source across the sky and frequently moving the telescope beam on and off the source. This was done using Vir A at Arecibo, and Cas A, Tau A and Cyg A at NRAO. The three sources at NRAO gave consistent results.

The error in normalization actually depends on the total system temperature because of the measurement method we used; a typical error is estimated to be about 8% for a single observation on a weak source. The error is larger, about 12%, for observations of the Crab nebula pulsar because the nebula greatly increases the total system temperature. Systematic errors occur due to uncertainty in the efficiencies; these are estimated to be less than 10%. Table II-2 contains average values of receiver temperature for each experiment. Table II-3 contains sensitivities calculated using the values of table II-2 and the equation

$$S_{min} = \frac{5\pi/2 \cdot \sqrt{T_{s1}T_{s2}}}{\sqrt{e_1 e_2}\sqrt{BT}} \qquad \text{(II-19)}$$

Table II-2

Average System Parameters, by station

Date	Parameter	196 MHz			111 MHz			74 MHz		
		A	N	S	A	N	S	A	N	S
Winter 1971-2	receiver temp. (K)	350	350	375	600	170	675	–	–	–
	efficiency (K/Jy)	1.3	.93	.31	3.5	.96	.30	–	–	–
Winter 1972-3	receiver temp. (K)	–	–	–	400	200	900	600	400	750
	efficiency (K/Jy)	–	–	–	2.6	1.0	.35	4.6	.60	.35

Table II-3

System sensitivity for weak sources, by baseline

	196 MHz			111 MHz			74 MHz		
	AN	AS	NS	AN	AS	NS	AN	AS	NS
Winter 1971-2 sensitivity (Jy)	0.5	0.8	0.9	0.5	1.2	.8	–	–	–
Winter 1972-3 sensitivity (Jy)	–	–	–	0.5	1.3	1.8	1.4	1.9	5.1
Average sky temp. used (K)		150			600			1800	

where B = 350 kHz, T = 180 sec (one tape), and T_{s1} and T_{s2} were calculated from the receiver temperatures at each station and average sky temperatures given in table II-3.

  d. Flux scale. The flux scale was established by assuming flux density values for Cas A, Cyg A, and Tau A at our observing frequencies. Table II-4 lists the fluxes. The values were obtained by computing a best fit, in the least squares sense, to the available absolute measurements at many frequencies. The details of this procedure are discussed by Resch (1974).

Table II-4

Standard source fluxes

Source	190 MHz	111 MHz	74 MHz
Cassiopeia A (epoch 1972.9)	10960 Jy	16680 Jy	22570 Jy
Cygnus A	8955	13275	17210
Taurus A	1525	1775	1980
Virgo A	1030	1575	2145

  Systematic errors in flux measurements can only be evaluated through comparison with other independent observations. Each of the seven experiments was normalized independently and then the values of correlated flux were inter-compared and also compared to source surveys made at frequencies near our observing frequencies. The procedures we used are as follows.

  Since the two long baselines are of nearly equal length, the correlated flux of a source observed on both baselines should be the same. This was tested by computing the ratio of the two fluxes (AN/AS) for runs in 1973 February. The average ratio was less than 5% different from unity

at both frequencies. This indicates that the NRAO and Sugar Grove effi-
ciencies have the correct ratio. Next, the observed fluxes of about six
sources which were expected to be unresolved on the short baseline were
compared to independent published flux measurements. It was found that
the fluxes agreed within 10% at both frequencies, indicating that the
short baseline stations had been calibrated correctly. Finally, the ratios
of the flux observed in 1972 December to that in 1973 February was computed
and the average ratio was found to be less than 5% different from unity.
This shows that both experiments were calibrated the same.

Unfortunately, we have no way of determining the systematic
errors involved with both long baselines because no independent measure-
ments exist. However, the agreement of our measurement of the pulsing
flux for the Crab nebula pulsar (using zero-baseline pulse profiles) with
the single-telescope measurements at Arecibo supports the accuracy of the
Arecibo baselines' calibration.

These arguments establish that all of the flux values presented
here are indeed consistent and on the same flux scale. Unknown systematic
errors may remain and their magnitude is estimated to be <10%. More de-
tails on the analysis of systematic errors are given by Resch (1974).

2. Polarization. Polarization observations with an interferometer
are more difficult than with a single telescope because of the heightened
instrumental effects. Incomplete isolation of the oppositely polarized
feeds results in an unwanted response. A right circularly polarized (RCP)
feed responds to a fraction, f, of the left circularly polarized (LCP)
component of the signal, and also to a fraction, 1 - f, of the RCP com-
ponent.

The quantity f is called the single-telescope instrumental polarization. For total power measurements with a single telescope it makes no difference that f is not zero, unless the source is polarized. However the response of an interferometer is reduced because the LCP and RCP components of the signal are not correlated. This effect can be corrected for if the value of f (or some other suitably calibrated quantity) for each antenna is known.

When the two stations of an interferometer observe with oppositely circularly polarized feeds, the interferometer responds to linearly polarized radiation of any position angle. However, due to the fact that the value of f for each station is not zero, the response to an unpolarized source is not zero. The quantity α is called the "interferometer instrumental polarization" and it is the ratio of the correlation coefficient due to an unpolarized source as observed with similarly- and oppositely-polarized feeds at the two stations. The instrumental polarization is approximately equal to the square root of the sum of the individual instrumental polarizations, f_1 and f_2 (see Appendix D). Since the values of f are fractions, the instrumental polarization of the interferometer can be considerably higher than either of the single-antenna instrumental polarizations. For example, to achieve an interferometer instrumental polarization of 15%, each antenna can have no worse than 1% instrumental polarization.

Values of α were obtained from observations of strong extragalactic sources which were assumed to be unpolarized (3C273, 3C286, 3C287, and 3C298). Tables II-5 and II-6 give the observed values of α and the derived values of f. The instrumental polarization was very high for all of the experiments, and it dominated most of the attempts to measure linear

Table II-5

Interferometer instrumental polarization (α)

Date	196 MHz			111 MHz			74 MHz		
	AN	AS	NS	AN	AS	NS	AN	AS	NS
Winter 1971-2	.14±.02	.20[+]	.32*	.20±.10	.25[+]	.32±.02	-	-	-
1972 December	-	-	-	-	-	-	-	-	.32±.08
1973 February	-	-	-	.34±.08	.31±.10	.17±.04	.42±.04	.34±.04	.18±.04

[+]derived by closure from AN and NS measurements

*assumed to be the same as at 111 MHz

Table II-6

Single-telescope instrumental polarization (f)

Date	196 MHz			111 MHz			74 MHz		
	A	N	S	A	N	S	A	N	S
Winter 1971-2	<.01	.03	.07	<.01	.03	.07	-	-	-
1972 February	-	-	-	-	.03*	.07	-	.03*	.07
1973 February	-	-	-	.09	.03	<.01	.10	.03	<.01

*assumed to be the same as 1973 February

polarization of pulsars. The results of the observations are discussed in the next chapters. One consequence of the large instrumental polarization is that the correction factor for observations with similar feeds at both stations is of the order of five percent, comparable to other calibration effects.

3. Noise fluctuation level and integration times. The complex correlation coefficient (fringe amplitude and phase) can be considered as an observed vector (R) which is composed of a signal vector (S) and a randomly oriented noise vector (N) as shown in figure II-9, where $|S| = \rho$, $|N| = \sigma$, and $|R| = \rho^{\circ}$. The noise vector has a Rayleigh distribution in amplitude and a uniform distribution in phase; the signal vector is a constant. The resultant vector then has a Rice distribution which approaches

Figure II-9. Signal, noise, and resultant vectors.

a Gaussian distribution as the signal-to-noise ratio increases. Because we measure a normalized correlation coefficient with a clipped system, the noise is a constant and does not depend on the signal level. The rms noise level is defined as

$$\sigma = \frac{\pi/2}{\sqrt{BT}} \qquad (II-20)$$

For a full-tape coherent average, T = 180 sec, and with a bandwidth of B = 350 kHz, $\sigma = 1.4 \times 10^{-4}$. For a reliable detection of fringes, we usually require the correlation to be above the 5σ level. However, a small residual fringe rate and time delay can be used to verify signals

as weak as about 3σ. To obtain an unbiased estimate of the fringe ampli-
tude we subtract the noise

$$\rho = \left[\rho^{\circ 2} - \sigma^2\right]^{1/2} \tag{II-21}$$

The rms uncertainty in the phase is

$$\sigma_\phi \cong \sigma/\rho \tag{II-22}$$

for measurements with a noise level of σ. More details and derivations
can be found in Whitney (1974) and Rogers (1970).

For coherent integration times less than a full tape in length, σ
increases as the square root of the time, and the level for detecting
correlation is higher. The need for shorter coherent integration times
is due to non-random phase noise such as oscillator jumps, or refraction
effects. A coherent integration which included these effects would give
a fringe amplitude which is lower than the true amplitude.

The phase perturbations with time scales of about one minute are
easily seen in the plots of fringe phase versus time which are output by
VLBI2. The deviations are probably due to ionospheric "blobs" moving
across the beam of one of the telescopes. In such cases broken coherence
averaging should be done: the data is coherently averaged over segments
for which the phase is fairly linear. This procedure gives a better esti-
mate of fringe amplitude but increases the uncertainty by reducing the
integration time.

If incoherent averaging is employed, it is not necessary to have
detected the signal in one short coherent integration time in order to
estimate the correlation coefficient. Moran (1973) states that the op-
timum estimator for incoherent averaging, in the weak signal case, is

the square root of the average of the squares of the coherently averaged
quantities. The noise level for the resulting estimate decreases only as
the fourth root of the total integration time.

In program VLBI2 the data is coherently averaged over segments of
lengths 0.2, 2, 20, and 180 sec and then each set of averages is inco-
herently averaged. For observations of most sources, the 20-sec averages
were routinely used unless examination of the phase for a particular run
indicated that either a longer or shorter time was more appropriate.

During all of the experiments we were plagued with an additional ran-
dom source of error: excessive tape errors which resulted from a fault
in the tape drive at Sugar Grove. Usually bad runs are easily detectable
because parity errors occurred on nearly every record and the fringe ampli-
tudes were anomalously low. Such runs, when obvious, were culled.

4. Interplanetary scintillation effects. Over all time scales in-
terplanetary scintillations (IPS) cause phase perturbations in the wave-
front arriving at the earth. This effect can be corrected for by using
a model of the solar wind, such as that proposed by Cronyn (1972). He
derived a formula for the amount of phase deviation in the wavefront, $\Delta\phi$,
as a function of observing wavelength, solar elongation, and coherent
integration time. The fringe amplitude will be reduced such that only
a fraction, $\exp(-\Delta\phi^2/2)$, of the true correlated power is detected, as
if the source were partially resolved. The amount of phase shift increases
with longer wavelength, smaller elongation, and longer coherent integration
times. Table II-7 lists, for elongation 90°, values of $\Delta\phi$ at 111 and 74 MHz
for various integration times. At 180° elongation the values of $\Delta\phi$ would be
smaller by a fraction of 0.7; for sources out of the ecliptic plane, $\Delta\phi$ will
also be reduced.

Table II-7

IPS phase deviations for $\epsilon \sim 90°$

Coherent integr. time		111 MHz		74 MHz	
Records	Seconds	$\Delta\phi$(rad)	$\exp(-\Delta\phi^2/2)$	$\Delta\phi$(rad)	$\exp(-\Delta\phi^2/2)$
900	180	1.7	0.25	2.5	0.05
100	20	0.68	0.79	1.0	0.57
10	2	0.20	0.98	0.30	0.95
1	.2	0.03	0.99	0.05	0.99

For sources in the ecliptic plane we should use not longer than 2-sec averages according to Cronyn's model. Alternatively, we could correct the observed correlation coefficients by the calculated factor. Short integration times of 20 sec were routinely used, but no correction factors for the solar wind were applied. Large phase deviations due to interplanetary scintillation of 3C48 were observed when the source was at a solar elongation of 60° in 1973 February. However, the data showed that the decorrelation effect was not nearly as severe as predicted by the model. These observations are discussed by Resch (1974). For the Crab nebula observations, slight decorrelation was observed with longer integration times; this is discussed in the next chapter.

D. Summary of Chapter II

The techniques involved in a VLBI experiment have been discussed from the point of view which is most useful for the results which are presented in the next two chapters. The focus in this chapter has been on acquiring and processing meter-wavelength pulsar data with a VLBI system. Part A described the experiments and observations; part B was concerned with the processing of interferometer data to obtain estimates of correlation

coefficients. Finally part C presented the various calibration procedures adopted for these particular experiments. The data presented in the remaining chapters has been through all of the procedures outlined above so that the best estimates of correlated flux have been obtained.

CHAPTER III

CRAB NEBULA PULSAR: TOTAL FLUX RESULTS

This chapter presents the results of our studies of the so-called "compact source" in the Crab nebula (Hewish and Okoye 1965). The spectrum of the compact source is very steep and its flux dominates the nebular emission at very low frequencies. Fluxes measured at 74, 111, and 196 MHz are reported here. The measurements were made with both long- and short-baseline interferometers so we have partially resolved the compact source and have made estimates of its angular size.

In 1968 Staelin and Reifenstein (1968) discovered a pulsar in the Crab nebula, and since then many arguments have been presented which point to the identification of the pulsar with the compact source. Most of the discussion in this chapter implicitly assumes that the compact source and pulsar are identical, and some additional, and very convincing, results are presented to support this view.

A.   Data presentation

1.   Definitions. There are two ways to consider the signal from the Crab nebula pulsar: either as a periodic waveform which can be analyzed into its Fourier components, or as an average power. These quantities were shown in figure II-5 and defined in equations II-4 and II-5 (pages 22-3). The time-averaged pulsing power is denoted as I_p, the non-pulsing or steady flux as I_S, and their sum as the total time-averaged flux, I_T. At frequencies above about 175 MHz, all of the power from the pulsar is pulsing so that $I_S = 0$ and $I_p = I_T$. Below about 70 MHz, essentially all of the power is non-pulsing, and $I_p = 0$ and $I_S = I_T$. Near 100 MHz the pulsing

45

and non-pulsing components contribute about equally to the total power and $I_P \sim I_S$ and $I_P \sim I_T/2$.

Considering the pulsar as a continuum source, i.e. the compact source in the Crab nebula, we process the data normally and obtain values for I_T. These results have the highest signal-to-noise ratio because all of the available power is being observed. The results of observations of I_T will be discussed in this chapter, and the results of the observations of I_P and I_S are in the next chapter.

Information on the size and spatial structure of a source can be obtained from total flux measurements. Normally, the fringe visibility of a source is calculated by comparing the flux observed with an interferometer to the total flux of the source observed with a single telescope (zero-baseline interferometer). For the Crab nebula pulsar, the nebula provides a strong continuum background against which it is only possible, with a single telescope, to observe the pulsing flux, I_P. We used a short-baseline interferometer to resolve the spatially large nebula so that only flux from the compact source is correlated; in this way we obtain a measurement of I_T which includes both continuous and pulsing components. The fringe visibility, γ, is defined as the ratio of the fluxes observed with the long baseline and short baseline. This assumes that the source is totally unresolved on the short baseline. The long-baseline flux is denoted by a subscript R which means partially resolved flux. We then have $I_{TR} = I_{PR} + I_{SR}$ and $\gamma = I_{TR}/I_T$.

2. Data lists and plots. In table III-1 are collected the one-day average fluxes for each frequency, the values of fringe visibility, and the over-all averages. The fluxes observed with the two long baselines were averaged together for this table. Figure III-1 is a plot of the flux

Table III-1

Total average fluxes of the Crab nebula pulsar

196.5 MHz

Date	I_T(Jy)	No.	I_{TR}(Jy)	No.	γ	Notes
1971 Nov. 23-24	8.1±0.1	2	4.9±0.5	7	0.61±0.10	(a)
1971 Dec. 19-20	7.3±0.7	6	6.2±1.5	14	0.85±0.26	
1972 Jan. 23-24	—	-	7.7±1.2	9	—	(b)
1972 Feb. 27-28	10.0±0.4	4	6.5±1.0	14	0.65±0.12	
1972 Mar. 22-25	—	-	6.9±0.5	3	—	(c)
averages	8.3±1.2	12	6.4±1.4	47	0.79±0.27	
	8.3±0.4 p.e.		6.2±0.2 p.e.		0.74±0.06 p.e.	(e)

111.5 MHz

Date	I_T(Jy)	No.	I_{TR}(Jy)	No.	γ	Notes
1971 Nov. 23-24	50.0±1.7	3	31.2±5.8	9	0.63±0.12	(a)
1971 Dec. 19-20	45.6±0.8	3	29.4±3.0	15	0.64±0.07	
1972 Jan. 23-24	—	-	28.9±3.2	9	—	(b)
1972 Feb. 27-28	49.3±1.5	4	28.8±3.4	14	0.58±0.07	
1972 Mar. 22-25	—	-	23.2±5.1	4	—	(c)
1972 Dec. 8	36.1±2.5	13	—	-	—	(d)
1972 Dec. 9	34.6±3.8	11	—	-	—	(d)
1973 Feb. 25	41.2±3.3	10	2⸵ ⸱.8	20	0.64±0.10	
1973 Feb. 26	40.2±4.3	11	2⸵ ⸱.0	17	0.72±0.11	
1973 Feb. 27	44.2±2.6	11	30.5±2.4	23	0.69±0.07	
averages	40.5±4.6	66	28.9±3.8	111	0.67±0.13	
adjusted avg.	40.5±0.6 p.e.		31.2±1.2 p.e.		0.72±0.03 p.e.	(e)

74.0 MHz

Date	I_T(Jy)	No.	I_{TR}(Jy)	No.	γ	Notes
1972 Dec. 5	105.3±19.4	11	—	-	—	(d)
1972 Dec. 6	110.4±12.1	11	—	-	—	(d)
1972 Dec. 7	101.6±11.1	11	—	-	—	(d)
1973 Feb. 28	96.0±3.6	3	30.7±2.8	17	0.32±0.03	
1973 Mar. 2	105.2±7.9	5	30.7±3.4	12	0.29±0.04	
averages	105.0±⸱ 5	41	30.7±3.0	29	0.29±0.05	
adjusted avg.	105.0± 2.1 p.e.		33.5±1.7 p.e.		0.32±0.02 p.e.	

Notes:
(a) Strong interference at Arecibo.
(b) Sugar Grove not on the air.
(c) Sugar Grove sensitivity low.
(d) Arecibo not on the air.
(e) See discussion on p. 49 .

48

Figure III-1. Total average flux of the Crab nebula pulsar. The error bars are the standard deviations of all the data points. Data points are listed in table III-1. The errors at 196 MHz are the same size as the points.

vs. time using the values in table III-1. The average fluxes at 196 and
111 MHz were computed from the data listed in the tables of Appendices E
and F. The error quoted following each flux value in the table is the rms
deviation of the data points and should be the random error in a single
estimate of the flux. This is the error plotted in the figure. Values
for fringe visibility were computed using the listed average fluxes. The
errors were calculated as the quadratic sum of the percentage error in each
flux used in the calculation. The overall average flux and fringe visibil-
ity at each frequency are weighted averages, and the associated error rep-
resents the rms deviation of all of the points. The error of the "adjusted
average" is the standard deviation of the mean value which takes into
account the total number of data points. The "adjusted" flux is discussed
next.

At all frequencies, full-tape (180-sec) coherent integration times
were used unless significant phase perturbations or a phase discontinuity
was noted and then a shorter time was used. Since the appropriate noise
level was subtracted from the fringe amplitudes (equation II-21), the cor-
related fluxes should be nearly equal for any integration time in which
the signal is detected. However, a calculation at 111 and 74 MHz using
20-sec coherent integration times increased the fringe visibilities
(because the long-baseline correlated flux was higher) by an average of
8±4%; this is within our estimated flux error. At both frequencies the
long-baseline fluxes are usually detected at about 15 times the rms noise
level for a 20-sec integration time. For 2-sec integration times the
fringe visibility is increased by 19±8% at 74 MHz and 13±6% at 111 MHz,
but, the flux is only a the 5σ detection level for this short integration
time. It was decided to use the 180-sec integration times in order to

retain a high confidence level in the correlated flux and the calculated
visibilities. Then, to remove the known systematic error, the average
long-baseline flux, the fringe visibility, and the error were raised by the factor
1.08, to yield the "adjusted averages." Because there are many runs the
probable error is still quite small.

This systematic effect is indicative of a true decorrelation effect as
predicted by Cronyn (1972), although the decorrelation is not as severe as
his model proposes. There is also no difference between the amount of
decorrelation as a function of solar elongation. This is not unexpected,
though, because our observations were made when the Crab nebula was be-
tween 180° and 80° elongation and the source was never very near the sun
where stronger effects are expected.

Figures III-2 and III-3 are plots of the individual-run fluxes for
111 and 74 MHz in 1973 February. They comprise our "visibility curves"
for the compact source. Most of the scatter in the data points is attri-
buted to random errors because the standard deviation is usually equal to
the expected errors. However, we note that the large variations in flux
at 111 MHz on 25 February (in figure III-2) are correlated on the long
and short baselines so that the fringe visibility remains approximately
constant. Therefore, some of the scatter in the average fluxes can be
attributed to variations in the total flux from the pulsar on a time scale
of minutes. On February 26 and 27 and for all of the 74-MHz observations
(figure III-3) the pulsar was not "active" during the hour we observed it,
and the scatter has the expected value.

As illustrated in figure III-2, values for the fringe visibility are
surprisingly constant in spite of the rapid and large variations in total
flux. The unresolved and partially resolved fluxes followed approximately

51

Figure III-2. Total average flux of the Crab nebula pulsar, 111 MHz. Data is for three days in 1973 February. Each point is a three-minute average.

Figure III-3. Total average flux of the Crab nebula pulsar at 74 MHz. Data is for several days in 1972 December and 1973 February. Each point is a three-minute average.

the same trends on all times scales so as to keep the fringe visibility
constant. Figure III-1 shows this on a yearly time scale. Although some
of the flux variation from month to month could be due to unknown system-
atic errors, the fact that the long and short baselines usually vary in
the same way argues for an interpretation of the changes which allows some
intrinsic variability in the pulsar's flux. The variability is discussed
in section B-1 of this chapter when the spectrum of the compact source is
considered.

   3.   Brightness distribution and angular size. The data presented in
table III-1 provide only a small range of points on the visibility curve
because the sparse hour-angle coverage allowed little foreshortening of
the long baselines. Interpretation of the visibility for any of the data
can be done only by assuming a source brightness distribution. In the
1971 March 144-MHz experiment the Crab nebula was observed at many dif-
ferent hour angles so that each baseline was foreshortened, and a crude
visibility curve is available. The data points are plotted in figure III-4.
The fringe visibility scale was set by normalizing each observed correla-
tion coefficient to the correlation observed on the shortest baseline.

   If the apparent angular size of the Crab nebula pulsar is due to in-
terstellar scattering, then according to the theory we expect the size of
the scattering disk to depend on the observing frequency to some power.
For certain types of irregularity spectra, we also expect the source to
have a Gaussian brightness distribution at all frequencies. Unfortunately,
the 144-MHz data points are consistent with many brightness distributions.
Superimposed on the data of figure III-4 are three visibility curves: a
Gaussian (FWHM = 0.055 arcsec), a uniform disk brightness distribution
(diameter 0.06 arcsec) and a point double (separation 0.04 arcsec). The

Figure III-4. Fringe visibilities of the Crab nebula pulsar observed in 1971 March at 144 MHz. Model visibility curves for three brightness distributions are shown.

55

Gaussian curve fits as well as the other two curves, so we can only say that the data are consistent with a Gaussian brightness distribution.

The observed fringe visibilities can be related to angular sizes by considering the Fourier transform relations. Assume the source's Gaussian brightness distribution is given by

$$B(\theta) = \exp\left[-4\ln2(\theta/\theta_s)^2\right] \qquad (III-1)$$

where θ_s = full width at half maximum (FWHM) of the Gaussian curve. The two-dimensional Hankel transform of $B(\theta)$ is the visibility function:

$$\gamma(b_\lambda) = \exp\left[-\pi^2 b_\lambda^2 \theta_s^2/4\ln2\right] \qquad (III-2)$$

where b_λ = baseline length in wavelengths. We observed a value of γ at some b_λ and we can calculate θ_s from equation III-2 or read its value from a graph of equation III-2 shown in figure III-5. The values of θ_s obtained from the fringe visibilities in table III-1 and figure III-4 are listed in table III-2 and plotted in figure III-6, along with several other measurements for comparison. The errors in the determination of θ_s are derived from the measurement error in γ by the formula for error propagation.

Table III-2

Apparent angular diameters of the Crab nebula pulsar

Freq (MHz)	Baseline	Baseline (Mλ)	γ	θ_s (arcsec)
196.5	2550	1.7	0.74±0.06	0.03±0.01
144.3	2700	1.3	0.65±0.15	0.05±0.03
111.5	2550	0.94	0.72±0.03	0.07±0.01
74.0	2550	0.63	0.32±0.02	0.18±0.01

56

Figure III-5. Fringe visibility vs. angular size of source for a Gaussian model. Analytic form for the curve is given in equation III-2.

Figure III-6. Measured values of the apparent size c: the Crab nebula pulsar at several frequencies. Sizes have been converted to Gaussian half-power diameter when necessary. The VLBI point at 26 MHz is by Mutel et al. (1974), the others are from this thesis. The references for the IPS points are: ◩ Cronyn (1970a), ⊟ Armstrong et al. (1973), ◪ Bell & Hewish (1967). The line through the points has a slope of 2.

The fractional error is

$$\Delta\theta_s/\theta_s = (-1/\ell n\gamma) \cdot (\Delta\gamma/\gamma) \qquad\qquad \text{(III-3)}$$

The value c. θ_s is much better determined if γ is very small even if it has a large uncertainty.

A weighted least-squares fit to a power-law wavelength dependence was made for the four values of θ_s in table III-2. An exponent of 2.0 ± 0.4 was ob·-·ned, which is consistent with the wavelength-squared dependence found ₐ₁ ₘₐ₁y scattering theories. The wavelength dependence of inter-stellar scattering is discussed in ₁ₒre detail by Mutel et al. (1974). Th·v have also collected many measurements of the apparent angular size of the compact source in the Crab nebula,and a fit to all of the data yields a power law of exponent 2.05 ± 0.25.

B. Discussion

1. Spectrum. The fluxes measured at our three frequencies give a spectral index of -2.9 ± 0.4, which is the same value and error quoted by Rankin et al. (1970) from observations of the pulsar between 430 and 196 MHz. Our total flux measurement at 196 MHz agrees with the Arecibo flux measurement at that frequency, and our measured total fluxes at the lower frequencies therefore lie on the extrapolation of the spectrum of the pulsing flux. Figure III-7 gives the soectrum of the compact source, including pulsar, IPS, and VLBI measurements.

The usefulness of a spectral index for this source can be questioned however, because of the variability observed in both the pulsing and the total flux. Simultaneous measurements at several frequencies have shown there is no correlation between variations in the pulsing power at 430 and

Figure III-7. Spectrum of Crab nebula compact source and pulsar. References for the spectral points are: ◨ Cronyn (1970a); ⊞ Harris (1973); ◪ Readhead and Hewish (1974); ⊟ Armstrong *et al*. (1973); ⊖ Erickson *et al*. (1972); ○ this thesis; ● Rankin *et al*. (1970).

111 MHz (Rankin et al. 1974), which means that even the shape of the spectrum

is variable. Changes in the pulsing flux of up to a factor of three in a

: w weeks time a.e common at 430 MHz where all of the flux is pulsing, while

at lower frequencies the changes in pulsing flux, though still apparent, are

not so drastic.

The behavior of the pulsing flux contrasts with our observations of

the total flux. We observed up to 25% variations in the total flux at

111 MHz, and no significant variations (<15%) at 74 MHz. This behavior

also differs from that of other pulsars which seem to be highly variable

at meter wavelengths (Huguenin et al. 1973). More monitoring of the total

flux is required to be able to derive statistical properties of the vari-

ations which can be compared to the variations in pulsing flux.

2.   Small structure in the nebula. Several lines of evidence suggest

that there could be small-scale emission structure (other than the pulsar)

in the Crab nebula at low frequencies. The observations of Matveenko (1968)

indicate there are two compact sources in the nebula. Using recent inter-

planetary scintillation observations Armstrong et al. (1973) suggest that

there may be several small sources in the nebula. It is also possible that

the wealth of detail present in the filaments, wisps, and continuum emis-

sion at optical wavelengths might continue to low frequencies. High-

resolution maps at centimeter wavelengths (Wilson 1972) reveal "ridges"

which are coincident with the filaments and have spectral indices approx-

imately equal to that of the continuum radiation. This information hints

that these structures might also be detectable at meter wavelengths.

Although our coverage of the (u,v) plane is meager, we can draw some

conclusions about small-scale emission structure in the nebula. A lack

of fine structure is indicated by our flat visibility curves at 111 and

74 MHz (figures III-2 and III-3). The fringe visibility as a function of hour angle at 111 MHz does not vary except for noise fluctuations. Also, there is no systematic trend in the time-delay and fringe-rate residuals which might indicate the presence of other sources. At 74 MHz the data spans two and one-half hours and again no changes in fringe visibility or residual parameters are evident.

If there were fine structure besides the pulsar in the nebula at our frequencies, that is, if there were many small sources, the visibility curve should show large fluctuations with small changes in hour angle. Except for a fortuitous arrangement of sources we conclude that there is no st ucture in the nebula on an angular scale of the order of the fringe spacing (0.3 arcsec at 74 MHz) or smaller. Similarly the smoothness of the short-baseline interferometer visibility curves also indicates a lack of structure with angular sizes smaller than 15 arcsec. More extended observations at these frequencies should be made in order to consider this problem in more detail.

Another argument which supports the absence of structure in the nebula relies on data presented in the next chapter. Anticipating the results, we observe that all of the flux at 196 MHz is contained in the pulsing component, and that at 111 MHz the phase of the pulsar's radiation agrees with that of the compact source. This is evidence that the pulsar is truly the only small object in the nebula, because if we were observing the coherent sum of radiation from the pulsar plus fine structure or other compact objects, then part of the total flux would not be pulsing at 196 MHz, and the continuous radiation would have a different phase from that of the pulsar. This is not the case, and we conclude there are no compact objects or structure in the nebula other than the pulsar.

3. Discrepancy with IPS flux. Interplanetary scintillation (IPS) observations of the compact source in the Crab nebula at 74 MHz have been reported by Armstrong et al. (1973). They derive an angular diameter of 0.18±0.01 arcsec at 1/e which corresponds to a half-power diameter of 0.15 and is consistent with our observations. The amount of scintillating flux which they quote is a factor of two higher than the total flux observed with VLBI techniques, although their value for the flux agrees with other IPS observations of the compact source by Harris (1973) and Readhead and Hewish (1974). The spectrum of figure III-7 contains several points which illustrate the discrepancy between the IPS and VLBI fluxes.

Armstrong et al. suggest there could be another source or sources in the nebula which could account for the extra flux they observe. The scintillating flux could come from any location within the telescope beam, and they would observe an incoherent average of the various source fluxes. Even though our hour angle coverage is incomplete we have shown above that there is no "structure" or other sources in the nebula except for a possible coincidental arrangement.

If there is only the pulsar which is small at 74 MHz they suggest we might be missing some of the flux due to decorrelation or other effects, but we believe we have accounted for all the flux. Decorrelation due to interplanetary phase fluctuations over the short 50-km baseline could not have occurred, especially since we were observing when the Crab nebula was near the anti-solar direction. Ionospheric phase fluctuations were accounted for by broken coherence averaging when necessary.

Accurate position measurements at low frequencies are impossible because of the unknown phase shifts imposed by the ionosphere, but we never found a correlation peak at any position in the nebula other than

near the pulsar. The small residual time delays and fringe rates serve
to confine the location of the compact source to the inner one-tenth of
the nebula.

The discrepancy between the IPS and VLBI techniques may have been
resolved recently. Coles et al. (1974) obtain a good fit to the curve of
scintillation index vs. solar elongation by using new theoretical calcula-
tions and normalizing their data with the VLBI-meas\ired flux. They con-
clude that they now agree with our results. Further comparisons between
VLBI and IPS results have been made by Resch (1974) using the data from
these experiments and the IPS survey by Readhead and Hewish (1974).

4. Polarization. The instrumental polarization was very high, as
shown in tables II-5 and II-6, and it was not well determined. Thus the
measured linear polarization of the pulsar's radiation has large uncertain-
ties. Table III-3 lists the fraction of linearly polarized radiation for
the total flux (m_T, from the short-baseline observations) and the partially
resolved fluxes (m_{TR}, from the long baselines). The limits on the linear
polarization at 111 and 74 MHz are due to the large error associated with
the determination of the instrumental polarization. At 196 MHz, about 50%
linear polarization was observed, which is consistent with the observations
by Manchester et al. (1972). They observed a mean linear polarization of
45% at 147 MHz and 55% at 281 MHz. Polarization of the pulsing power alone
will be considered in the next chapter.

Table III-3

Polarization of total average flux

Frequency	m_T	m_{TR}
196 MHz	$0.40^{+0.10}_{-0.30}$	$0.50^{+0.10}_{-0.20}$
111 MHz	<0.15	<0.25
74 MHz	<0.15	<0.25

C. Summary of Chapter III

Values for the total flux of the compact source in the Crab nebula at 74, 111, and 196 MHz were presented in this chapter. The source was observed with both short- and long-baseline interferometers so that measurements of the fri e visibility allowed angular diameters to be estimated at each frequency. The angular sizes scale as frequency-squared which is consistent with interstellar scattering theories.

An absence of small structure other than the pulsar in the Crab nebula is indicated by the lack öf structure in our observed visibility functions. The results of these measurements combined with those of the next chapter will be compared to predictions of interstellar scattering theories in Chapter V.

CHAPTER IV

CRAB NEBULA PULSAR: PULSING FLUX RESULTS

The results of our determinations of the Crab nebula pulsar's pulse
shapes are discussed in this chapter. The profiles were reconstructed
from the Fourier components according to the method outlined in Chapter II,
and further analysis is described in the first part of this chapter. Sample
profiles are presented in the second and third parts of the chapter, and
the implications of differences and similarities between the correlated
and single-telescope pulse profiles are discussed.

The single-telescope pulse shapes at several frequencies are shown
in figure IV-1. which is taken from the paper by Rankin et al. (1970).
The general pulse morphology
changes with frequency because
the components of the pulse
which are distinct at high
frequencies become blended
due tc scattering. There are
: components of the pulse,
all of which contain com-
parable amounts of energy.

The precursor occurs just

Figure IV-1. Single-telescope
pulse shapes.

before the main pulse, and an interpulse is located approximately half
way through the pulse. Between the main pulse and interpulse is a base-
line component.

A.   General discussion of Fourier components

1.   Review of method. Besides the total time-averaged flux from the
compact source in the Crab nebula, we also considered separately the two
components of the radiation: the pulsing (I_p) and non-pulsing or steady
(I_s) fluxes. As described in Chapter II the data tapes are processed with
appropriate time-delay and fringe-rate offsets so as to make the interferom-
eter respond to the nth Fourier harmonic of the pulse shape. The tapes are
processed 2N+1 times to yield values of fringe amplitude and phase for n=0,
±1, ±2, ... N, where N is the highest order harmonic which can be detected.
The pulse shape is recovered by adding the complex components, including
n=0, in a Fourier sum, as discussed in detail in Chapter II (pages 22-27).

2.   Number of components. For a simple single pulse shape (ignoring
the Crab nebula pulsar's interpulse for now) the amplitude of each Fourier
component decreases monotonically with increasing harmonic number, but the
rate of decrease depends on the pulse width. A sharp pulse (such as the
196-MHz pulse) has a broad Fourier transform and high-order components
have appreciable amplitude, whereas a broad pulse (such as at 111 MHz)
has a narrow Fourier transform so that the amplitudes of the components
fall rapidly with higher harmonic number. With comparable sensitivity at
the two frequencies, we therefore expect to be able to detec_ more com-
ponents at 196 MHz than at 111 MHz. In practice, we usually detected five
Fourier components in one run (one three-minute average) at 196 MHz. Since
the pulses do not have simple shapes, at 196 MHz the amplitude of the n=2
component is higher than that cf n=1 because of the strong influence of
the interpulse. At 111 MHz three Fourier components were usually detect-
able in one run, although the actual number varied with changes in the
pulse shape and level of pulsing power.

As discussed in Chapter I, we had expected to observe a narrower
pulse with the long-baseline interferometer than with the short baseline
because of the scattering geometry. This means we should have detected
more Fourier components in the higher resolution data. For example, we
might have observed a pulse similar in shape to the 196-MHz pulse when
we observed with the long-baseline interferometer at 111 MHz. This turned
out not to be the case, as the pulse shapes on all baselines are similar.
This fact and its implications are discussed in later sections.

Because the pulse waveform is a real quantity, we expect the +n and
-n components to have equal amplitudes and opposite phases. Due to the
presence of noise, this is not always the case. Corresponding components
hardly ever have equal amplitudes, and the phase noise is typically about
one-half radian. Occasionally, for high values of n, one or the other of
a component pair will not be detected. On some tapes, perhaps, components
up to n=8 at 196 MHz could be detected, but to prevent waste of computer
time we processed the tapes for only five components. Similarly, experi-
ence showed that n=3 was the highest component number to be used at 111 MHz
because higher order components were rarely detectable.

Tests were made in which the component amplitudes and phases were
perturbed by various amounts in order to investigate the effect on the
profile. It was found empirically that the phase could be perturbed by
up to one-half radian and the amplitudes could be adjusted by about 50%
without distorting the original profiles beyond recognition. Correct
amplitudes but corresponding random phases do not result in a "believable"
profile. The waveforms at 111 MHz observed at Arecibo under the Crab
nebula pulsar surveillance program are analyzed into six Fourier harmon-
ics (Counselman and Rankin J 72), twice as many as we could detect. This

is presumably due to the fact that the components with n > 3 are only marginally detectable. Since these components are very weak, their presence or absence does not affect the pulse profile significantly.

   3.   Lack of components at 74 MHz. At 74 MHz we never detected any Fourier components with the long-or short-baseline interferometers, although the single-telescope waveforms observed at Arecibo can usually be analyzed into at least one Fourier component. This discrepancy is not readily understandable; it could possibly be due to several effects which are considered next.

One difference between the two observing methods is the relative sensitivities of the Mark I system and the Arecibo receivers. Table IV-1 gives the parameters for the two systems; the Arecibo parameters were

Table IV-1

System parameters for Crab nebula pulsar observations

System	Freq. (MHz)	Bandwidth (kHz)	Integr. time (min.)
VLBI Mark I	all	350	3
Arecibo	196	4-10	18
Arecibo	111	2-10	18
Arecibo	74	1-5	18

taken from the paper by Rankin et al. (1970). These and other system parameters from tables II-2 and II-4 were used to calculate the sensitivity, when observing the Crab nebula, for Arecibo (A) and for each interferometer (double letters). Table IV-2 presents these numbers. The zero-length baseline (AA) is formed by "auto-correlating" and dedispersing the Arecibo Mark I data tape. This procedure was discussed in Chapter II, section B-3 (page 27).

Table IV-2

System sensitivities in Jy

for observations of the Crab nebula

Frequency (MHz)	A	AA	AN	AS	NS
196	2.8	1.7	1.7	2.3	2.3
111	4.1	2.0	2.2	3.0	3.4
74	5.1	2.4	3.6	4.5	7.0

Our short-baseline sensitivity is nearly the same as that of Arecibo but no Fourier components were detected on a few test runs. This lack of detection is not due to the flux being below the detection limit since on these runs the Arecibo system recorded between 15 and 25 Jy of pulsing flux (Rankin et al. 1974). With the long baselines, the interferometer partially resolved the total flux and the amplitudes of the Fourier components are reduced by this factor also because the effect of a sharper pulse with high resolution does not occur. This puts even the n=1 component well below the detection limit on the long baseline.

Table IV-2 shows that the zero-baseline interferometer formed using the Arecibo data is the most sensitive; this is due to the relative e Mark I bandwidth. We did detect the first Fourier component at an amplitude of about 3±1 Jy on one data tape from 1973 February 28. On that day the Arecibo system detected 15±6 Jy of pulsing flux (Rankin et al. 1974). Even considering the large errors, our marginal detection is not entirely consistent with the Arecibo observations.

One possible problem involves curvature of the pulses our passband since, as shown in Chapter II, we approximate the dispersion of the pulses as a straight line. The effect of the curved pulse was estimated

by calculating the difference between the pulse time-of-arrival at the top and bottom of the passband using both the straight-line approximation and the true dispersion relation. At 74 MHz the difference between these two times is about 3 msec. This corresponds to about one-half radian of phase difference when we integrate across the passband, resulting in a signal degradation by a factor about 0.7. This would decrease the zero-baseline interferometer's sensitivity but only to about that of the Arecibo system.

Several runs were processed in searches for Fourier components, but no general production runs were made because of the low signal level. In order to draw better conclusions about possible difficulties with the de-dispersing method at very low frequencies more runs should be processed to confirm the lack of detection; this processing is in progress.

4. Epoch determination. The phase of each Fourier component is referenced to the time at which the offset oscillator used in the processing was started. This time was the same for all values of n. This means that the peak of the reconstructed pulses occurs at a phase which can be referred to UT. We have compared pulse arrival times obtained this way to those measured at Arecibo and the epochs agree to within a few percent of the pulse period. Pulse shapes an be coherently averaged using the epoch information if accurate times-of-arrival can be predicted.

B. Results at 196 MHz

1. Sample profiles and Fourier components. The five Fourier component amplitudes and phases for each three-minute run at 196 MHz were added in Fourier sums, interpolated, and the resulting smooth profile was

plotted. Figure IV-2(a) shows typical pulses from the short and long baselines and Arecibo. The component amplitudes and phases for the profiles are in the next two diagrams: Figure IV-2(b) is a plot of the Fourier component amplitudes, normalized to the n=0 component amplitude, against harmonic number; figure IV-2(c) is a polar plot of the phases, relative to the phase of n=0, for the short-baseline profile. The phases of each component pair (+n and -n) are symmetrical about the phase of n=0 with an rms deviation of 9°4 for this run. Appendix E contains a catalogue of 196-MHz average pulse shapes and a listing of the Fourier components and other relevant quantities.

2. Discussion. Both of the interferometer profiles and the Arecibo profile are similar and the amount of resolution is slight. All of the flux is pulsing ($I_T = I_p$), and the baseline level set by the interferometer is the same as that of the single-telescope observation. The reason for not using 196 MHz for the second set of experiments was that the interferometer provided no unique information compared to a single telescope.

Since all of the power is contained in the pulsing component, the linear polarization of the total flux is the same as that of the pulsing flux. The fraction of linear polarization, m, is ~50%, as in Table III-3. We have not attempted to determine m separately for the main pulse and interpulse because of the high instrumental polarization.

C. Results at 111 MHz

1. Sample profiles and variation of I_p/I_T. At 111 MHz the pulsing (I_p) and steady (I_s) components of the pulse shape contribute about equally to the total flux from the compact source ($I_s \sim I_p \sim I_T/2$). Thus the ratio I_p/I_T is approximately equal to one-half, although it was found to vary with

Figure IV-2. (a) Typical pulse profiles, 196 MHz. (b) Amplitudes, relative to n=0, of Fourier components of the pulses in (a). (c) Phases, relative to n=0, of Fourier components of the short-baseline pulse in (a). Vector length indicates component strength.

time. In the data from the first five experiments, Fourier compon ats up to n=3 were usually detected. The resulting pulse shapes are oi _dt than the 196-MHz pulse shapes and they also have an offset bascline bias and continuous non-pulsing power. Pulses from a typical run in 1971 November are shown in figure IV-3(a). The comparison Arecibo pulse has been raised above the baseline to coincide with the short-baseline interferometer pulse. Figure IV-3(b) is a plot of Fourier component amplitude vs. harmonic number; figure IV-3(c) is a polar plot of the phases. The average (signed) deviation of the phases from symmetry around n=0 is 9°.8 and the rms deviation is 24°.6.

The value of I_S is taken as the minimum of the pulse profile. The total flux I_T is the amplitude of the n=0 component (A_0), and I_P is calculated as $I_P = I_T - I_S$. This underestimates I_S because some "ringing" of the Fourier harmonics is expected and the minimum of the profile may be below the true basc level. This is evident on the 196-MHz profiles where the amplitude is sometimes negative. For the first set of five experiments (1971-2) the average value of I_P/I_T was 0.6 for both long- and short-baseline pulse profiles. The ratio of I_P/I_T is 0.72 for the short-baseline profile of figure IV-3.

For the last two experiments most of the data revealed only two Fourier components, and $I_P/I_T \sim 0.4$ for all the profiles. Figure IV-4(a) is a reconstructed pulse observed in February 1973. The pulse shape is clearly broader than that in figure IV-3. Figures IV-4(b) and IV-4(c) give the component amplitudes and phases relative to n=0. Appendix F is a catalogue of 111-MHz average pulse shapes from all experiments, and a list of the components and values of I_P/I_T.

Figure IV-3. (a) Typical pulse profiles, 111 MHz, 1971 November.
(b) Amplitudes, relative to n=0, of Fourier components of the pulses
in (a). (c) Phases, relative to n=0, of Fourier components of the
short-baseline pulse in (a). Vector length indicates component strength.

Figure IV-4. (a) Typical pulse profiles, 111 MHz, 1973 February.
(b) Amplitudes, relative to n=0, of Fourier components of the pulses
in (a). (c) Phases, relative to n=0, of Fourier components of the
short-baseline pulse in (a). Vector length indicates component
strength.

Figure IV-5 is a plot of the average value of I_p for each observing day, and also the average value of I_p/I_T. Table IV-3 lists the values in the plot and the fringe visibility of the pulsing flux, γ_p. The expected uncertainty in I_p is quite large, about ±15%, because I_p is derived from a sum of 2N+1 amplitudes and phases which each have an error. The scatter about the mean value of I_p is about ±20%, only slightly higher than the predicted value.

The total amount of pulsing power was determined in a variety of ways: with the short-baseline cross-correlation interferometer, by auto-correlating the Arecibo tape to form a zero-baseline interferometer, and from the single-telescope observations made at Arecibo. The results of each method are plotted in figure IV-5. All these methods give approximately the same value of I_p, although the short-baseline correlated flux is systematically lowest by about 20%. This is somewhat disturbing since it occurs only for the cross-correlation observations. However the large error bars allow the several flux values to be consistent. The Mark I auto-correlation data agrees well with the Arecibo fluxes which were observed simultaneously with the VLBI experiment.

2. Polarization. The polarization of the total flux at 111 MHz was presented in table III-3. With the pulse profiles in hand we can separate the pulsing and non-pulsing flux and determine the polarization of each component separately. Table IV-4 lists m_p (the fraction of linear polarization in the pulsing power) and m_T (fraction in the total power, from table III-3). The values for m_p are consistent with the results of Manchester et al. (1972) who observed m_p = 35% at 114 MHz. There is a formal difference between the value of the polarization of the pulsing and total fluxes, but within experimental uncertainty the two polarizations are the same.

Figure IV-5. Average values of pulsing flux (I_P) and the ratio of pulsing to total flux (I_P/I_T).

Table IV-3

Pulsing flux of the Crab nebula pulsar at 111 MHz

Date	I_P/I_T	I_P	No.	I_{PR}/I_{TR}	I_{PR}	No.	γ_P
1971 Nov. 23–24	0.59±0.18	28.6±6.3	3	0.66±0.09	22.5±4.0	7	0.79±0.1
1971 Dec. 19–20	0.53±0.04	23.7±1.6	3	0.63±0.16	18.9±5.6	14	0.80±0.07
1972 Jan. 23–24	--	--	-	0.61±0.04	17.7±4.7	9	--
1972 Feb. 27–28	0.61±0.09	29.7±3.1	4	0.59±0.13	17.0±4.7	12	0.57±0.05
1972 Mar. 22–25	--	--	-	0.54±0.06	12.8±3.9	4	--
1972 Dec. 8	0.34±0.11	11.9±3.6	11	--	--	-	--
1972 Dec. 9	0.40±0.10	13.7±4.0	8	--	--	-	--
1973 Feb. 25	0.39±0.12	16.0±4.4	5	0.48±0.14	13.1±5.0	15	0.82±0.13
1973 Feb. 26	0.42±0.11	17.1±5.2	11	0.48±0.13	13.9±4.1	16	0.81±0.10
1973 Feb. 27	0.46±0.07	20.4±3.3	11	0.51±0.09	15.3±3.0	22	0.75±0.05

Table IV-4

Polarization of total

and pulsing flux at 111 MHz

Fraction	Total flux	Resolved flux
m_P	$0.27^{+0.10}_{-0.20}$	$0.22^{+0.15}_{-0.20}$
m_T	<0.15	<0.25

3. Dependence of visibility on pulse phase. The predicted dependence of fringe visibility on pulse phase, illustrated in figure I-3, was not observed. The pulse shapes observed on both long and short baselines appear to be similar, in that the pulse derived from the partially resolved flux is uniformly reduced in amplitude but not changed in shape. Values of I_P/I_T were calculated separately for the pulses observed with long and short baselines and, to within the rather large error limits, are equal. Also, figures IV-2b, 3b, and 4b indicate there is no systematic trend toward having γ increase (approach unity) for higher Fourier components.

A quantitative test was made by computing the mean values for the flux of each Fourier component using all the available data. (The individual components are tabulated in Appendices E and F.) Then the fringe visibility was calculated for each component at both 111 and 196 MHz, and the results are plotted in figure IV-6. The error bars represent the standard deviation of γ as calculated from the standard deviations of the mean fluxes. The figures show that each component has approximately the same visibility as the $n=0$ component, and within the errors there is no trend toward unity. All of the phenomena mentioned in this section are of course inter-related, and they all give useful ways of indicating

Figure IV-6. Figure visibility vs. harmonic
number for (a) 111 MHz and (b) 196 MHz.

the lack of strong evidence for a source which expands with pulse

phase.

4. Identification of pulsar with compact source. The arguments

which support the identification of the low-frequency compact source with

the pulsar in the Crab nebula were summarized by Erickson et al. (1972)

and also by Lang (1971b). High-resolution VLBI observations of the Crab

nebula can be used to distinguish between the compact source and the pul-

sar if the phases of the radiation are known. The correlated flux obtained

through processing the data as for a continuum source is due to the compact

source, and the phase of these fringes provides the position of the com-

pact source. The fringe amplitudes and phases obtained for n ≠ 0 obviously

are due to the pulsar, and the average phase of the +n and -n components

will give the position of the pulsar. Only if the compact source is in

the same position as the pulsar will the fringe phases be the same. The

phases of the Fourier components which were detected at 121 MHz were used
by Erickson et al. (1972) to identify the pulsar with the compact source.
The data presented in this thesis extend their results and tighten the
limits on the identification.

The method they used, and which is used here, is the measurement of
differential phase, which is a powerful tool for determining accurate
relative source positions. If the sources on which the differential mea-
surement is to be made are in the beam of the telescopes at the same time
then all instrumental phase deviations, including differences between lines
of sight through the atmosphere and ionsophere, are greatly reduced. The
difference in fringe phase between the sources is then a direct measure of
their position difference. The test is very sensitive because we can mea-
sure a difference in phase to a fraction of a fringe.

The problem is formulated as a null test: the signed deviations of
the average phase of ea⁻: pair (+n and −n) of components from the phase
of the corresponding n=0 component are summed and averaged to yield $\langle\delta\phi\rangle$.
If $\langle\delta\phi\rangle$ = 0, then the pulsar would occupy the same position in the sky as
the compact source. The values of $\langle\delta\phi\rangle$ are listed in the tables of Ap-
pendices E and F, for individual runs, and were averaged fo⸱ the values
listed in table IV-5. The averages were formed for both frequencies. The

Table IV-5

Average phase differences between pulsar and compact source

Frequency	$\langle\delta\phi\rangle$ (degrees)	(milli-arcsec)	No. runs	Total no. of components
196 MHz	2.5±4.0	0.8±1.3	41	205
111 MHz	−1.4±3.6	0.8±2.0	98	241

values were computed using all the long-baseline data, the quoted error is the standard deviation of the mean. At 111 Hz the average phase difference implies that the pulsar and compact source are coincident to about 0.8 milli-arcsec in a position angle along the baseline. This corresponds to a linear distance limit of ~2 a.u., assuming 2 kpc for the distance to the Crab nebula (Trimble 1973).

As a test of the method, the same procedure was followed using the 196-MHz Fourier components. At this frequency we know that all of the power is pulsing because the baseline level of the pulse profiles is at zero, so $\langle \delta \phi \rangle$ must be zero. The error gives an idea of the noise level. As the numbers in table IV-5 show, the result and error are approximately the same as at 111 MHz. These results were used in Chapter III, part B-2 as evidence against small structure in the Crab nebula other than the pulsar.

D. Summary of Chapter IV

The body of data presented in this chapter consists of the Fourier components of the Crab nebula pulsar's radiation at 196 and 111 MHz. Analysis of the amplitudes, phases, and pulse shapes has shown that the shape changes with time and that the baseline offset contains a variable fraction of the total flux. We have seen that the fringe visibility of all components of the radiation is not a function of pulse phase. Finally the pulsar has been undoubtedly identified with the compact source, and is coincident with it to within 2 a.u. at the distance of the nebula. The next chapter will use these results and those of the previous chapter to examine various models and theories.

CHAPTER V

MODELS FOR THE CRAB NEBULA AND INTERSTELLAR MEDIUM

A.   Review of observed phenomena

Many of the spatial, temporal, and spectral features which we observe

in the radiation from the Crab nebula pulsar are due to the influence of

the media through which the radiation passed. Models for the radiating

mechanism, and of the nebular, interstellar, and interplanetary media

should account for all the observed phenomena, a brief review of which

follows.

1.   Spatial features. As described in the previous two chapters,

the spatial features are uniquely observed via VLBI and ⊤⌐⌐ This thesis

presents consistent observations of apparent angular si. . ⌐s a function

of frequency. The brightness distribution has been observed at one fre-

quency (144 MHz) and is consistent with a Gaussian. The fringe visibil-

ities which we measured have been interpreted in terms of Gaussian bright-

ness distributions and yield the angular sizes listed in table III-2

(page 55). The fringe visibilities measured for the total flux apply

to all the components of the radiation: there is no systematic dependence

of fringe visibility on pulse phase, and the pulsing flux has the same

visibility as the total flux. The technique of interplanetary scintil-

lations can also be used to study angular structure of radio sources.

Early IPS observations at 81 MHz (Bell and Hewish 1967) were used to

estimate a size which is consistent with our observations and recent

IPS observations at 74 MHz (Armstrong et al. 1973) derive the same size

as was measured with our VLBI experiments.

2. Temporal features. Many aspects of the temporal features of the radiation are being monitored with the twice-weekly observing program at Arecibo. During time intervals from weeks to months every observable parameter appears ' vary in a non-systematic way. The pulse shape, dispersion measure, amount of pulsing power, pulse period, and the period time-derivative all vary (Rankin and Counselman 1973). In the seven VLBI experiments, we observed in addition that the total flux and the ratio of pulsing to total flux are also variable. No temporal changes were observed in the angular structure of the radiation.

3. Spectral features. Narrow-band spectral features have not been observed for the Crab nebula pulsar, probably because the scintillation bandwidth of the features, predicted from the pulse broadening ($\sim$15 msec), is only about 10 Hz at 111 MHz. If a filter this narrow could be made it would be difficult to achieve an adequate signal-to-noise ratio. For other pulsars, Rickett (1970) observed a relation between the dispersion measure and the maximum bandwidth over which scintillations are correlated. This implies an association between the "dispersing" electrons and the "scattering" electrons. They may be the same electrons, meaning that electron density irregularities occur wherever there are electrons. This is the basis for the belief that the scattering is truly an interstellar phenomenon and that it occurs all along the path.

Several models have been proposed which attempt to explain these observed spatial, temporal, and spectral features, but so far none has succeeded in predicting all of the observations. There are one or more aspects of each theory which, considering especially the new data presented in this thesis, do not agree with the observations. In sections B through E which follow, we discuss four models and point out their virtues and

deficiencies. In section F, we have combined the best features of each model into yet another model which does in fact explain the observations. More refined observations in the future will require alterations to these theories.

B.   Thin screen model

The first attempt to explain what happens in the interstellar medium to affect pulsars' radiation was the "thin screen model." This model was briefly discussed in the introduction and now will be considered in more detail. The discussion draws upon the work of Lang (1971a), Cronyn (1970a and b), and Lovelace (1970).

1.   Assumptions.   (a) The artifice of the thin screen can be used if it is assumed that the density irregularities in the medium are iso- tropic and homogeneous; in view of Rickett's work this may be a fair assumption. The irregularities are collapsed onto a plane approximately midway between observer and source; the screen in thin enough that it produces only phase deviations in the wavefront while the amplitude remains unchanged.   (b) Another assumption is that geometrical optics is a valid approximation so that ray tracing can be used.   (c) Finally the time de- lays caused by variations in the group velocity through the density ir- regularities are ignored because they are much smaller than the delays due to geometrical effects. This last assumption is valid only for Gaussian and shallow power-law spectra of irregularity sizes, however. Cronyn (1973) specifically discards this assumption and proposes that the group delays are as large as geometrical delays if a steep power-law spectrum of sizes is used. This important model will be discussed later. Jokipii (1973) notes that the thin screen is really only a convenient contrivance and not the limit of a more rigorous theory.

2. __Theory__. The theoretical predictions which can be compared to our observations are derived next. First the relation between scattering time delay and apparent angular diameter for the thin screen model is stated. Then the impulse response of the model, convolved with a model pulse shape, is used to predict the observable ratio I_p/I_T. Figure V-1 is a drawing of the thin screen configuration. The difference in the light-travel time between rays which arrive from the edges of the scattering cone and those which arrive from the center is

Figure V-1. Thin screen configuration.

$\tau_o = (\delta_1 + \delta_2)/c$. The relation between τ_o and θ_o can be derived from the geometry assuming that θ_o is a small angle:

$$\tau_o = qZ\theta_o^2/2c \qquad (V-1)$$

where $q = L/(Z - L)$, $\qquad\qquad$ (V-2)

$\quad$ Z = total path length from source to observer,

$\quad$ L = distance of observer from the screen.

The quantity q is a proportionality factor which indicates the location of the screen. It is the ratio of the distances of observer and source from the screen, and if the screen is halfway between observer and source $q = 1$. Note that as the screen is moved closer to the source q becomes very large, thus allowing a large time delay to be associated with a very small angular size simply due to the geometrical configuration.

The rms scattering angle is θ_o, defined through the two-dimensional brightness distribution:

$$B(\theta) = \exp - (\theta^2/2\theta_o^2) \quad . \qquad\qquad \text{(V-3)}$$

θ_o is related to measured θ_s by

$$\theta_s = 2(2\ell n2)^{1/2} \theta_o \cong 2.3 \theta_o \quad . \qquad\qquad \text{(V-4)} \quad \cdot$$

The time delay τ_o is the e-folding time of the exponential decay of the impulse response of the thin screen. The impulse response is also called the "probability density function" (pdf) for the scattering time delay τ. For a single thin screen, the pdf has the form e^{-x} which is plotted in figure V-2.

The convolution of the impulse response with the emitted pulse shape yields the predicted pulse shape. For the calculations which were made here, the emitted pulse was

Figure V-2. Impulse response of thin screen.

represented as two delta functions: one for the combined main pulse, precursor, and baseline component; and one for the interpulse. The second delta function followed the first by 13 msec and had one-third of the total energy. The period was taken as 33 msec. This model is taken from Cronyn (1970a). A different model in which the delta functions had equal energies and were separated by 10 msec (combining the main pulse with the precursor and the interpulse with the baseline component) gave the same results to within a few percent for the calculation of the fraction of pulsing flux. A more complicated model which would

include all four components separately was not tried, but for the purpose
of calculating I_p/I_T such a model would probably not change the results
significantly. Figure V-3 is the predicted pulse shape assuming $\tau_o \sim 15$
msec at 11: MHz.

The convolution of the pdf
with a train of pulses yields
the "steady state" observed
power as a function of time,
including any flux which is
delayed enough to appear as

Figure V-3. Predicted pulse shape
for thin screen.

unpulsed radiation. Evaluating this function at the pulse period (the
minimum of the curve) gives the amount of flux which is in the steady
source, thus accounting for the contributions from the exponential tails
of all previous pulses. For the thin screen model, figure V-4 is a plot
of the fraction of the total
flux which is still contained
in the pulsing component, as
a function of the character-
istic time delay. At a time
delay approximately equal to
the pulse period only about
one-third of the flux is still
pulsing.

Figure V-4. Predicted I_p/I_T for
thin screen model.

3. Comparison to observations. The pulse shape of figure V-3 is
obviously not in good agreement with the observed pulse shape because of
the discontinuities. The exponential decay in the latter part of the
pulse is observed however.

We observed $I_p/I_T \sim 0.6$ in 1971-2; from the graph of figure V-4 this corresponds to a time delay of 15±3 msec. If we let q = 1 in equation V-1 and take the distance to the Crab nebula (Z) as 2 kpc (Trimble 1973) we calculate θ_s = 0.18±0.02 arcsec. This is more than a factor of two larger than the size which we observed, 0.07±0.01 arcsec. Alternatively, the observed angular size implies a time delay of only 2.3 msec.

The calculated θ_s could be changed by making q $\sim$ 6 and thus placing the screen at a distance L $\sim$ 1.7 kpc from the earth. There have been suggestions that scattering may occur primarily in spiral arms which would constitute single screens. There is no strong spiral feature at 1.7 kpc in the anticenter direction, although the structure in this part of the Galaxy is not well known.

Before our measurement of θ_s at 111 MHz, the size most often quoted was that derived from 81-MHz IPS observations by Bell and Hewish (1967) of θ_s = 0.2±0.1 arcsec which scales as wavelength-squared to 0.11±0.05 arcsec at 111 MHz. If we assume this is a diameter at 1/e and convert to a half-power diameter, we obtain 0.09±0.05 which is consistent with our observations but, again, not with the observed pulse broadening. More recently Readhead and Hewish (1974) published an angular diameter of 0.25±0.1 arcsec, which is close to the previous value. The size derived from other IPS observations by Armstrong et al. (1973) at 74 MHz also agrees with our observations.

Another problem with the thin screen treatment is that, to within our errors, we observed no change of visibility across the pulse. There is no way to avoid this phenomenon with the thin screen model since it is due to geometrical effects and derives from the assumptions mentioned

above. More accurate observations of correlated pulse shapes should be made before this effect can be ruled out completely, however.

Besides the discrepancy between the temporal and angular broadening, a major problem with the thin screen theory is the concept: it is too simple. We know that between the earth and the Crab nebula there are many parsecs of interstellar matter, and it seems unlikely that the effects along the entire path can be represented by a single thin screen. In fact the basic assumption of the thin screen approximation, that the medium is isotropic and homogeneous, is undoubtedly false. However, this approach was useful for the Crab nebula pulsar as a first step toward explaining the observations.

For other pulsars the thin screen approximation also appeared to work well. Lang (1971c) showed that fits to the pulse shape predicted with the thin screen theory are generally quite good. Using more sensitive data on these same pulsars, though, Counselman (1974) showed that the residuals from a fit to the predicted pulse shapes for two pulsars are small but significant. Now that more accurate and extensive observations of pulse shapes and angular sizes are available a more sophisticated theory than the single-screen model is warranted.

C. Two-screen model

1. The model. The next step toward improving agreement between observations and theory was made by Counselman and Rankin (1972) who proposed that two scattering screens affect the radiation of the Crab nebula pulsar: the Crab nebula itself and the interstellar medium. In a later paper, Rankin and Counselman(1973; hereafter called R&C) suggested that the nebular screen is variable in that sometimes it would be a stronger

scatterer than the interstellar medium, other times its effects would disappear, and often it would be comparable in scattering strength to the interstellar medium. R&C point out that the average electron density and number of density irregularities in the 2-kpc path between the earth and the nebula should be constant in time, and they attribute the observed temporal variations in dispersion and pulse shape to changes taking place within the nebula.

The identification of the nebula as a scattering screen was made because of other activity associated with the nebula and pulsar. About the time of the first observed large increase in dispersion measure (1969 September), a major timing irregularity ("glitch") also occurred. This activity was also accompanied by movement of the optically-observed wisps near the pulsar (Scargle and Harlan 1970). No such correspondence of these phenonema has occurred again, and it is likely that the 1969 September events were chance coincidences. Nevertheless the concept of the nebula as a scattering screen is attractive. The nebula surrounding the pulsar must have some unique effect on the pulsar's radiation, and the influence of the nebula should be assessed even if it can be shown to be negligible. This question is considered in section F.

2. Theory. Functions similar to those plotted for the single-screen model will be developed now so that we can compare our observations to the predictions of the two-screen model. The model of R&C is shown in figure V-5. They assigned 6.2 msec of time delay (at 100 MHz)

to each screen, thus choosing an epoch when the nebula and interstellar medium were of comparable strength. The scattering pdf for two thin

Figure V-5. Two-screen model configuration.

screens with equal time delays $(\tau_N = \tau_0)$ is shown in figure V-6; it is

a function of the form xe^{-x},

which results from the con-

volution of two exponential

functions.

The pulse shape result-

ing from the convolution of

this pdf with the model emit-

Figure V-6. Impulse response of two-screen model.

ted pulse is shown in figure V-7, for a frequency near 100 MHz with

$\tau_0 = 6.2$ msec. This predicted

pulse shape is in much better

agreement with observations

than the shape predicted using

a single thin screen (figure

V-3).

Figure V-7. Predicted pulse shape for two-screen model.

The relative amount of

pulsing power as a function of τ_0 is plotted in figure V-8. The pdf for

equal time delays was used

for simplicity. Comparison

to figure V-4 shows that the

pulsating component is cut

off more efficiently with

two screens than with one

screen. Note that <u>each</u> of

the two screens in the two-

Figure V-8. Predicted I_P/I_T for two-screen model.

screen model has a time delay

τ_0 so that the scales for comparing figures V-4 and V-8 are different by

approximately a factor of two.

If each screen has a Gaussian irregularity spectrum there should also be a decrease of visibility across the pulse as in the single-screen case, although the effect is not as pronounced here because the pulse is already partially broadened when it reaches the interstellar screen. The visibility function for pulsar radiation scattered by two thin screens is discussed in more detail by Cronyn (1974).

3. Comparison to observations. During all of our observations the time delays of the two screens were almost certainly never equal. The time delay τ_o which is associated with the stable interstellar medium was usually much larger than : a time delay τ_N which is associated with the nebula (J. M. Rankin, private communication). This means that the effect of the nebular screen was small enough that the data are consistent with scattering in a single screen having $\tau_o \sim 10$ msec at 100 MHz.

The angular size observed at the earth due to scattering in a single screen with $\tau_o \sim 10$ msec is predicted to be 0.15 arcsec at 100 MHz, using Z = 2 kpc in equation V-1. This angular size scales as frequency-squared to 0.10 arcsec at 111 MHz. The agreement with observations is better than for the single-screen model only because the value of τ_o is smaller. The predicted angular size is still 50 percent larger than our observed value. Since our errors are only 15 percent, this is a significant difference.

Our observations of changes in I_p/I_T are in qualitative agreement with the trends in the dispersion measure and scattering variations. Between the winters of 1971-2 and 1972-3 we observed that the value of I_p/I_T decreased from ~ 0.6 to ~ 0.4, while during this period the dispersion measure showed a dramatic increase and the scattering certainly increased also. Quantitatively though, the observed angular size is associated with a smaller interstellar time delay than the model, whereas

the observed value of I_p/I_T (as in the single-screen case) predicts a
larger time delay than the model. Since the interstellar time delay is
not variable, this is a basic discrepancy of the observations with the
model. Finally, the predicted decrease of fringe visibility with pulse
phase is not observed, although the experimental uncertainty is high.

D.   Extended medium model

From the discussion of the last two sections, it is apparent that
either the thin screen approximation or the Gaussian irregularity spec-
trum, or perhaps both, must be abandoned. Williamson (1972) derived
probability density functions for the case of an extended medium in which
the source's radiation executes a random walk along the entire path length.
Figure V-9 shows the impulse response as computed by Williamson. The
rounded peak and long rise
time are reflected in the
predicted pulse shapes. Both
features are due to the fact
that with an extended medium
there is very little "straight-
through" radiation; the rays
which arrive near the start of
the pulse may come from any part
of the scattering disk, and the
rays which arrive from exactly
the source direction may not have

Figure V-9. Impulse response of
extended medium.

suffered the smallest delay. This also results in an absence of fringe
visibility dependence on pulse phase.

On this model the time delay associated with a given angular diameter
is $\pi^2/3 \sim 3.3$ times <u>smaller</u> than that for the thin screen model. There-
fore our observed angular size of 0.07 arcsec at 111 MHz corresponds
to less than 1 msec of time delay, implying that most of the pulse broad-
ening must occur elsewhere than in the "extended medium." Alternatively
the observed pulse broadening of 10 to 15 msec implies an angular size
which is much larger than that observed.

The pulse shapes predicted using this model have rise times which
are too long to agree with observations. The observed 111-MHz pulse from
the Crab nebula pulsar has a steep initial rise, about 4 to 5 msec from
baseline to peak, whereas the predicted shape using this model has a rise
time of about 9 msec. After comparing the theoretical and observed pulse
shapes, Williamson (1974) concludes that the extended medium approach is
definitely excluded and that the scattering medium must be concentrated
in a few locations along the path.

E.   Square-law structure function

Cronyn (1974) proposed that the "structure function" of the inter-
stellar dispersion measure have the form $D_N(b) = D_o b^2$ where D_N is the
variance (mean square) of the difference in electron density between two
lines of sight separated by a baseline b, and D_o is a constant. Thus a
Gaussian size spectrum is rejected in favor of a more realistic power
law spectrum. It has been established that for the interplanetary medium
a power law size spectrum probably exists, and the same proposal for the
interstellar medium is a natural extension of this idea.

For a square-law structure function the group delays, due to a slower
propagation speed through the largest irregularity sizes, are comparable

to the geometrical delays. The additional group delays are randomly dis-
tributed about their mean, and they effectively randomize the dependence
of fringe visibility on pulse epoch.

This theory does not require the Crab nebula to be scattering screen.
Indeed the nebula cannot be important for scattering and, in particular,
it cannot be the cause of the variable dispersion measure and pulse shapes.
According to Cronyn, these variations are simply manifestations of statis-
tical fluctuations in the line-of-sight electron column density. He as-
sumes implicitly that dispersion measure and scattering are intimately
related as suggested by Rickett (1970). Another feature of Cronyn's
theory is that it predicts the occurrence of dispersion measure fluctu-
ations for all pulsars. The rms variations should depend on distance,
relative velocities, and length of observing period. To date no changes
other than for the Crab nebula pulsar have been observed but dispersion
measures are being monitored at several observatories.

Due to the group delays there is very little "straight-through"
radiation, as in the extended medium case, and the predicted pulse shapes
again have too-round peaks and too-slow rise times. The impulse response
is the convolution of an exponential function (for the thin screen) with
a Gaussian (for the random delays); it is plotted in figure V-10. The
predicted pulse shapes cannot be
actually compared to observations,
however, because the essence of
this theory is the statistical
nature of the scattering medium.
Therefore the predicted pulse
shape is the average, over as

Figure V-10. Impulse response
for square-law structure function.

long a time as possible, of all the pulses which are observed. The rms
variation in pulse shapes will continue to grow until we have observed
the largest deviations from the average value; until a suitably large
body of data is in hand adequate comparisons cannot be made.

F.   The Crab nebula as scattering scr

This section addresses the question. Is the Crab nebula a scattering
screen which has a major effect on the pulsar's radiation? That it con-
stitutes a screen is certain because there must be some thermal electrons
which are in some way irregularly distributed; but the screen's effective-
ness depends on the magnitude of the density fluctuations. We will assume
that the nebula is responsible for most of the observed pulse broadening
and see what this implies about the density fluctuations and scale sizes.
Then considering what is known about the nebula we can decide whether this
model is reasonable.

1.   Values for τ_N, θ_N, and scale sizes. The discussion in this
section concerns only the scattering phenomena which occur in the nebula;
the effect of the interstellar medium is considered separately. We
adopt a value for the characteristic time delay of τ_N = 15 msec at
111 MHz, where the subscript N refers to the nebula. We take the path
length through the nebula as 1 pc and let the screen be effectively 0.5
pc from the pulsar. Then with the total path as Z = 2 kpc we have
q ~ 4000 from equation V-2. Thus from equation V-1 and the above values
for τ_N, Z, and q, we obtain θ_N = 2.8 milli-arcsec. The angle θ_N is
the half-power diameter of the angular spectrum (equivalent to θ_s of
equation V-4). What does the value of θ_N imply about structure in the
nebula? Following Cohen and Cronyn (1974) we can consider three charac-

teristic linear sizes in the screen which are important for scattering.
The smallest significant size is $\ell_\phi \sim \lambda/2\theta \sim 10^{10}$ cm, the linear dis-
tance across which one radian of phase shift occurs. Sizes smaller than
ℓ_ϕ produce too small a phase shift to influence the angular broadening.
The Fresnel zone size, $\sqrt{\lambda Z} \sim 10^{12}$ cm, is the largest size which is sig-
nificant for angular scattering; sizes larger than $\sqrt{\lambda Z}$ cause refraction
and have little effect on source broadening. Finally, the scattering
disk size, $2\theta_N \cdot 10^{14}$ cm, defines the distance over which we can receive
radiation from the source.

Such a wide range of sizes (four orders of magnitude) might be rep-
resented by a power law spectrum of irregularity sizes in the nebula.
The small and large lengths are equal to the gyroradii of electrons
in a 100-μG field with energies of 100 and 10^6 Mev, respectively. In
the nebula there are electrons between these extreme energies; they would
produce synchrotron radiation between 6 MHz and optical frequencies.
Could these sizes become thermal electron density irregularities? Wentzel
(1969) suggested a way for this to happen by noting that since streaming
cosmic rays are scattered by their own Alfven waves, they interact most
strongly when they travel through one wavelength in one gyro-period. An
investigation of the possible hydromagnetic waves in the nebular plasma
would be interesting in that it could provide information about possible
density irregularity sizes. One important parameter for such a study
would be the thermal electron density in the nebula since this influences
both the excitation and damping of the waves (Scheuer and Tsytovich 1970).
The various determinations of the electron density are considered next.

2. Thermal electron density. a. Expansion. A firm limit can
be set on the thermal electron density along the line of sight to the

pulsar from the lack of an observed temporal monotonic decrease in the dispersion measure. Since the nebula is expanding, the volume density systematically decreases with time. Using the known expansion rate, the fractional change in the dispersion measure of the nebula is calculated to be ~0.2% per year. Since no monotonic decrease in dispersion measure (i.e. column density) has been observed to a limit of about $\Delta N < 10^{16}$ cm^{-2} per year, the average volume density of electrons must be $n_e < 1$ cm^{-3} along the line of sight to the pulsar. The contribution of the nebula to the total dispersion measure is then <1 pc cm^{-3} if we take 1 pc as the path length through the nebula. This argument was first used by Drake (1969) to establish an upper limit to the mass of the nebula.

b.   Comparison with PSR 0525. Other ways of determining the electron density involve comparisons between the Crab nebula pulsar (PSR 0531+21) and the nearby pulsar PSR 0525+21. They are separated on the sky by about 1°5 and have similar dispersion measures and rotation measures. The dispersion measures and rotation measures are listed in table V-1 for both pulsars and the nebula; these values are given by

Table V-1

Dispersion and rotation measures

for pulsars and nebula

Object	Dispersion (pc cm^{-3})	Rotation (rad m^{-2})
PSR 0531	56.8	-42.2
PSR	50.9	-39.6
.	<1	-25.6

Manchester (1971). The near equality of the rotation measures of the two pulsars led Wilson (1974) to conclude that the radiation from

PSR 0531+21 is not Faraday-rotated in the nebula; rather he postulates that the rotation measures of both pulsars are due entirely to the interstellar medium. In fact he used the difference in their rotation measures ($\sim$2 rad m^{-2}) as an upper limit to the effect of the nebula and derived $n_e < 0.01$ cm^{-3} along the line of sight to the pulsar within the nebula. Manchester (1971) notes, however, that the similarity of the two rotation measures could be coincidental and that a small filament in front of the pulsar in the nebula could account for the difference between the nebular and pulsar rotation measures.

Wilson's treatment assumes that the interstellar magnetic field and electron density are the same along the path to both pulsars, and that both pulsars are at approximately the same distance. Consequently we must also be able to say that the difference in the dispersion measures of the pulsars indicates the contribution of the nebula to PSR 0531+21's dispersion measure. The difference is $\sim$6 pc cm^{-3}, giving $n_e = 6$ cm^{-3} averaged through the nebula. But this is in conflict not only with the limit on n_e set by the expansion but also with the value just derived from comparing the rotation measures of the two pulsars. We must conclude that the interstellar medium is not the same along the two paths to the two pulsars, and look for other means of determining n_e.

c. Optical observations. Filaments of all sizes thread the nebula and it would seem that any one line of sight should encounter at least one. In fact there is a small filament which appears to overlie the pulsar. In Trimble's (1968) system it is number 159; its radial velocity of -162 km/sec means it ought to lie on our side of the pulsar and be about 0.2 pc in front of it. The filament is very faint, and probably has an electron density of about 100 cm^{-3}, derived from photometric observations. It is unresolved on photographs with resolutions

of one arcsec and so it must be smaller than 0.01 pc. Its contribution

to the dispersion measure of the pulsar is thus <1 pc cm^{-3}. If there

were no other electrons along the line of sight through the nebula, the

average electron density over the 1 pc path would be $n_e < 1$ cm^{-3}. Com-

bined with the limit set by the expansion, the total average electron

density along the line of sight to the pulsar is $n_e < 2$ cm^{-3}.

For the region near the center of the nebula, Scargle (1969)

derived $n_e \sim 10^{-3}$ cm^{-3} and suggested that the density might increase

further from the pulsar.

The discussion of this section has shown that the thermal electron

density of the Crab nebula along the line of sight to the pulsar is not well

known. However an upper limit of $n_e < 2$ cm^{-3} can be set confidently.

3. __Filament 159__. The small filament mentioned in the previous sec-

tion which lies between us and the pulsar could be, literally, a thin

scattering screen. The configuration is shown in figure V-11. In this

section some consequences of
the location of this filament
are explored. We specify some
irregularity scale sizes and
velocities and attempt to
justify them as physically
reasonable. We begin by
assuming, as stated at the
beginning of section F,

Figure V-11. Filament 159
configuration in Crab nebula.

that most of the temporal broadening occurs in the nebula.

a. __Numerical quantities__. For the filament in the location

shown in figure V-11, we have q $\sim$ 10000 from equation V-2. With the adopted

time delay of τ_N = 15 msec at 111 MHz, we calculate the apparent angular size of the pulsar as observed at the earth to be θ_N = 1.2 milli-arc-sec. To proceed, we need a relation between the rms scattering angle and the irregularity scale sizes and density fluctuations. Derivations have been given by Cronyn (1970a) and Lovelace (1970) and the result is:

$$\theta_o = \frac{r_e \lambda^2 \Delta n_e}{2\pi} \sqrt{\frac{d}{a}} \qquad (V-5)$$

where r_e = classical electron radius (2.8×10^{-13} cm),

  Δn_e = rms deviation from average electron density,

   a = typical "scale size" of irregularities,

   d = thickness of screen.

We have assumed that the irregularities have a typical scale size a, and that they are Gaussian-distributed. This may not be the most physically reasonable assumption, but for ease of calculations and for simplicity, let us continue with the Gaussian spectrum.

We take the scale size as the linear distance over which one radian of phase shift occurs: a ～ 10^{10} cm (this was defined as ℓ_ϕ in section F-1). From equation V-5 we can then calculate the rms density fluctuations which could account for θ_N. This yields Δn_e ～ 4×10^{-4} cm^{-3}, where we used d = 0.01 pc and the values of a and θ_N given above. If the filament is actually thinner than 0.01 pc, the required rms density fluctuations would be larger. These calculations have ignored the regions of the nebula outside the filament because nothing is known of possible thermal electron density irregularities there.

If the average electron density in the filament is n_e ～ 100 cm^{-3}, the value of Δn_e implies <0.01% density fluctuations would be required to occur over a length scale of 10^{10} cm. Such deviations from the average

electron density are reasonable, and could reflect spatial variations in the ionization and recombination occurring in the filament. We can therefore explain all of the temporal broadening as a result of density fluctuations in the filament.

b. Time delay variations. Another requirement of the model is that changes in τ_N which are impl: ed by our observations of changes in the ratio I_p/I_T should also follow from physically reasonable variations. From the graph of figure V-4, the change in the value of I_p/I_T from 0.6 (observed in 1971-2) to 0.4 (observed in 1972-3) implies a change in τ_N from 15 to 25 msec over a time interval of one year (3×10^7 sec). This in turn yields a change in θ_N of a factor of ~1.3, and a corresponding variation of Δn_e from 4 to 6×10^{-4} cm^{-3}.

The pulsar's proper motion is ~100 km/s (Trimble 1968) and the filament also has a proper motion of ~30 km/s (Trimble 1968) in a direction approximately perpendicular to that of the pulsar. It is not unreasonable to suppose that relative motion of the pulsar, filament, and observer could carry the line of sight through regions of the filament where the ionization is more or less patchy. These quite minor variations in the mean electron density of the filament can easily account for the observed variations in scattering parameters.

c. Changes in dispersion measure. Can irregularities in the filament also be used to explain the observed variations in dispersion? The variations reported by Rankin and Counselman (1973) can be viewed as random, overlapping "events" which result in increases and decreases in the column density of thermal electrons. These changes could conceivably be due to "clouds" of appropriate size, velocity, and thermal electron density moving across the line of sight. Rough values of the required

cloud parameters were estimated by Rankin and Roberts (1971) based on "typical" magnitudes and durations for the "events." Subsequent observations revealed that the variations are much more complicated, as shown in the two-year span of data presented by Rankin and Counselman (1973).

It is possible that within the filament there exist large-scale irregularities which are responsible for the changes in dispersion. These irregularities would be of the order of ,or larger than,the linear diameter of the scattering disk in size. Smaller sizes will be numerous enough that as many will move into as out of the area of the disk and no changes in dispersion measure due to these would be observed. Let us suppose there are clouds of size $a_D \sim 2$ a.u. in the filament, and let each have an average density of $n_e \sim 200$ cm^{-3}. Then with a 50% filling factor we can produce the observed emission measure of 200 pc cm^{-6} and the limit on the average density of $n_e \sim 100$ cm^{-3}. If the clouds have velocities of $v \sim 100$ km/s (which could be due to the proper motion of the pulsar and filament), one "cloud" would pass across the scattering disk in a time $t = a_D/v = 3 \times 10^6$ sec ~ 1 month, and its passage would cause a change in electron column density of $\Delta N = n_e a_D = 6 \times 10^{15}$ cm^{-2}. The observed dispersion variations have approximately these time scales and magnitudes.

Until more extensive observations are available so that statistical methods can be used, these simple calculations must remain suspect because there are too many unknown and arbitrary parameters.

d. Scintillations. Temporal variations in the pulsar's intensity are also predicted due to irregularities in the filament. A diffraction pattern would be formed by interference between various scattered rays. The scale of the pattern will be on the order of $\ell_\phi \sim 10^{10}$ cm. The scintillations would exhibit a time scale of

$\ell_\phi/v \sim 10^3$ sec and be correlated over a bandwidth of $1/2\pi\tau_N \sim 10$ Hz at 111 MHz. The observable variations will be discussed in the next section.

e. Interstellar scattering. On the model described above, the source which appears at the edge of the nebula at 111 MHz has been broadened into an apparent angular size which, viewed from the earth, is a few milli-seconds of arc; the pulse shape has been broadened to display a characteristic time delay of ~15 msec; and intensity scintillations have been built up in the radiation.

The source is now larger than the critical size required for interstellar intensity scintillations (Cohen and Cronyn 1974), though its passage through the interstellar medium will not alter the already-present variations. Interstellar scattering will additionally broaden the angular size and pulse shape of the source, however. If we adopt Williamson's model for an extended medium (described in section D) we can achieve an angular diameter of 0.07 arcsec while convolving only 0.7 msec of temporal broadening into the pulse shape. An earth-based observer would then perceive a source which has the requisite combination of temporal and angular broadening.

On this model, or any model in which appreciable temporal broadening occurs in the nebula, narrow-band structure observed in the pulsar's spectrum will be indicative only of the nebular time delay. This model therefore predicts that the total observed time delay (τ_0) and the width of the frequency structure (f_D) will not be in the relation $2\pi\tau_0 f_D = 1$ as was observed for the Vela pulsar by Backer (1974).

At 111 MHz, where $\tau_N \sim 15$ msec, the decorrelation bandwidth is only $f_D \sim 10$ Hz. At higher frequencies f_D approaches a feasible observing

bandwidth and this prediction is testable. Hugu nin et al. (1969) observed
this pulsar at 151 MHz and observed no frequency structure in the radiation.
However they used a passband of 0.1 MHz which would have blurred any scin-
tillations.

G.   Summary of models

The five models presented above all attempt to explain the observed
features in the radio radiation from the Crab nebula pulsar. The major
observation which any model must explain is the combination of angular
and temporal broadening which have both been observed at 111 MHz. Based
on the temporal broadening, the simplest model, a single thin screen,
predicts an angular size which is about a factor of two larger than the
size measured with VLBI. A similar discrepancy exists for the two-screen
model. Also for both models, the predicted decrease of fringe visibility
with pulse phase is not observed. The extended medium model of Williamson
again predicts an angular size which is much too large to agree with the
VLBI observations. To evaluate the structure function of Cronyn, more
observations of other pulsars are still needed. Finally, the model in
which nearly all of the temporal broadening occurs in the nebula and only
a few milliseconds are added in the interstellar medium does predict the
observed combination of temporal and angular broadening.

CHAPTER VI

OBSERVATIONS OF OTHER PULSARS

This chapter discusses the observations of pulsars other than the

Crab nebula pulsar. The first part of the chapter is a presentation of

the results and their implications. The second part is a discussion of

various interstellar scattering effects.

A. Results and implications

1. Strong pulsars. a. Observations and processing. Four strong,

low-dispersion pulsars were observed during each session; table VI-1 lists

the pulsars' parameters. Although many tapes on each pulsar were recorded

Table VI-1

Low-dispersion pulsar parameters

PSR	Period (sec)	Equivalent width (msec)	Duty cycle %	Dispersion measure (pc cm^{-3})	Gate width (msec)
0834+06	1.274	20	4	12.9	50
0950+08	0.253	10	4	3.0	10
1133+16	1.188	20	4	4.8	50
1919+21	1.337	25	2	12.4	25

during every observing session, results are reported here for only a few

runs. One reason for the small number of runs is that since all pulsars

are highly variable sources, many times they were too weak to be detected

in a three-minute integration. If the correlated signal could be detected,

individual pulses were usually quite easily visible on the total power

records. Due to the complexity of having three stations on the air

107

simultaneously, it was not possible to revise the schedule when it appeared that a pulsar happened to be weak at the time we observed.

The other reason for the few runs is that we consider here only those observations for which fluxes on all three baselines are available. This is again because pulsars are highly variable sources, and the fringe visibility on the long baseline can be calculated only if a simultaneous measurement of the total flux was made using the short baseline. This excludes the 1972 January, March, and December data when only one baseline was active. As in the case of the Crab nebula pulsar, the fringe visibility, γ, is defined as the ratio of long-baseline (S_{PR}) to short-baseline (S_p) flux. γ is also the fringe visibility of the pulse energy, since the gate width was the same for all baselines. Finally, only the 111-MHz observations of pulsars are reported here. At 196 MHz few three-baseline observations are available, and at 74 MHz the spectra of most of the pulsars have turned over making the pulsars too weak to detect.

The gating method was used for all the pulsars listed in table VI-1. If, through an error or mishap, the pulse epoch was not determined, searches for the correct epoch were not made because of the large amount of computer time involved. The gating method was necessary on every pulsar observation because the enhancement of the signal-to-noise ratio meant the difference between detection and non-detection. Several runs were processed both without a gate (treating the pulsar as a continuum source) and with a gate, and only those runs processed with the gate showed fringes. Table VI-2 gives the detection limits at 111 MHz for each pulsar, both for a full-tape integration and for a single pulse.

b. Average fluxes and fringe visibilities. Table VI-3 lists the average fluxes, fringe visibilities, and angular sizes at 111 MHz for

Table VI-2

System sensitivity (5σ level) for pulsar

at 111 MHz, by baseline

Pulsar	No. pulses per tape	T_{sky} (K)	S_{min} (Jy) for full tape			S_{min} (Jy) for one pulse		
			AN	AS	NS	AN	AS	NS
0834+06	141	380	1.4	2.6	3.7	17	31	44
0950+08	711	470	1.6	2.9	4.2	42	76	112
1133+16	151	540	1.7	3.0	4.4	20	37	55
1919+21	134	1500	8.9	8.9	14.6	61	103	170

all three-baseline runs. The total flux is S_p (observed with the short

baseline), and the partially-resolved flux is S_{PR} (observed with the

long baselines). The angular sizes were obtained from the fringe visi-

bilities by using figure III-5 (page 56).

The variability of the average flux is readily apparent. The

fringe visibility varies also, though this effect is only evident for

daily, or longer, time differences. On time scales of several minutes

(run-to-run) the flux may vary considerably but the fringe visibility

remains approximately constant. This behavior was also exhibited by

the Crab nebula pulsar (see figure III-2).

c.   Strong-pulse fluxes and fringe visibilities. Individual

pulse intensities often exceed many times the mean intensity, and during

each three-minute run there occur pulses which have strengths which are

several standard deviations above the average flux. For each run the

pulse amplitudes which were above the 4σ level on both long and short

baselines were used to calculate individual-pulse fringe visibilities.

Because the noise level for detecting a single pulse is high, only the

Table VI-3

Average pulsar parameters, 111 MHz

Pulsar	Date	No.	S_P(Jy)	S_{PR}(Jy)	γ	θ_s (arcsec)
0834+06	1971 Nov. 24	3	7.4±0.9	3.6±1.3	0.49±0.19	0.10±0.05
	1973 Feb. 24	0	36.4±2.7	38.3±2.6	1.05±0.10	<0.04
	1973 Feb. 25	4	39.0±1.8	30.5±2.1	0.78±0.06	0.06±0.02
0950+08	1973 Feb. 24	5	13.1±2.3	10.5±2.3	0.80±0.06	0.05±0.03
1133+16	1973 Feb. 24	2	15.6	14.7±1.1	0.78±0.17	0.06±0.04
1919+21	1971 Dec. 19	3	37.7±4.1	33.6±6.6	0.89±0.11	<0.04
	1973 Feb. 25	3	31.2±5.1	23.3±6.0	0.75±0.13	0.06±0.03

strongest pulses could be use., there were typically a dozen or so pulses in each run.

It was found that there is no difference between the visibilities deriᵥed from the single pulses and those derived from the average fluxes. This is in contrast with the predictions of Cronyn (1972) that the fringe visibility should decrease for longer coherent integration times, and indicates that decorrelation across the long baseline due to interplanetary scintillations was not as severe as indicated by the rms phase deviations presented in table II-7. None of the pulsars lies in the ecliptic plane, the closest being PSR 0950+08 which is 5° above the plane, so that a decrease of scintillations away from the plane might explain the lack of an appreciab ᵥ effect on these pulsars. Also, most of the observations were made at solar elongations greater then 90° which could account for a reduced solar wind effect.

d. Single-pulse amplitude and phase plots. All of the pulsars we observed have pulse widths less than 0.2 sec (the length of one record) so that the correlation amplitude of a single record reflects the pulse intensity. To show that the same amplitudes were observed on each baseline, the single-pulse fringe amplitudes were plotted as a function of time or pulse number. The amplitudes observed on all three baselines were superimposed and the pulse-energy measurements made at Arecibo were also plotted when they were available. Figure VI-1 shows the pulse-to-pulse amplitudes and phases for an observation of PSR 1919+21 in 1971 December. The data were smoothed by a five-pulse running average. The dramatic increase in flux during the latter half of the run illustrates the variability of the pulsar flux and also shows that both the unresolved
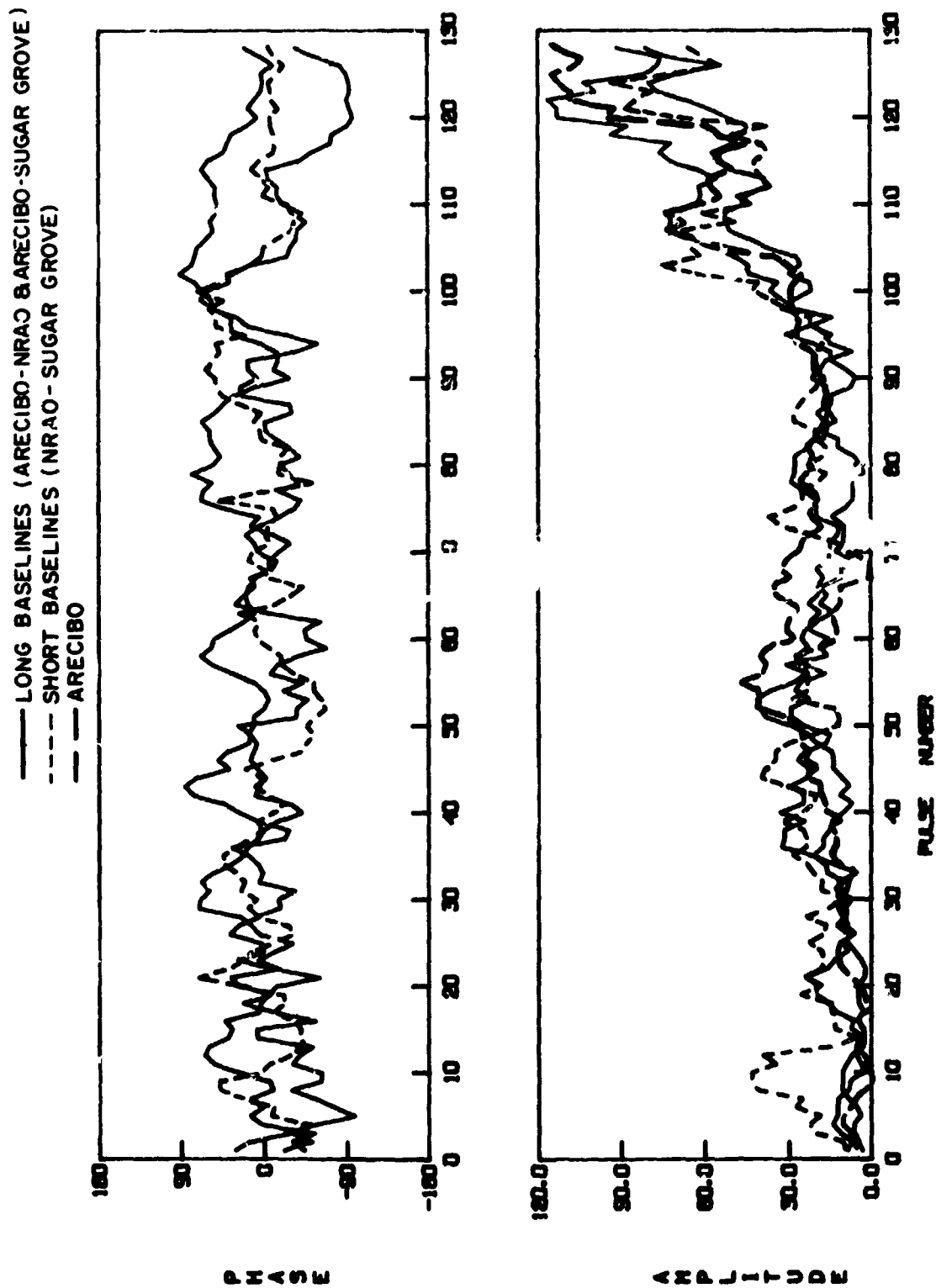
Figure VI-1. Pulse-to-pulse amplitude and phase at 111 MHz for 'SR 1919+21 in 1971 December. The data were smoothed with a five-pulse running average. The total length of the pulse series is three minutes.

and partially-resolved fluxes exhibit the same variations. The pulse am-
plitudes plotted in figure VI-2 offer a bet er example of the closeness
of the variations on all baselines. This data was obtained for PSR 0834+06
in 1973 February; although Arecibo pulse-energy measurem its were recorded
they are not yet available for comparison with the interferometer data.
The amplitudes and phases were smoothed with a five-pulse-wide filter to
narrow the noise spectrum.

The presence of very strong pulses distorts the dist.ibution of
fringe amplitudes: pulsars display amplitude distributions which have
long high-amplitude tails in contrast with the distributions for continuum
sources which are Kicean. Figure VI-3 is a plot of the distributions of
fringe amplitude and phase for the quasar 3C286 and for the pulsar PSR 0950+08.
The amplitude distribution for PSR 0950+08 is similar to other histograms pub-
lished for this pulsar (Smith 1973). The two phase distributions are both
approximately Gaussian. This illustrates that the correlated pulse ampli-
tudes have the same characteristics as those observed with a single tele-
scope.

e. Polarization. Most pulsars are highly polarized, so that
even though our instrumental polarization was very high, we could measure
the linear polarization of pulsars. During the 1973 February experiment
we made several observations in linear polarization on PSR 0834+06 and
0950+08. The fluxes were corrected for instrumental polarization accord-
ing to the equations derived in Appendix D. We observed less than 15%
linear polarization for PSR 0834+06, and 90±20% linear polarization for
PSR 0950+08; these numbers are derived from the average of the flux ob-
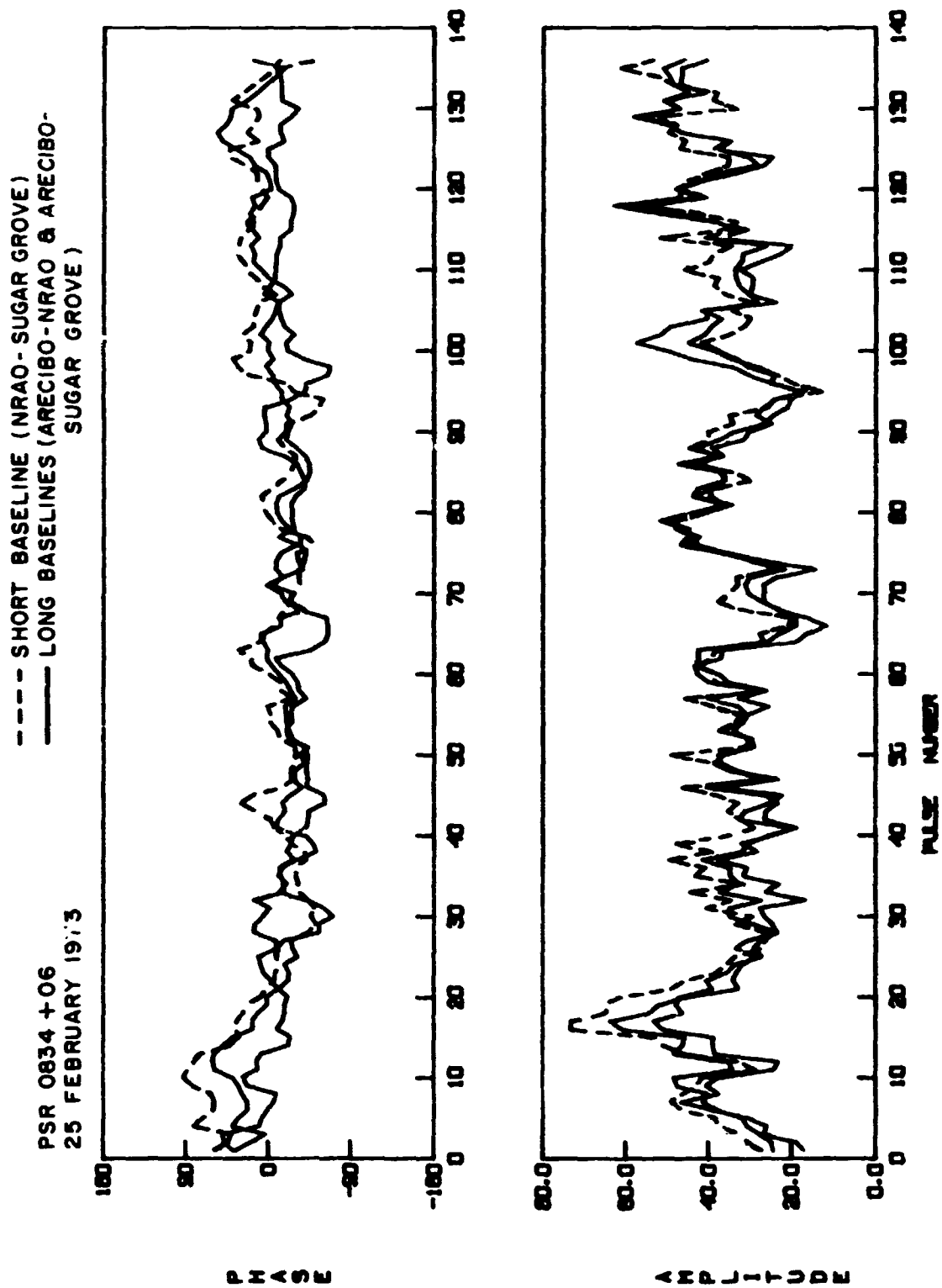served during three runs on each pulsar.

Figure VI-2. Pulse-to-pulse amplitude and phase at 111 MHz for PSR 0834+06 in 1973 February. The data were smoothed with a five-pulse running average. The total length of the pulse series is three minutes.
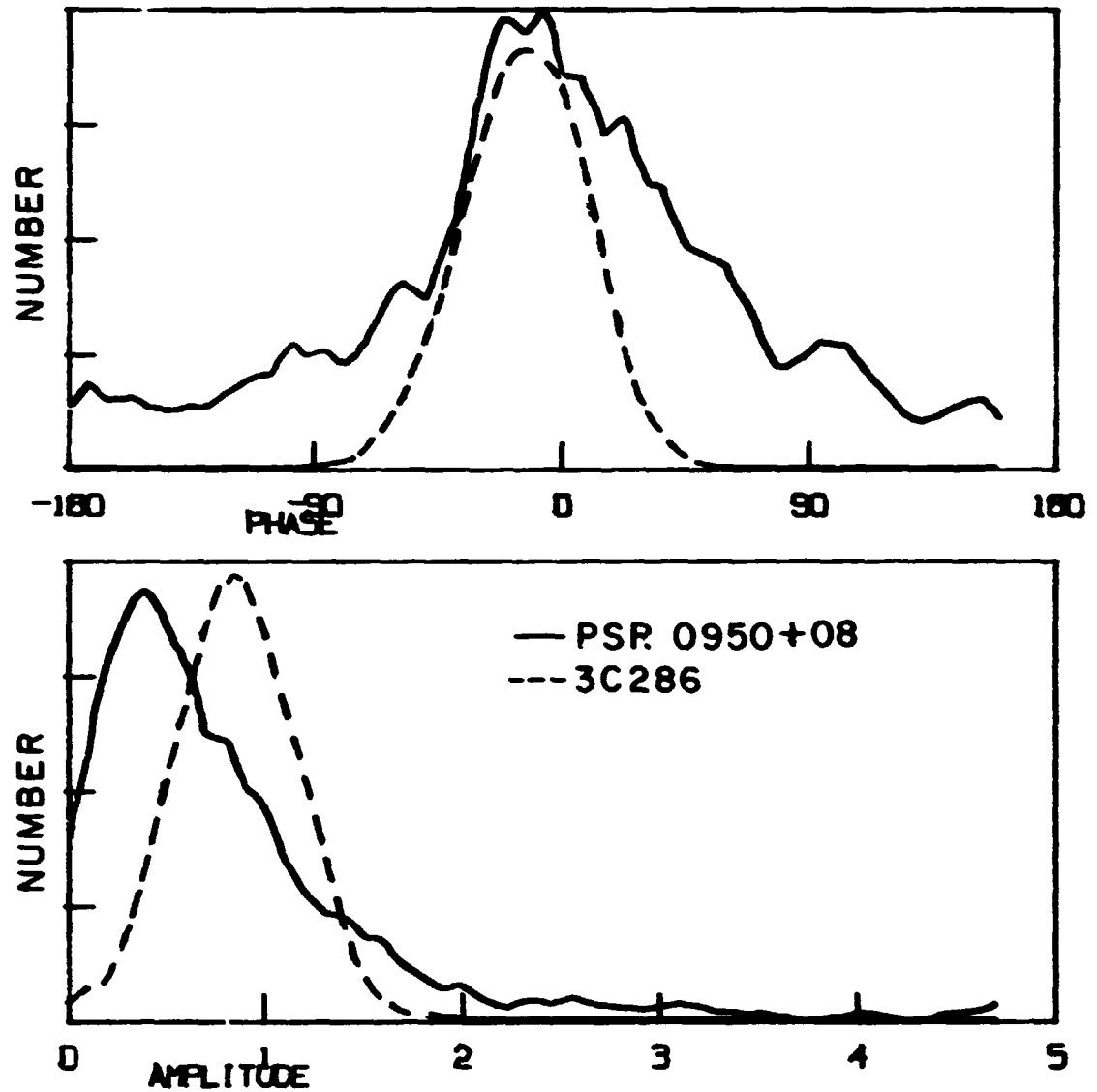
114

Figure VI-3. Distribution of amplitude and phase for PSR 0950+08
and 3C286. Both runs were made at 111 MHz in 1973 February. There
are a total of 710 pulses for the pulsar and 900 samples for the
quasar. The amplitude scale is in units of the mean amplitude.
The phase distribution is wider for the pulsar because the signal-
to-noise ratio is lower (see equation II-22, page 41).

Manchester et al. (1973) collected polarization measurements for 20 pulsars at many frequencies and concluded that most pulsars exhibit a constant fractional linear polarization below some critical frequency while the polarization decrease above that frequency. Although our measurement for PSR 0950+08 is consistent with the limiting polarization of 65% assigned by Manchester et al., it may be that this pulsar does not reach the limiting polarization until below 100 MHz. Our measurement for PSR 0834+06 is not consistent with the measurements of Manchester et al. They find ~25% polarization at 151 MHz and believe that the limiting polarization has not been reached. According to this, we should have observed about 25% polarization; however, the high instrumental polarization precluded more accurate measurements.

2. Weak pulsars. We hoped to observe substantial resolution and to measure an apparent angular size for distant pulsars other than the Crab nebula pulsar to establish a dependence of angular size on distance. For this reason, we observed four weak, high-dispersion pulsars at 111 and 74 MHz during 1972 December and 1973 February. Table VI-4 lists the pulsars' parameters, as given by Lang (1971c). These pulsars were processed as continuum sources because they all have little flux which is pulsing at low frequencies. No correlated flux was detected for any of the pulsars on either the long or short baseline.

Table VI-4

High-dispersion pulsar parameters

PSR	Period (sec)	Dispersion measure (pc cm^{-3})	ℓ	b
1858+03	0.655	402	37.2	-0.6
1933+16	0.359	158	52.4	-2.1
1946+35	0.717	129	70.6	5.0
2003+31	2.111	225	69.0	0.0

There are many reasons for not observing fringes, but ruling out errors in recording or processing leaves only two possible reasons. First, the source size may be comparable to the fringe spacing and therefore the source is partially resolved by the interferometer. This possibility could obtain for these four pulsars since their asymmetrically broadened pulse shapes (Lang 1971c) indicate that interstellar scattering should also produce a broad angular size. Second, the source may be actually smaller than the fringe size but too weak to detect. This could occur if the emitted spectra of these pulsars turn over at frequencies above about 100 MHz; then the flux probably would have been below our detection limits on all baselines.

Seiber (1973) compiled all the available flux measurements for PSR 1933+16 and published a spectrum which exhibits a turnover near 300 MHz. Therefore the flux was well below our detection limit on all baselines. Insufficient flux measurements have been published for the other three pulsars to enable this same statement to be made, but some limits can be established. Recently McLean (1973) published spectral indices for PSR 1858+03 and 1946+35 using observations at 922 and 408 MHz. Extrapolating to our frequencies we obtain the fluxes listed in table VI-5. Our upper limits on the flux indicate that the spectra of these two pulsars could turn over below 408 MHz. Alternatively, the pulsars could have been weak at the times we observed.

Table VI-5

Fluxes of PSR 1858+03 and 1946+35

PSR	Spectral Index	Frequency (MHz)	Extrapolated Flux (Jy)	Observed Flux (Jy)	No. of runs
1858+03	-2.9	111	3.3	<4±2	4
		74	10.6	<10±5	2
1946+35	-2.7	111	4.0	<1.9±1	8
		74	11.9	<4.5±2	5

Without better knowledge of the spectra we cannot interpret the lack of detection on the long baselines quantitatively. The apparent angular sizes of these pulsars are probably partially resolved but actual total flux measurements rather than limits are needed to calculate even a limit on the fringe visibility.

B. Discussion of interstellar scattering effects

The plane wave which starts out from the pulsar and propagates toward the observer is perturbed during its passage through the irregular interstellar medium. Both amplitude and phase fluctuations are imposed on the wave, and each manifests itself in a different way. Amplitude variations (due to interference effects) are the basis for the observed scintillation phenomena, and phase perturbations in the wave give rise to predicted, but not yet observed, apparent source motion. The multipath scattering also produces angular and temporal broadening of the radiation; this aspect was discussed in Chapter V. Each of these phenomena will be discussed with regard to the pulsar observations.

1. Scintillations. The characteristic time delay discussed in Chapter V also implies a characteristic frequency width, $1/2\pi\tau_o = f_D$, over which intensity fluctuations are correlated. The quantity f_D is called the "decorrelation bandwidth," and in order for intensity scintillations to be observable the instrumental bandwidth must be smaller than f_D so that the frequency-dependent diffraction pattern is not blurred or "decorrelated." At 111 MHz, estimates for f_D are 1 to 2 kHz for all the low-dispersion pulsars we observed except PSR 0950+08 which has $f_D \sim$ 100 kHz. The Mark I bandwidth of 350 kHz is thus many times wider than f_D and for this reason it is unlikely that the observed variability is due to

interstellar scintillations. Interplanetary scintillations are also
probably not the cause of the flux variations either, because the time
scales for IPS are very short. Instead, we attribute all flux changes
to intrinsic source variability. Possibly for PSR 0950+08 some variations
are due to scintillations since the observing and scintillation bandwidths
were quite close.

The observed fluctuations in intensity occurred over time scales from
ε 2 pulses to over one year. The similarity between the individual
pulse energies measured at Arecibo and the single-pulse correlated fluxes
(figure VI-1) implies that the variability observed with the interferom-
eter reflects the true pulse-to-pulse fluctuation. Over monthly intervals
the flux changes are also probably intrinsic to the source. Huguenin et al.
(1973) note that changes of up to a factor of 10 occur on characteristic
time scales which are different for each pulsar. Over several months we
observed large changes in flux, but from day-to-day within an observing
session the average flux stayed approximately the same.

2. Source motion. The possibility of apparent position variations
due to interstellar scattering is discussed by Lovelace (1970). This
phenomenon is analagous to the effect called "seeing" by optical obser-
vers. Lovelace notes that the apparent position changes should usually
be caused by the largest irregularity sizes in the medium. For a Gaussian
irregularity spectrum there is no predicted apparent source motion because
only for a steep power law spectrum (with spectral index >2) are there
sufficiently large irregularity sizes to produce the effect. It is dif-
ficult to predict the magnitude and time scale of the variations without
knowledge of the irregularity size spectrum. We would expect, however,

that observable position variations would be at least several times larger

than the scattering size, θ_s, and that the time scale would depend on the

linear size and relative transverse velocity of the irregularity which

produces the effects. Typically, we expect an excursion of one scattering

size in one intensity scintillation time.

Since our interferometer fringes are on the order of the apparent

angular size of the pulsars, we would observe phase excursions of at least

several turns over time intervals of up to several years depending on the

physical parameters of the irregularities. Without any more precise

specifications, this effect of interstellar scattering is hopelessly en-

tangled with ionospheric refraction effects. Over our long baseline (2500 km)

ionospheric scintillations are completely decorrelated and at 111 MHz we

could observe changes in the source's apparent direction of several hun-

dred fringes (equivalent to about one minute of arc) due to the ionosphere.

Such deviations are within the interferometer's response pattern but changes

this large could completely mask source position fluctuations which are due

to interstellar scattering.

Our observations of pulsars show no position variations which cannot

be attributed to the ionosphere. To properly investigate source motion,

differential techniques should be used in which one measures the phase

difference between the pulsar and another source also in the telescope

beam. Such a technique was successfully used to put a limit on the posi-

tion difference between the Crab nebula pulsar and compact source (Chap-

ter IV, section C-4).

3. **Angular broadening.** Apparent angular sizes at 111 MHz for a

total of five pulsars were measured during the experiment. If we look at

equation V-5 (page 102), we see that (apart from wavlength) the angular

size depends directly on the source distance (Z) and the rms electron
density variations (Δn_e), and inversely on the irregularity size (a). If
we assume that the irregularities are associated with the electrons res-
ponsible for the dispersion (D) and that the interstellar medium is similar
along lines of sight to all pulsars, then the observed angular sizes should
scale as the square root of the dispersion. The observed angular sizes at
111 MHz are plotted against dispersion measure in figure VI-4, and the
values for θ_s, D, and Z are listed in table VI-6. The distances are those
assigned by Prentice and ter Haar (1969) who took account of the known HII

Table VI-6

Pulsar sizes (at 111 MHz) and distances

PSR	θ_s (arcsec)	$D(\text{pc cm}^{-3})$	Z (pc)
0531+21	0.07±0.01	56	2000
0834+06	0.06±0.01	13	400
0950+08	0.05±0.03	3	60
1133+16	0.06±0.04	5	130
1919+21	0.06±0.03	13	250

regions and early-type stars along the line of sight to the pulsars. In
figure VI-4 a line of slope one-half is drawn for both 111 and 74 MHz.
The line for 111 MHz passes through the point for the Crab nebula pulsar
since this is the best-determined size. The nearby pulsars appear to be
too large at 111 MHz, but the large error bars do include the predicted
values.

What do the changing angular sizes (table VI-3) indicate? A de-
crease in angular size means that the rms density fluctuations along the
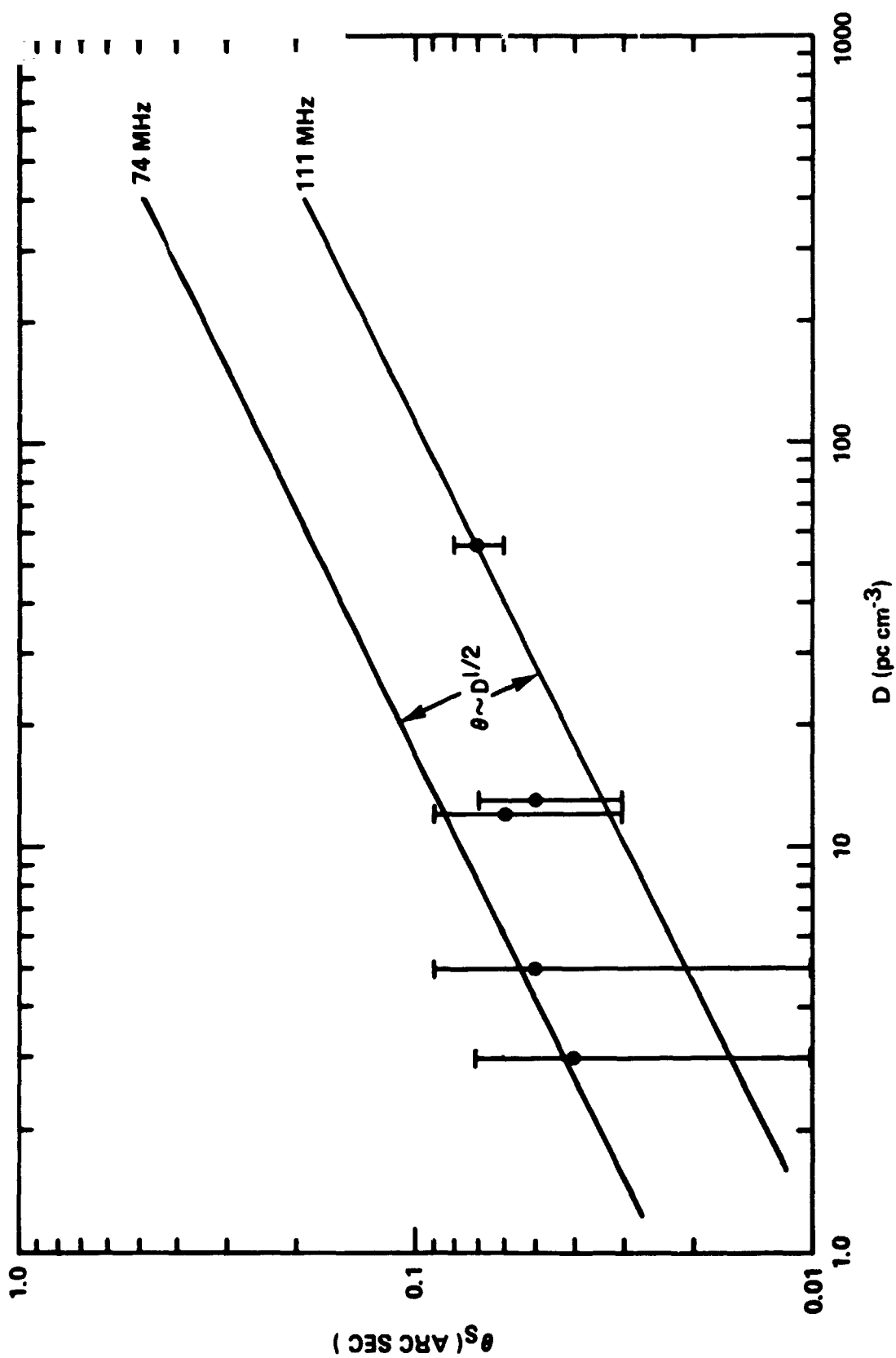line of sight have smoothed out, or that larger scale sizes drifted into

Figure VI-4. Apparent angular size vs. dispersion measure for five pulsars at 111 MHz. Lines have slope one-half, and at 111 MHz the line passes through the size of the Crab nebula pulsar. The 74-MHz line is shown in order to indicate the wavelength dependence. The 1973 February points from table VI-3 are plotted.

the line of sight. For the pulsar observations in 1973 February, D. C. Backer and G. A. Zeissig recorded individual pulse intensities simultaneously with our experiment at Arecibo and NRAO so that the drifting diffraction patterns could be observed. The data have not yet been analy.ed, but it will be interesting to see if the patterns are different during the two days when different values for the angular size were measured. We predict that the observed patterns should be larger on the day when the pulsar was smaller.

The question remains, what in the interstellar medium causes the scattering? The evidence from the angular broadening is that there are myriad irregularities with linear sizes $\ell_\phi \sim 10^9$ cm, the distance over which one radian of phase shift occurs. The latest diffraction pattern measurements (Slee et al. 1974) indicate a similar irregularity size. Such sizes are much too small to be observed with the conventional techniques used for studies of the interstellar medium. The existence and prevalence of small scale sizes are strongly indicated by various observations of pulsars using quite disparate techniques, and new theories concerning the interstellar plasma need to consider this fact.

CHAPTER VII

SUMMARY, CONCLUSIONS, AND SUGGESTIONS FOR FURTHER WORK

This thesis presented angular size measurements for five pulsars,
with the body of data heavily weighted toward the Crab nebula pulsar. A
visibility function for the Crab nebula pulsar which is consistent with a
Gaussian brightness distribution was measured in an early 144-MHz experi-
ment. Assuming a Gaussian distribution at all frequencies, we have also
made estimates of apparent angular sizes at 196, 111, and 74 MHz. These
sizes scale as wavelength-squared in accordance with interstellar scatter-
ing theories, and the angular sizes for all five pulsars show a dependence
on the square root of distance (or dispersion measure) which is consistent
with theoretical predictions.

We have also measured the flux of the compact source in the Crab neb-
ula at 196, 111, and 74 MHz, and find that the fluxes lie on the extrapo-
lation from high frequencies of the pulsing flux. Using differential fringe
phase measurements we have tightened the limit on the coincidence of the
pulsar and compact source to a separation of ~2 a.u. at the distance of
the nebula.

We have shown that the apparent angular size and temporal broadening
of the Crab nebula pulsar cannot both be explained with a single thin
screen model for interstellar scattering. A two-screen model improves
the situation, but equal-strength screens predict results inconsistent
with observations. It appears that for this pulsar, the observed com-
bination of angular and temporal broadening may be intimately related to
the presence of the nebula. A model in which the small filament lying in

front of the pulsar is responsible for the temporal broadening while the

extended interstellar medium causes the angular broadening does enable

the otherwise-discordant angular and temporal effects to be explained.

Further observations of this pulsar, and comparisons to observations of

other pulsars, would help to determine if the Crab nebula does indeed have

a unique effect.

The results presented in the previous chapters naturally lead us to

ask many more questions about the Crab nebula, about interstellar scatter-

ing effects, and about interplanetary scintillations. Possible future

projects involving the study of these media include the following.

1.   The theories which propose the Crab nebula as a scattering screen

predict that the narrow-band frequency structure in the radiation of the

pulsar will not follow the relation $2\pi\tau f = 1$. This prediction could be

tested with observations made near 400 MHz with a frequency resolution of

3 kHz or less. If   scintillations are observed which are not in accord

with the time delay then we could conclude that the Crab nebula does play

an important role as a scattering screen.

2.   The total flux of the pulsar (i.e. the compact source) at 111 MHz

does not appear to vary as substantially as the pulsing flux, although we

were able to observe only once per month. A program to monitor the com-

pact source over short time intervals with an interferometer could de. -

mine if the variations in total flux and pulsing flux are correlated. This

would help determine how much of the variability is attributable to scat-

tering and how much is intrinsic.

3.   The absence of small-scale structure in the Crab nebula other

than the pulsar was inferred through arguments concerning our flat visi-

bility curves, the total flux agreement between pulsar and compact source

at 196 MHz, and the position agreement between pulsar and compact source
at 311 MHz. More complete coverage of the (u,v) plane at these frequencies
would provide a good test of our inferences, and also of our assumption
that the brightness distribution of the scattering disk is Gaussian. A
VLBI experiment employing fully-steerable telescopes and baselines at
least as long as those used in this project would be needed.

Another way of investigating the small-scale structure in the nebula
would be to determine the spectra of the radiation from the filaments by
obtaining high-resolution synthesis maps of the nebula at several fre-
quencies between 1 and 10 GHz. Such a project would be an extension of
Wilson's (1972) work to higher resolutions and more frequencies and could
be done using the 35-km interferometer at NRAO or the proposed Very Large
Array (VLA).

4. The dispersion measures of many pulsars are being monitored at
several observatories. Detection of variations in this quantity would
support Cronyn's (1973) theory of a power law spectrum of irregularity
sizes. If variations are detected, monitoring of other pulsars' disper-
sion measures could provide more statistical information on the dynamics
of large irregularity sizes in the interstellar medium. Also, a detection
of dispersion measure variations in pulsars other than the Crab nebula
pulsar would also indicate a need for re-examination of the models which
propose that the nebula is responsible for the variations.

5. A concentrated program to perform simultaneous observations of
drifting diffraction patterns and angular sizes for many pulsars would
yield much-needed statistical data on the smaller irregularity sizes.
The observations presented here have shown that interstellar angular

scattering is an observable, and possibly changing, phenomenon. There is a need for simultaneous observations of every possible observable parameter of pulsars because of their great variability.

6. An investigation of the angular extent, time scale, and wavelength dependence of predicted apparent source motion could be done using an interferometer and differential phase techniques. This also would provide information on the sizes and velocities of the largest irregularities in the interstellar medium.

One should ask how or if the experiments and techniques used for the present work could be improved upon to facilitate future investigations. Unfortunately, a consideration of limiting instrumental effects shows that no order-of magnitude increase in sensitivity or accuracy can be made in the study of pulsars' angular structure for the following reasons.

To measure the apparent angular diameters more accurately, we can increase the interferometer's sensitivity or its angular resolution. For better sensitivity we require a wider bandwidth, a longer integration time, or a reduced system temperature. None of these can be achieved at low frequencies, however. Wide bandwidths cannot be used because of interference problems; the integration time cannot be increased because of ionospheric and interplanetary phase fluctuations which decorrelate the signal; and the system temperature cannot be reduced because it is dominated by the galactic background at frequencies below about 200 MHz. Even worse, for observations of the Crab nebula pulsar the nebula dominates the system temperature at all frequencies. Conventional means of increasing sensitivity do not work at low frequencies for interferometry.

Instead of reducing the noise level, we could perhaps increase the resolution so that the relative error in fringe visibility is smaller. In raising the observing frequency, we must realize that the interstellar angular scattering effect decreases as λ^2 while the fringe spacing of an interferometer only increases as λ/D where D is the baseline length. Thus, the relevant parameter for interferometric observations of interstellar scattering effects is λD. (The dependence of angular scattering on distance is also important but the effect is smaller.) To illustrate the numbers involved, table VII-1 lists the parameters for our observations

Table VII-1

Observing parameters for Crab nebula pulsar

Freq.	Wavelength	γ	$\lambda D (m^2)$
196 MHz	1.5 m	0.85	3.8×10^6
111 MHz	2.7 m	0.68	6.9×10^6
74 MHz	4.0 m	0.27	10.2×10^6

of the Crab nebula pulsar. From this table we see that to avoid complete resolution of a pulsar, we require $\lambda D \lesssim 10^7$ m^2 and to achieve partial resolution we need $\lambda D \gtrsim 10^6$ m^2. At a frequency near 400 MHz, a λD product of 5×10^6 m^2 requires a baseline $D \sim 6700$ km. Any baseline is limited to the diameter of the earth, and more reasonably to an earth radius so that mutual visibility of sources is possible. A fundamental limit to the baseline is therefore $D \lesssim 6400$ km. We can hope to observe substantial resolution of the apparent sizes only of the most distant pulsars.

The possible projects mentioned above which require VLBI techniques could be done using existing telescopes which have low-frequency capabilities.

Table VII-2 lists a few possible baselines using such telescopes at 200 MHz. The advantage of having fully-steerable dishes to provide good (u,v)-plane

Table VII-2

Possible baselines at 200 MHz

Stations	Baseline length (km)	Baseline length (Mλ)	λD product (m^2)
Jodrell Bank - Arecibo	6400	4.2	9.6×10^6
Jodrell Bank - NRAO	5720	3.8	8.6×10^6
Arecibo - Owens Valley	5260	3.5	8.0×10^6
NRAO - Owens Valley	3320	2.2	5.0×10^6
Arecibo - NRAO	2550	1.7	3.8×10^6

coverage indicates that the Jodrell Bank to NRAO baseline may be the best for the experiments proposed. When more definite programs are designed, the sensitivity of each baseline should also be taken into account.

The work presented in this thesis has only begun to untangle the many effects imposed on pulsars' radiation by the irregular interstellar medium. There are many more inquiries to be formulated and investigations to be undertaken which will shed light on the structure and dynamics of the interstellar medium.

APPENDIX A

SCHEDULING AND PREPARATION PROCEDURES

A. Pre-scheduling program

Obtaining observing time at more than one station simultaneously requires cooperation and coordination between the experimenters and telescope schedulers. Once time has been allocated, the experimenters must schedule observations such that all stations can point their telescopes to the same sources at the same time, and that there is ample time allowed to move each telescope from source to source.

We use a computer program called PRESKED which has as input a list of sources, station locations, and telescope limit stops. It calculates the times at which each source rises and sets at the selected stations. "Rise" and "set" define the time interval when the source is within the telescope's limits. The mutual visibility of a source at all the stations is also calculated. The program output is a list of the rising and setting times for each source at each telescope, accompanied by a bar graph where the mutual visibility time is blocked out in UT. This facilitates scheduling individual observations by showing at a glance which sources are "up" at which times.

B. Scheduling program

We employ computer programs for scheduling purposes also. The main program examines a proposed observing schedule and checks each run against each telescope's hour angle and elevation limits and slew   es. It flags runs which cannot be made and also indicates the error, e.g. elevation

limit or azimuth slew rate. Based on this program's output, a new schedule

is tried. After several iterations a schedule acceptable at all stations

is finalized. The program produces a copy of an observing schedule for each

station, which lists for each observation the starting time and source posi-

tion and other information. The same program prints a label for each tape

which is scheduled to be recorded and also punches the input cards for the

processing program. Because communication between the stations is not always

possible, changes to the schedule are rarely made during the course of the

experiment. Notes are added to the schedule during the experiment, such

as which tapes started late, interference levels, and clock drift rates.

The annotated schedule then serves as a station log.

C.   Station set-up

Each station in the experiment has its own peculiar set-up which de-

pends on available equipment and normal operating procedures at that tele-

scope. Figure A-1 is a block diagram of a typical station which is set up

for pulsar VLBI Mark I observations. Usually a 30-MHz IF signal is avail-

able from the front end of the telescope and is delivered to the Mark I

controller. Extra equipment is necessary for pulsar and total power record-

ings. Pulse epochs are measured (several millisecond accuracy) at one or

more stations and individual pulse intensities are recorded simultaneously

with the Mark I recording. The total power in the Mark I bandwidth is also

monitored and system calibration observations are made periodically to

measure receiver temperature and dish efficiency. Table A-1 lists the

adopted system parameters for each observing session.

Figure A-1. Typical station set up for Mark I recording of pulsar data. Several of the elements in this diagram are discussed in the text. The tape hanger is not drawn to scale and is not appropriately dressed.

Table A-1

Adopted system parameters for low-frequency experiments

Station	Parameter	Freq	Nov 71	Dec 71	Jan 72	Feb 72	Mar 72	Dec 72	Feb 73
Arecibo	Receiver temp. (K)	196	500	280	300	200	350	——	——
		111	700	650	600	600	500	400	400
		74	——	——	——	——	——	600	600
	Efficiency (K/Jy)	196	1.3	1.3	1.3	1.3	1.3	——	——
		111	3.5	3.5	3.5	3.5	3.5	2.6	2.6
		74	——	——	——	——	——	4.6	4.6
NRAO	Receiver temp. (K)	196	350	350	350	350	350	——	——
		111	170	170	170	170	170	200	200
		74	——	——	——	——	——	400	400
	Efficiency (K/Jy)	196	.93	.93	.93	.93	.93	——	——
		111	.96	.96	.96	.96	.96	1.0	1.0
		74	——	——	——	——	——	.60	.60
Sugar Grove	Receiver temp. (K)	196	375	375	375	375	375	——	——
		111	675	675	675	675	675	930	530
		74	——	——	——	——	——	900	610
	Efficiency (K/Jy)	196	.31	.31	.31	.31	.31	——	——
		111	.30	.30	.30	.30	.30	.35	.35
		74	——	——	——	——	——	.35	.37

The receiver configuration and observing techniques varied substantially from one experiment to the next. As we gradually learned better ways of handling the many potential problems involved in low-frequency VLBI observations, we altered the original receivers and other equipment and made changes in calibration procedures. Some of the items shown in figure A-1 should be mentioned as examples of the special circumstances encountered.

The feeds at NRAO and Arecibo were the standard low-frequency feeds; at Sugar Grove a special 74-MHz feed was built by A. Youmans for our experiments. At low frequencies the size of the feed can be quite large and interaction between parts of the feed and feed-support legs can result in an unusual antenna response. This is probably the cause of the asymmetric 74-MHz efficiency curve at NRAO (see figure II-8, page 33).

Tunable RF filters were used to reject as many interfering signals as possible before mixing. An interference survey was done at each station in the fall of 1972 to identify the exact band near our nominal frequencies which had the least interference. As a consequence of interference signals which did get throu..., the clipper would often saturate making some data meaningless. Big, 250-milli-watt IF amplifiers were obtained for use at each station to insure linearity of the system even when strong interference was present.

The galactic background temperature is very irregular over the sky, and since it forms a substantial fraction of the total system temperature at low frequencies, measurement of the total system emperature during each run is very important. Calibration of the last two experiments was done using a variation of the "Y-factor" method. To determine the system temperature,

we measured the amount of attenuation required to keep the signal level constant. For the earlier experiments, system temperatures were estimated using information gained from the later experiments.

At 100 MHz, the natural fringe rate on the short baseline (NRAO to Sugar Grove) is only about 1 Hz. Since earlier experiments had revealed troubles with clippers which did not give an equal number of zeros and ones, we introduced a 1-kHz offset in the local oscillator at Sugar Grove to avoid clipper bias at such a low fringe rate. This resulted in an artifical fringe rate of about 1.001 kHz on the short baseline and also added 1 kHz to the natural fringe rate on one long baseline (Arecibo to Sugar Grove). Another problem with the short baseline was that the same interference signals might occur at both NRAO and Sugar Grove, and we could observe correlation due to interference. However, such a correlation would occur at the 1-kHz fringe rate and only the true fringes would show up at a fringe rate near 1.001 kHz.

The Mark I recording system consists of a standard Ampex computer tape drive and a controller. The IF signal from the telescope is converted to video with a bandwidth of about 350 kHz. The controller clips the signal, samples it at 720 kbits/sec and sends the data, buffered in 6-bit characters, to the tape drive. One function of the controller is to start the tape recording at the time set in the schedule so that the run starts simultaneously with the other stations. The tape drive uses standard half-inch magnetic tape; it is run at its fast limit of 150 in/sec, 800 bits/in. One record is 0.2 sec long, and there are about 900 records on one tape. Table A-2 contains the data acquisition specifications. Because of the many reels of tape involved, the observing program at each station requires an observer (tape-hanger) present at all times. More detailed information on the recording system is given by Hinteregger (1972).

Table A-2

Mark I data acquisition specifications

Quantity	Value
Bandwidth	350 kHz
Sample rate = tape bit rate	720 kbit/sec
One bit	1.3888889 sec
One record	0.2 sec
Inter-record gap	~5 msec
One tape	900 records = 180 sec
One observation	one tape
Tape speed	150 inches/sec
Tape density	800 6-bit characters/inch

In order to be able to synchronize the tapes during play-back in the computer we need to know the offset from UT of the VLBI master clock. We attempt to insure that the clock at each station is set to within a few microseconds of UT. This is usually done in one of three ways: (1) We believe that the observatory clock has the correct time and use that. This has proven to be a disastrous assumption on enough occasions that (2) we require that the station clock be checked against Loran and WWV transmissions. For best insurance, however, (3) we carry a rubidium clock standard to the Naval Observatory or the Goddard Space Flight Center clock laboratory, set the time, and transport the clock to the telescope. The clocks are "set" most accurately after the experiment by processing several tapes which were recorded on strong sources and searching for the clock offset which yields the largest correlation coefficient.

APPENDIX B

INTERFEROMETER PHASE

The expression used to calculate the **a priori** phase is derived below,
and the result is used in the description of the operation of the two main
processing programs, VLBI1 and VLBI2, in Chapter II.

In general, the fringe phase is given by

$$\phi(t) = \omega\tau_g(t) + \Delta\omega_{LO}\Delta t_{LO} \qquad (B-1)$$

where ω = total local oscillator frequency,

τ_g = true geometrical delay which changes with hour angle,

$\Delta\omega_{LO}$ = offset between local oscillators,

t_{LO} = time elapsed since $\Delta\omega_{LO}$ started at τ_{LO}.

Note that only the total local oscillator frequency enters the calculation.
This is because the geometrical time delay, τ_g, occurs in the RF signal and
the compensating delay introduced by the processing programs is inserted
into the video signal.

A Tay or series expansion is made for the true time delay:

$$\tau_g(t) = \tau_g(t_o) + \dot{\tau}_g(t)(t - t_o) \qquad (B-2)$$

where t_o = nominal start time of the observation, in univ\rsal time,

$\dot{\tau}_g$ = time rate of change of geometrical delay.

The total calculated phase is

$$\phi_{calc}(t) = \left[\omega\,\tau_g(t_o + \tau_e)\right] + \left[(\dot{\tau}_g(t)\omega + \Delta\omega_{LO})\,\Delta t_R\right]$$
$$+ \left[\Delta\omega_{LO}\Delta t_{LO}\right] \qquad (B-3)$$

where τ_e = difference between clock epochs at the two stations,

$\Delta\tau_R$ = time elapsed since the reference time t_o.

Each term of equation B-3 will be discussed separately next.

The first term in square brackets of equation B-3 is called the "funda-mental phase," ϕ_o,

$$\phi_o = \omega\tau_g(t_o + \tau_e) \qquad \text{(B-4)}$$

which accounts for the geometrical delays. The delay is calculated at the nominal start of the observations, including the known clock offsets. The next term refers to the change of geometrical delay as the earth rotates; this is the fringe rate. The fringe phase is counted from the reference time t_o. The "total fringe rate," f, is

$$f = \dot{\tau}_g\omega + \Delta\omega_{LO} \qquad . \qquad \text{(B-5)}$$

The last term is the phase of the oscillator which is used to offset the fringe rate if necessary. Its phase is counted from the time at which the oscillator was started. This time, t_{LO}, is specified in UT. The total calculated phase can now be written as:

$$\phi(t)_{calc} = \phi_o + f\Delta t_K + \Delta\omega_{LO}\Delta t_{LO} \qquad . \qquad \text{(B-6)}$$

This expression is used in Chapter II, section B, as equation II-1.

APPENDIX C

REPLICATION OF PULSAR FRINGES

Pulsar fringes are replicated because the source signal is a periodic function. As an aid to understanding how this happens, figure C-1 is presented. The symbols and functional representations used here follow the style of Bracewell (1965). Explanations for the symbols and values of the numerical quantities used are given in table C-1. (These symbols are used only in this appendix and are no' the same as in the main text.)

Part (a) of figure C-1 is a sample of a span of data recorded on a pulsar with a period of about 0.62 sec using the Mark I system. An ana-lytic representation of the interferometer response as a function of time is shown in (b). Graphical sketches of each term are in (c). The fringe rate spectrum is the Fourier transform of the response; a representation is shown in (d). The convolution theorem for Fourier transforms was employed in passing from the time domain to the frequency domain. Sketches of each term in the fringe rate spectrum are given in (e) and the total spectrum is drawn in (f). The spectrum illustrated is a cut through the (τ_R, f_R) plane of figure II-7 (page 25) along the sloping axis. For most pulsars, the parameter G is very small so the spectrum lies nearly along the f_R axis.

The basic sampling interval, with the gating technique, is the pulse period, and the noise spectrum extends only out to frequencies $\pm 1/2P$ Hz instead of ± 2.5 Hz as for a continuum source. However, note that the amplitudes of the Fourier harmonics are modulated both by the pulse shape transform and by the basic sampling window transform of full width 10 Hz. The true amplitudes can be obtained by first demodulating with the calculated

141

REPLICATION OF PULSAR FRINGES

(a) SAMPLE SPAN OF DATA.

$$\mathbb{R}(t) = \left[A(t) \times \pi(T)\right] \times \left[I_P(t) \times \pi(W_G) * \text{Ш}(P)\right] \times \left[\text{Ш}(R) * \pi(D)\right] \times \left[\text{Ш}(R)\right]$$

FRINGES OBSERVING PULSE GATE PULSE RECORD DATA SAMPLING
WINDOW SHAPE WINDOW REPETITION REPETITION WINDOW FUNCTION

(b) REPRESENTATION OF (a) IN FUNCTIONAL FORM.

(c) GRAPHICAL REPRESENTATION OF (b).

$$\mathbb{P}(f) = \left[F(f) * \text{sinc} (1/T)\right] * \left[F_P(f) * \text{sinc} (1/W_G) \times \text{Ш}(1/P)\right] * \left[\text{Ш}(1/R) \times \text{sinc} (1/b)\right] * \left[\text{Ш}(1/R)\right]$$

FRINGE RESOLUTION PULSE GATE SAMPLING SAMPLING FRINGE REPLICATION
SPECTRUM MODU- SHAPE MODULATION FUNCTION FUNCTION MODU- OF PATTERN
LATION TRANSFORM LATION

(d) FOURIER TRANSFORM OF (b).

(e) GRAPHICAL REPRESENTATION OF (d)

(f) TOTAL FRINGE RATE SPECTRUM (Entire pattern replicated every 1/R Hz).

Figure C-1. Replication of pulsar fringes. Refer to table C-1 and the text for explanation of the symbols used. The fringe amplitude in (f) will be modulated by the long-dashed curve as well as by the short-dashed curve.

Table C-1

Explanation of symbols in figure C-1

Symbol	Explanation
t	time
f	fringe frequency
P	pulse period, ~0.62 sec in this example
w_P	pulse width
w_g	gate width, ~50 msec in this example
D	data span ~190 msec
I	inter-record gap ~5 msec
R	record interval = 0.2 sec
T	total length of observation = 180 sec
$\Pi(x)$	box-car function of width x
$\mathrm{III}(y)$	picket fence function: infinite series of delta functions spaced y apart
sinc(z)	$\sin(\pi z)/\pi z$ function of half-width z
x	multiplication
*	convolution

value of sinc x at the appropriate frequencies. We could then turn to
the Fourier component method described in Chapter II se. _ion B-3 and re-
construct a pulse shape using equation II-14.

INTERFEROMETER INSTRUMENTAL POLARIZATION

A. Theory

An unwanted response results from incomplete isolation of the right circularly polarized (RCP) feed from the left circularly polarized (LCP) feed of an antenna. The RCP feed responds to a fraction (f) of the LCP component of the signal, and only responds to a fraction (1-f) of the RCP component. The quantity f is the single-telescope instrumental polarization. The response of an interferometer formed by two telescopes which have non-zero values for f is reduced because the RCP and LCP components of the signal are not correlated. This effect can be corrected for if values of f, or some other calibrated quantity, are known. The expression for a correction factor is derived as follows.

The total power observed with an RCP feed at stations 1 and 2 is,

$$P^o_{1R} = (1 - f_1)P_{1R} + f_1 P_{1L}$$

$$P^o_{2R} = (1 - f_2)P_{2R} + f_2 P_{2L}$$

where P_{1R} and P_{2R} = true RCP component of power,

P^o_{1R} and P^o_{2R} = observed RCP component of power,

f_1 and f_2 = fractional response of antenna to oppositely polarized radiation; "instrumental polarization" of single telescopes (ideally, $f_1 = f_2 = 0$).

If we assume all the phase angle differences average to zero and there is no circular polarization in the source radiation, then $P_{1R} = P_{1L}$ and $P_{2R} = P_{2L}$.

145

Let

$$\beta = f_1 + f_2 - 2f_1 f_2$$

and

$$m = \rho_{LR}/\rho_{RR} \quad .$$

The quantity m is **the true** fractional linear polarization of the source's correlated flux; ρ_{RR} and ρ_{RL} are the total and linearly polarized flux, respectively. When each antenna observes with an RCP feed the observed correlated power is

$$\rho_{RR}^{o} = \rho_{RR} \left[1 - \beta + m^2 \beta \right]^{1/2} \quad .$$

When one antenna observes with an RCP feed and the other with an LCP feed, the correlation coefficient is:

$$\rho_{RL}^{o} = \rho_{RR} \left[\beta + m^2 \right]^{1/2} \quad .$$

Let the fraction α be the ratio of the correlation coefficient observed with similarly- and oppositely-polarized feeds and call it the "instrumental polarization" of the interferometer. Then α is a directly observable quantity (we assume the term $m^2 \beta$ is negligible):

$$\alpha = \rho_{RL}^{o}/\rho_{RR}^{o} = \left[\frac{\beta + m^2}{1 - \beta} \right]^{1/2}$$

The true correlation coefficient for an unpolarized source can be obtained by:

$$\rho_{RR} = \rho_{RR}^{o} (1 + \alpha^2)^{1/2} \quad .$$

To determine m, an unpolarized calibrator source must be observed
to obtain values of α_c for the calibrator source. The polarized source
determines α_p. Then

$$m = \left[\frac{\alpha_p^2 - \alpha_c^2}{1 + \alpha_c^2}\right]^{1/2}$$

In principle, very low values of m can be measured even though α_c is large,
provided that α_c and α_p can be accurately determined. Figure D-1 contains
curves from which m can be read once α_p and α_c are known.

Unless the source is circularly polarized we should observe that
$\rho_{RR} = \rho_{LL}$ and unless there is a nonlinear effect at one antenna we should
also observe that $\rho_{RL} = \rho_{LR}$. Deviations from these equalities are attrib-
utable to noise, coupling between dipoles, interaction between the feed
and feed-support legs, or other unknown factors.

B.   Application

The values of α were obtained from observations of strong extra-
galactic sources which were assumed to be unpolarized. The sources we
used were: 3C273, 3C286, 3C287, 3C298. At the NRAO station, the received
signal was switched at a 2.5 Hz rate so that alternate records on the tape
were recorded with the RCP and LCP feeds. At Arecibo and Sugar Grove, the
entire tape was recorded with either the RCP or LCP feed. Then the cross-
correlation output from the Arecibo-NRAO or NRAO-Sugar Grove baselines is
alternately ρ_{RR} and ρ_{RL}, or whatever combination occurred. An estimate
of the quantity α can then be computed from each tape without the need
for normalization and its attendant errors. The only assumption necessary
is that the LCP and RCP feeds have the same efficiency.

148

Figure D-1. Intrinsic fractional linear polarization of a
source (m) vs. observed fraction of linear polarization (α)
for various values of instrumental linear polarization (α_c).

This procedure was followed in 1972 January and February and the calibrations were assumed to apply for the remaining months since the feeds were the same. In 1972 December and 1973 February extensive polarization observations were made for calibration purposes. Since the feeds were different for each experiment the values of f and α are different also. The observed values of α and the derived values of f are in Tables II-5 and II-6 of Chapter II (page 39). The calibrations and effect on the experiment are discussed in the main text (pages 37-40).

APPENDIX E

CATALOGUE OF FOURIER COMPONENTS AND PULSE SHAPES

FOR THE CRAB NEBULA PULSAR AT 196 MHZ

The tables which follow contain the amplitudes and phases of the
complex correlation coefficients detected in each three-minute observa-
tion of the Crab nebula pulsar at 196 MHz. The title of each table indi-
cates whether the data is from short- or long-baseline runs. Each column
of the tables is labelled as to its contents,a description of which follows.

Columns 1 and 2 give the run number and date of each observation.
Column 3 (TIME) contains the UT at which the observation started. Column 4
(BASE) indicates the baseline on which the observation was made, and each
letter indicates the station (A for Arecibo, N for NRAO, S for Sugar Grove).
Column 5 contains the TOTAL FLUX (in Janskys); this is the total time-averaged
flux, i.e. the compact source flux. These numbers were used to compute the
average fluxes presented in table III-1 (page 47). Columns 5, 6, 8, 10, 12,
and 14 are the amplitudes, A_n where n=0 to 5, and columns 7, 9, 11, 13, and
15 are the phases, φ_n where n=1 to 5, of the Fourier components of the aver-
age pulse shape (see equation II-5, page 22). The top line for each run
contains the components for n > 0, the second line is for n < 0. The phases
are given in degrees relative to the phase of the n=0 component. The phase
convention used for this table is that, apart from noise, phases of a pair
of components for the same value of n should be equal. Runs for which only
the amplitude of the n=0 component is listed were usually too weak, contained
excessive tape errors after many processings, or had components which were
too noisy to be reliably detected.

150

The fifth column from the right (3 SIG LEVEL) contains the 3σ de..ection level; any component amplitudes below this value were probably not detected. The third and fourth columns from the right (PHASE) indicate the signed deviation of the +n and -n component phases from equality and the rms deviation. These numbers were used in calculating the averages found in table IV-5 (page 81). The second column from the right (PULSE PEAK) gives the height of the maximum of the pulse profile. This was used for editing purposes. The last column (FRACTION PULSING) indicates the fraction of the total flux which is contained in pulsing power; at 196 MHz all of the power is pulsing.

Plots of the pulse profiles follow the tables. The baseline, frequency, and the month and year are indicated; the flux scales are in Janskys. The profiles have been superimposed by simply matching the peaks. The average profiles are therefore incoherent averages.

Table E-1

CRAB NEBULA PULSAR FLUX FOR SHORT BASELINE AT 196 MHZ

RUN NUMBER	DATE	TIME (UT)	BASE	TOTAL FLUX(JY) N=0	±1 AMP	±1 PHASE	±2 AMP	±2 PHASE	±3 AMP	±3 PHASE	±4 AMP	±4 PHASE	±5 AMP	±5 PHASE	3 SIG LEVEL (JY)	PHASE DEV (DEGREES)	PHASE RMS	PULSE PEAK (JY)	FRACTION PULSING
23063	23NOV.71	6:27	NS	8.0	3.8	327	5.4	209	2.9	165	3.1	46	2.9	13	1.8	6.2	13.2	31.6	1.00
					4.0	296	5.0	219	3.5	161	2.6	56	2.7	-35					
23070	23NOV.71	7: 2	NS	7.9	3.5	149	5.4	230	3.1	28	3.3	137	1.7	221	1.8	0.9	9.7	32.0	1.00
					4.4	151	5.1	235	4.3	15	3.9	106	2.4	248					
19042	19DEC.71	4:36	NS	5.9	2.9	57	5.4	109	2.3	183	3.0	228	3.1	299	1.9	-10.6	10.7	28.5	1.00
					3.8	78	5.7	121	2.7	172	2.4	266	2.4	345					
19043	19DEC.71	4:42	NS	7.4	5.8	107	6.5	45	4.5	228	3.9	210	3.1	138	3.5	-30.4	37.2	23.7	1.00
					6.1	107	6.7	94	3.7	326	4.7	250	2.7	257					
19058	19DEC.71	5:12	NS	8.0	4.2	150	5.9	278	3.6	75	3.2	213	2.5	-70	2.8	-30.7	05.7	28.9	1.00
					3.7	236	4.7	324	3.4	111	3.4	215	3.1	105					
19059	19DEC.71	5:18	NS	7.3	2.0	339	3.2	333	0.0	24	0.0	264	3.1	356	9.9	8.0	23.1	17.2	0.91
					1.9	350	2.9	336	0.0	-54	2.1	302	0.0	303					
1905A	19DEC.71	5:24	NS	7.6	4.0	209	4.9	352	2.4	216	2.6	-98	2.2	153	1.8	-37.7	48.8	22.9	1.00
					3.3	299	5.2	334	3.1	251	2.8	64	2.1	276					
1905B	19DEC.71	5:30	NS	7.7	4.1	33	5.5	26	4.3	55	3.0	60	2.9	133	1.9	7.0	21.0	30.0	1.00
					4.6	43	5.2	33	3.3	59	2.7	65	1.8	38					
28001	28FEB.72	0:10	NS	9.7	4.9	336	6.8	253	4.0	218	3.2	133	2.8	144	1.7	2.9	10.9	00.2	1.00
					5.5	320	6.2	251	4.3	242	4.2	137	3.6	105					
28004	28FEB.72	0:28	NS	10.4	5.2	352	6.9	323	4.3	-26	3.9	299	2.7	-11	1.7	-18.3	22.6	00.9	1.00
					5.5	345	7.1	351	4.6	43	3.6	357	3.8	21					
28005	28FEB.72	0:34	NS	10.2	4.9	145	7.0	243	4.0	41	3.9	112	2.8	299	1.7	-10.2	16.1	01.8	1.00
					6.0	163	7.0	253	5.0	70	3.8	167	3.6	331					
28008	28FEB.72	0:52	NS	9.5	4.6	179	6.7	-16	4.7	220	4.0	32	3.4	131	0.8	0.6	9.2	00.5	1.00
					4.8	176	6.4	9	4.9	180	4.3	25	2.6	201					

Table E-2

CRAB NEBULA PULSAR FLUX FOR LONG BASELINES AT 196 MHZ

RUN NUMBER	DATE	TIME BASE (UT)	TOTAL FLUX(JY) N=0	FOURIER COMPONENTS — AMP(JY) AND PHASE (DEG. REL. TO N=0) ±1	±2	±3	±4	±5	3 SIG LEVE. (JY)	PHASE DEV (DEGREES)	RMS (DEGREES)	PULSE PEAK (JY)	FRACTION PULSING
23061	23NOV.71	6:13 AM	5.1	128	233	10	43	0	1.5	-32.1	36.7	21.7	1.00
23062	23NOV.71	6:20 AS	4.6	185	273	47	167	0	1.7	25.1	48.6	18.0	1.00
23063	23NOV.71	6:27 AN	4.9	68	41	37	75	179	1.4	-19.5	39.1	21.9	1.00
23063	23NOV.71	6:27 AS	4.3	76	24	91	-59	19	1.6	-13.3	38.1	20.5	1.00
23072	23NOV.71	7:?	5.8	307	208	134	-20	-133	1.8	14.3	21.4	24.8	1.00
24065	24NOV.71	6:?	4.5	0	0	0	0	0	1.7	0.0	0.0	0.0	0.0
24067	24NOV.71	6:5	5.3	89	84	186	144	233	1.4	1.2	11.0	21.9	1.00
19031	19DEC.71	3:22	6.1	77	95	157	180	266	1.6	16.8	22.1	24.6	1.00
19032	19DEC.71	3:30 AS	6.8	230	353	159	337	161	1.6	28.5	45.8	13.7	1.00
19033	19DEC.71	3:38 AS	7.1	141	296	153	273	209	2.7	1.6	40.3	20.3	1.00
19042	19DEC.71	4:36 AN	4.6	55	-104	278	38	257	1.6	1.3	16.6	21.0	1.00
19042	19DEC.71	4:36 AS	3.5	18	312	143	44	180	1.6	0.0	0.0	0.0	0.0
19058	19DEC.71	5:12 AN	7.1	-20	323	289	284	319	1.4	4.0	11.1	29.3	1.00
19058	19DEC.71	5:12 AS	7.8	64	119	268	178	241	1.6	-10.0	34.6	32.1	1.00
19059	19DEC.71	5:18 AN	6.7	91	284	202	166	273	1.3	-14.0	17.7	22.9	1.00
19059	19DEC.71	5:18 AS	8.2	173	276	160	176	53	1.6	17.0	21.5	32.0	1.00
19059	19DEC.71	5:24 AN	6.1	172	301	96	222	7	8.2	8.1	9.4	26.3	1.00
1905A	19DEC.71	5:24 AS	7.2	198	292	110	223	19	1.7	1.2	16.8	27.8	1.00
1905A	19DEC.71	5:24 AS	6.9	181	327	99	235	167	1.4	-4.3	12.2	29.1	1.00
19058	19DEC.71	5:30 AN	4.1	-18	336	112	282	309	1.6	0.0	0.0	0.0	0.0
20044	20DEC.71	4:44 AN	4.1	296	300	51	208	40	1.4	0.0	0.0	0.0	0.0
20045	20DEC.71	4:50 AN	4.2	164	280	154	316	40	1.3	-6.2	44.9	14.4	1.00

Table E-2 (continued)

CRAB NEBULA PULSAR FLUX FOR LONG BASELINES AT 196 MHZ

RUN NUMBER	DATE	TIME BASE (UT)	TOTAL FLUX(JY) N=0	FOURIER COMPONENTS AMP(JY) AND PHASE (DEG. REL. TO N=0) ±1	±2	±3	±4	±5	3 SIG LEVEL (JY)	PHASE DEV (DEGREES)	RMS	PULSE PEAK (JY)	FRACTION PULSING
23022	23JAN.72	2:23 AM	11.0	5.2 / 213	7.1 / 329	5.4 / 170	3.7 / 320	3.3 / 124	1.3	4.1	9.0	42.5	1.00
23023	23JAN.72	2:29 AN	6.8	5.0 / 125	7.3 / 314	5.4 / 190	4.2 / 294	4.4 / 120		3.4	11.8	28.6	1.00
23026	23JAN.72	2:47 AM	7.8	3.4 / 47	3.6 / 50	3.6 / 64	2.7 / 69	2.0 / 73	1.8	5.4	7.6	33.1	1.00
23027	23JAN.72	2:53 AM	7.6	4.3 / 13	5.1 / 24	3.9 / 54	2.7 / 78	2.7 / 101	1.2	-15.3	20.8	32.3	1.00
23031	23JAN.72	3:11 AM	7.9	3.6 / 311	5.8 / 211	4.1 / 149	3.1 / 55	2.5 / 10	1.7	3.8	9.0	33.8	1.00
24021	24JAN.72	2:7 AM	7.0	3.8 / 291	5.8 / 193	4.1 / 138	3.1 / 47	2.6 / -6	1.3	1.9	18.0	27.3	1.00
24022	24JAN.72	2:13 AM	7.8	4.4 / 162	4.9 / 246	2.6 / 9	2.6 / 143	2.6 / 264	1.0	20.5	35.5	29.1	1.00
24025	24JAN.72	2:31 AN	6.6	4.7 / 141	5.8 / 288	4.2 / 70	3.5 / 191	2.6 / 288	1.9	-1.7	8.9	28.9	1.00
24026	24JAN.72	2:37 AM	6.9	4.1 / 62	5.8 / 112	4.4 / 158	3.1 / 167	2.9 / 234	1.2	23.4	32.6	24.5	1.00
26235	26FEB.72	23:56 AM	6.0	3.9 / 71	5.3 / 76	4.1 / 137	3.7 / 171	2.9 / 239	1.7	32.1	33.0	25.9	1.00
27000	27FEB.72	0:2 AM	8.6	4.0 / 11	5.3 / 18	3.3 / 88	2.2 / 333	2.8 / -19	1.4	1.2	8.8	40.1	1.00
27003	27FEB.72	0:20 AM	8.2	2.5 / 10	4.8 / 8	3.2 / 21	3.4 / 349	1.9 / 22	1.3	-22.8	24.3	30.9	1.00
27004	27FEB.72	0:26 AM	6.9	3.6 / 277	4.4 / 88	3.1 / 6	3.1 / 112	1.6 / 276	1.3	-11.7	18.5	33.0	1.00
27007	27FEB.72	0:44 AM	6.6	4.6 / 223	4.9 / 57	3.5 / -81	3.4 / 15	3.4 / 341	1.3	-9.1	1.0	29.8	1.00
27008	27FEB.72	0:50 A	5.7	3.6 / 169	4.3 / 305	3.3 / 112	4.5 / 229	2.2 / 46	1.3	-11.9	15.3	25.8	1.00
28000	28FEB.72	0: AM	5.6	3.3 / 43	5.4 / 314	3.1 / 112	4.1 / 236	2.8 / 73	1.3	3.7	25.9	21.8	1.00
28000	28FEB.72	0:10 AM	5.5	4.2 / 62	5.6 / 49	3.5 / 45	3.1 / 22	2.8 / 92	1.2	12.8	19.5	23.2	1.00
28001	28FEB.72	0:10 AS	6.8	3.5 / -24	6.6 / -40	2.6 / 81	3.8 / -9	2.6 / 20	1.5	10.3	12.2	26.0	1.00
28004	28FEB.72	0:28 AS	5.0	3.7 / 51	4.5 / -20	2.4 / 0	2.1 / 57	1.7 / 86	1.5	19.8	47.0	11.7	1.00
28005	28FEB.72	0:34 AM	6.5	3.3 / -11	4.9 / -32	3.4 / -43	2.6 / -21	2.0 / 2	1.2	5.8	18.6	28.6	1.00

Table E-2 (continued)

CRAB NEBULA PULSAR FLUX FOR LONG BASELINES AT 196 MHZ

RUN NUMBER	DATE	TIME BASE (U.T)		TOTAL FLUX(JY) N=0	AMP(JY)/PHASE ±1	±2	±3	±4	±5	3 SIG LEVEL (JY)	PHASE DEV (DEGREES)	RMS	PULSE PEAK (JY)	FRACTION PULSING
2800 5	28FEB.72	0:34	AS	6.8	3.0 158	4.2 254	2.1 3	2.7 126	1.7 312	1.5	4.7	17.9	27.6	1.00
2807 8	28FEB.72	0:52	AN	6.3	4.0 167	4.7 271	3.8 27	2.5 57	2.1 292	1.0	-2.0	20.0	25.5	1.00
					3.1 190	4.0 -37	2.5 226	2.5 333	2.2 193					
2800 3	28FEB.72	0:52	AS	6.7	3.1 171	4.8 -	3.6 157	2.6 353	2.1 236					
					2.2 211	3.9 1	2.9 213	2.3 358	1.8 223	1.5	4.1	10.0	26.5	1.00
					3.3 205	4.9 6	3.4 226	3.0 347	2.0 182					
25222	25MA/	2 22:12	AN	7.6	0.0 0	0.0 0	0.0 0	0.0 0	0.0 0	1.3	0.0	0.0	0.0	0.0
25223	25MA	2 22:18	AN	6.4	0.0 0	0.0 0	0.0 0	0.0 0	0.0 0	1.7	0.0	0.0	0.0	0.0
25226	25MAR.72	22:36	AN	6.6	0.0 0	0.0 0	0.0 0	0.0 0	0.0 0	1.2	0.0	0.0	0.0	0.0

Figure E-1. Individual and average pulse shapes at 196 MHz.

Figure E-1. (continued)

APPENDIX F

CATALOGUE OF FOURIER COMPONENTS AND PULSE SHAPES

ιυR THE CRAB NEBULA PULSAR AT 111 MHZ

The tables which follow contain the amplitudes and phases of the
complex correlation coefficients detected in each three-minute observa-
tion of the Crab nebula pulsar at 111 MHz. Explanations of the contents
of each column were given on the first page of Appendix E, page 150.
For the 111-MHz data, the last column (FRACTION PULSING) was used to
compute the averages found in table IV-3 (page 78) and plotted in fig-
ure IV-5 (page 77). Although three Fourier components are listed for
each run, the n = ±3 components are often not detected in December 1972
and February 1973. For these dates, only the first two components were
used in constructing the pulses.

Table F-1

CRAB NEBULA PULSAR FLUX FOR SHORT BASELINE AT 111 MHZ

RUN NUMBER	DATE	TIME (UT)	BASE	TOTAL FLUX(JY) N=0	FOURIER COMPONENTS AMP(JY) AND PHASE (DEG. REL. TO N=0) ±1	±2	±3	±4	±5	3 SIG LEVEL (JY)	PHASE DEV (DEGREES)	PHASE RMS	PULSE PEAK (JY)	FRACTION PULSING
240J0	24NOV.71	6: 2	2 NS	48.8	10.9 / 340	8.9 / 23	4.4 / 114	0.0 / 0.0	0.0 / 0.0	3.3	9.8	24.6	87.1	0.72
24063	24NOV.71	6:23	NS	52.4	11.4 / 322	8.2 / 58	4.9 / 38	0.0 / 0.0	0.0 / 0.0	3.9	0.0	0.0	0.0	0.0
24068	24NOV.71	6:58	NS	48.8	5.9 / 11	5.8 / 115	5.7 / 164	0.0 / 0.0	0.0 / 0.3	2.9	-17.5	41.2	69.8	0.46
20062	20DEC.71	4:22	NS	46.8	10.3 / 90	5.4 / 268	3.7 / 100	0.0 / 0.0	0.0 / 0.0	3.0	-2.8	15.5	79.8	0.50
20063	20DEC.71	4:36	NS	45.5	8.3 / 261	6.1 / 238	3.5 / 50	0.0 / 0.0	0.0 / 0.0	8.4	18.4	19.9	75.2	0.48
20051	20DEC.71	5: 8	NS	44.9	9.2 / 211	6.6 / 190	3.2 / 117	0.0 / 0.0	0.0 / 0.0	2.9	-3.2	16.2	76.4	0.57
27001	27FEB.72	0: 8	NS	50.5	7.9 / 269	6.0 / 146	1.9 / 102	0.0 / 0.0	0.0 / 0.0	2.9	7.4	34.0	78.2	0.48
27002	27FEB.72	0:14	NS	50.2	10.2 / 294	6.4 / 301	3.2 / 120	0.0 / 0.0	0.0 / 0.0	2.9	17.1	24.4	79.3	0.65
27005	27FEB.72	0:32	NS	49.6	9.2 / 74	6.1 / 263	3.5 / 153	0.0 / 0.0	0.0 / 0.0	2.6	-16.4	21.5	81.4	0.61
27006	27FEB.72	0:38	NS	46.8	7.8 / 93	7.3 / 277	3.5 / 98	0.0 / 0.0	0.0 / 0.0	2.8	-1.9	62.8	79.0	0.68
08050	08DEC.72	5: 3	NS	36.1	9.4 / 341	7.1 / 321	4.9 / -9	0.0 / 0.0	0.0 / 0.0	3.7	-0.9	47.3	50.3	0.20
08051	08DEC.72	5: 9	NS	37.0	10.6 / 323	6.2 / 31	5.2 / 155	0.0 / 0.0	0.0 / 0.0	4.0	-26.2	52.1	50.3	0.34
08052	08DEC.72	5:15	NS	37.6	8.6 / 296	6.6 / 29	5.7 / -73	0.0 / 0.0	0.0 / 0.0	4.2	13.2	57.4	49.9	0.27
08053	08DEC.72	5:21	NS	37.6	9.6 / 293	7.1 / 319	3.9 / -46	0.0 / 0.0	0.0 / 0.0	3.9	53.4	53.6	48.0	0.26
08054	08DEC.72	5:27	NS	40.0	8.4 / 113	6.5 / 357	4.9 / 17	0.0 / 0.0	0.0 / 0.0	3.9	0.0	0.0	0.0	0.0
08055	08DEC.72	5:33	NS	35.0	9.0 / 196	9.4 / 308	5.2 / 80	0.0 / 0.0	0.0 / 0.6	3.8	9.2	49.7	45.1	0.29
08056	08DEC.72	5:39	NS	36.0	15.2 / 143	8.8 / 134	5.2 / 182	2.5 / 89	0.0 / 0.0	3.6	49.7	52.4	83.7	0.35
08057	08DEC.72	5:45	NS	34.3	2.1 / 188	5.2 / 83	3.1 / 236	2.0 / 45	0.0 / 0.0	8.0	29.4	31.1	45.4	0.53
08058	08DEC.72	5:51	NS	33.4	5.7 / 11	2.7 / -28	3.3 / 340	0.0 / 0.0	0.0 / 0.0	3.8	21.5	25.5	87.9	0.56
08059	08DEC.72	5:57	NS	34.5	6.0 / -6	5.0 / 89	2.6 / 187	0.0 / 0.0	0.0 / 0.0	3.7	21.3	42.0	47.8	0.29
0-060	08DEC.72	6: 3	NS	31.2	4.4 / 253	3.3 / 269	2.6 / 183	0.0 / 0.0	0.0 / 0.0	3.7	41.7	56.9	41.7	0.36

Table F-1 (continued)

CRAB NEBULA PULSAR FLUX FOR SHORT BASELINE AT 111 MHZ

RUN NUMBER	DATE	TIME BASE (UT)	TOTAL FLUX(JY) N=0	FOURIER COMPONENTS AMP(JY) AND PHASE (DEG. REL. TO N=0) ±1	±2	±3	±4	±5	3 SIG LEVEL (JY)	PHASE DEV (DEGREES)	RMS	PULSE PEAK (JY)	FRACTION PULSING
08061	08DEC.72	6: 9 NS	39.1	5.3 / 74	5.3 / 241	3.6 / 202	0.0 / 0	0.0 / 0	5.8	9.7	68.7	46.8	0.27
08062	08DEC.72	6:15 NS	38.2	0.0 / 0	0.0 / 0	0.0 / 0	0.0 / 0	0.0 / 0	4.4	0.0	0.0	0.0	0.0
08065	09DEC.72	4:59 NS	32.0	0.7 / 21	2.7 / 93	2.2 / 44	0.0 / 0	0.0 / 0	4.0	-26.4	32.2	43.7	0.49
09050	09DEC.72	5: 5 NS	32.5	2.3 / 188	3.5 / 316	4.1 / 191	0.0 / 0	0.0 / 0	4.2	39.6	44.1	39.3	0.37
09053	09DEC.72	5:23 NS	39.0	0.0 / 0	0.0 / 0	0.0 / 0	0.0 / 0	0.0 / 0	3.8	0.0	0.0	0.0	0.0
09055	09DEC.72	5:35 NS	28.8	2.5 / 62	2.5 / 284	2.0 / 190	0.0 / 0	0.0 / 0	3.7	27.3	31.7	36.2	0.41
09056	09DEC.72	5:41 NS	37.4	2.0 / 53	0.7 / 204	2.0 / 117	0.0 / 0	0.0 / 0	3.6	-5.3	34.5	51.1	0.39
09057	09DEC.72	5:47 NS	30.3	5.9 / 260	2.0 / 185	2.5 / 103	0.0 / 0	0.0 / 0	3.6	-7.2	37.0	63.0	0.31
09058	09DEC.72	5:53 NS	30.8	6.8 / 291	1.4 / 290	2.0 / 245	0.0 / 0	0.0 / 0	3.7	0.0	0.0	0.0	0.0
09059	09DEC.72	5:59 NS	38.0	4.0 / 18	5.0 / 202	2.0 / 315	0.0 / 0	0.0 / 0	4.5	-11.2	54.7	53.2	0.50
09060	09DEC.72	6: 5 NS	37.0	4.0 / 80	7.4 / 242	4.0 / 0	0.0 / 0	0.0 / 0	3.7	0.0	0.0	0.0	0.0
09061	09DEC.72	6:11 NS	38.7	4.5 / 55	4.0 / 228	4.0 / -98	0.0 / 0	0.0 / 0	3.9	-50.3	52.1	55.6	0.23
09062	09DEC.72	6:17 NS	36.5	7.0 / -30	0.0 / 0	0.0 / 69	0.0 / 0	0.0 / 0	8.0	18.8	34.7	50.6	0.51
24237	24FEB.73	23:56 NS	45.0	6.4 / -89	4.3 / 155	3.8 / 133	0.0 / 0	0.0 / 0	4.5	0.0	0.0	0.0	0.0
25000	25FEB.73	0: 4 NS	39.0	3.3 / 5	5.9 / 226	2.7 / 270	0.0 / 0	0.0 / 0	3.5	0.0	0.0	0.0	0.0
25001	25FEB.73	0:10 NS	38.8	6.0 / -3	5.0 / 293	4.3 / 0	0.0 / 0	0.0 / 0	3.2	-24.1	43.8	55.4	0.56
25002	25FEB.73	0:16 NS	41.0	7.1 / 17	5.0 / 197	0.0 / 0	0.0 / 0	0.0 / 0	3.3	-2.2	25.9	58.4	0.47
25004	25FEB.73	0:28 NS	42.8	6.1 / 129	5.7 / 320	2.7 / -74	0.0 / 0	0.0 / 0	3.3	12.1	39.2	55.2	0.25
25005	25FEB.73	0:34 NS	34.0	7.4 / 94	4.4 / 357	1.8 / 68	0.0 / 0	0.0 / 0	3.2	0.0	0.0	0.0	0.0
25006	25FEB.73	0:40 NS	42.1	4.7 / 244	5.8 / 172	1.6 / 66	0.0 / 0	0.0 / 0	3.3	-4.4	4.4	62.0	0.36
25007	25FEB.73	0:46 NS	43.0	8.7 / 178	4.7 / 227	2.7 / 90	0.0 / 0	0.0 / 0	4.3	0.0	0.0	0.0	0.0
25008	25FEB.73	0:52 NS	45.0	3.6 / 95	5.2 / 221	3.0 / 146	0.0 / 0	0.0 / 0	3.5	0.0	0.0	0.0	0.0
25009	25FEB.73	0:58 NS	41.8	3.0 / 149	3.0 / 320	1.2 / 21	0.0 / 0	0.0 / 0	3.4	34.6	43.9	57.5	0.33
26237	25FEB.73	23:54 NS	44.9	5.4 / 271	4.8 / 231	8.7 / 0	0.0 / 0	0.0 / 0	3.8	-12.4	24.8	67.4	0.46

CRAB NEBULA PULSAR FLUX FOR SHORT BASELINE AT 111 MHZ

Table F-1 (continued)

RUN NUMBER	DATE	TIME BASE (UT)	TOTAL FLUX(JY) N=0	FOURIER COMPONENTS AMP(JY) AND PHASE (DEG. REL. TO N=0) ±1		±2		±3		±4	±5	3 SIG LEVEL (JY)	PHASE DEV (JY)	PHASE RMS (DEGREES)	PULSE PEAK (JY)	FRACTION PULSING
26000	26FEB.73	0: 0 0 NS	46.1	206	8.2	7.3	323	3.0	52	0	0.0	3.5	14.0	17.7	61.4	0.60
26001	26FEB.73	0: 6 NS	31.9	238	7.3	4.5	311	0.0	39	0	0.0	3.1	23.6	24.3	49.4	0.38
26002	26FEB.73	0:12 NS	40.1	75	4.6	3.4	151	1.2	190	0	0.0	3.1	14.9	19.7	66.3	0.37
26003	26FEB.73	0:18 NS	42.8	144	5.8	4.3	96	2.1	134	0	0.0	3.1	-26.7	48.3	61.6	0.49
26004	26FEB.73	0:24 NS	38.8	149	7.1	6.3	336	2.2	174	0	0.0	3.3	17.9	34.6	57.6	0.34
26005	26FEB.73	0:30 NS	37.9	226	6.7	4.4	260	2.6	137	0	0.0	3.1	-36.5	36.6	52.2	0.35
26006	26FEB.73	0:36 NS	38.7	233	7.4	4.0	209	2.7	101	0	0.0	3.1	-2.7	30.8	47.3	0.44
26007	26FEB.73	0:42 NS	37.4	-12	6.7	3.7	195	2.7	268	0	0.0	3.4	11.8	53.3	50.2	0.54
26008	26FEB.73	0:48 NS	45.9	1	5.4	4.6	336	1.8	184	0	0.0	3.4	45.1	66.5	58.6	0.20
26009	26FEB.73	0:54 NS	38.3	-1	4.8	4.6	334	0.7	65	0	0.0	3.2	28.2	45.3	30.9	0.50
26236	26FEB.73	23:50 NS	44.1	70	5.2	4.4	163	1.3	142	0	0.0	2.5	-12.5	15.7	65.6	0.51
26237	26FEB.73	23:56 NS	42.9	200	5.3	3.6	237	2.2	215	0	0.0	2.4	10.2	28.2	65.9	0.51
27000	27FEB.73	0: 2 NS	44.2	121	6.2	2.7	65	1.8	43	0	0.0	3.4	9.8	35.8	63.8	0.48
27001	27FEB.73	0: 8 NS	45.2	260	6.5	2.4	96	1.8	107	0	0.0	3.5	2.6	18.1	56.7	0.55
27002	27FEB.73	0:14 NS	39.9	230	6.9	6.1	174	4.2	293	0	0.0	3.3	-4.8	33.5	56.3	0.54
27003	27FEB.73	0:20 NS	39.9	13	4.6	1.3	281	1.9	166	0	0.0	3.3	-6.1	61.2	54.3	0.34
27004	27FEB.73	0:26 NS	43.6	60	5.5	4.6	284	1.3	118	0	0.0	3.4	20.4	33.2	58.6	0.47
27005	27FEB.73	0:32 NS	48.0	113	6.6	1.2	119	0.6	-34	0	0.0	3.4	-16.0	80.1	72.6	0.37
27006	27FEB.73	0:38 NS	45.9	144	6.6	7.0	35	1.2	26	0	0.0	3.4	5.7	8.0	69.4	0.52
	48.73	0:40 NS	46.2	208	9.1	0.0	58	0.0	103	0	0.0	9.9	24.2	46.0	59.5	0.38

Table F-1 (continued)

CRAB NEBULA PULSAR FLUX FOR SHORT BASELINE AT 111 MHZ

RUN NUMBER	DATE	TIME BASE (UT)	TOTAL FLUX(JY) N=0	FOURIER COMPONENTS AMP(JY) AND PHASE (DEG. REL. TO N=0)					3 SIG LEVEL (JY)	PHASE DEV RMS (DEGREES)	PULSE PEAK (JY)	FRACTION PULSING
				±1	±2	±3	±4	±5				
27008	27FEB.73	0150 NS	146.2	7.2 290	1.4 ?21	3.5 157	0.0 0	0.0 0	3.6	13.8	37.7	62 0	0.41
				6.8 327	5.4 3.(	2.5 31	0.0 0	0.0 0				

Table F-2

CRAB NEBULA PULSAR FLUX FOR LONG BASELINES AT 111 MHZ

RUN NUMBER	DATE	TIME BASE (UT)	TOTAL FLUX(JY) N=0	FOURIER COMPONENTS — AMP(JY) AND PHASE (DEG. REL. TO N=0) ±1	±2	±3	±4	±5	3 SIG LEVEL (JY)	PHASE DEV (DEGREES)	RMS	PULSE PEAK (JY)	FRACTION PULSING
23065	23NOV.71	6:41 AN	25.7	5.3 / 237	3.2 / 248	2.1 / 179	0.0 / 0	0.0 / 0	1.6	12.2	22.4	45.1	0.52
23067	23NOV.71	6:55 AN	25.3	5.8 / 265	4.1 / 207	2.3 / 119	0.0 / 0	0.0 / 0	2.0	0.0	0.0	0.0	0.0
24042	24NOV.71	4:52 AS	22.3	0.0 / 0	0.0 / 0	0.0 / 0	0.0 / 0	0.0 / 0	2.6	0.0	0.0	0.0	0.0
24052	24NOV.71	5:16 AS	34.1	6.5 / 61	4.2 / 259	1.9 / 145	0.0 / 0	0.0 / 0	2.5	2.5	25.5	51.9	0.72
24061	24NOV.71	6:9 AN	36.2	6.8 / 74	5.9 / 316	4.7 / 70	0.0 / 0	0.0 / 0	2.8	-27.1	37.8	54.5	0.71
24062	24NOV.71	6:16 AS	41.7	6.3 / 48	4.4 / 231	3.5 / 9	0.0 / 0	0.0 / 0	2.8	31.6	42.4	66.0	0.62
24063	24NOV.71	6:23 AN	31.5	6.1 / 72	4.5 / 242	3.5 / 136	0.0 / 0	0.0 / 0	1.6	0.8	15.5	52.6	0.74
24063	24NOV.71	6:23 AS	34.8	9.9 / 180	5.4 / 99	4.0 / 71	0.0 / 0	0.0 / 0	3.4	-20.3	36.8	58.8	0.59
24071	24NOV.71	7:12 AS	33.0	5.0 / 165	6.6 / 67	5.0 / -70	0.0 / 0	0.0 / 0	4.7	-9.4	23.4	55.4	0.74
19044	19DEC.71	4:45 AN	31.4	6.1 / 260	4.1 / 265	2.2 / 204	0.0 / 0	0.0 / 0	1.6	37.4	50.6	48.5	0.68
19045	19DEC.71	4:54 AN	28.8	7.0 / 237	6.6 / 241	3.9 / 246	0.0 / 0	0.0 / 0	1.6	-1.2	2.4	51.3	0.66
19056	19DEC.71	5:0 AN	31.1	8.5 / 273	4.7 / 207	2.6 / 99	0.0 / 0	0.0 / 0	2.0	-6.2	27.6	53.6	0.42
20031	20DEC.71	3:18 AS	30.2	6.8 / 231	6.7 / 250	3.1 / 219	0.0 / 0	0.0 / 0	2.5	23.3	42.2	50.0	0.44
20032	20DEC.71	3:26 AS	23.8	7.6 / 162	5.9 / 138	3.1 / 180	0.0 / 0	0.0 / 0	2.5	0.0	0.0	0.0	0.0
20033	20DEC.71	3:34 AS	31.3	5.2 / 198	6.8 / 96	3.8 / 241	0.0 / 0	0.0 / 0	2.5	34.4	44.7	45.1	0.61
20042	20DEC.71	4:32 AN	28.1	7.2 / 253	3.8 / 245	2.2 / 326	0.0 / 0	0.0 / 0	2.1	-43.2	48.8	49.5	0.53
20042	20DEC.71	4:32 AS	32.5	7.0 / 219	6.8 / 226	2.8 / 156	0.0 / 0	0.0 / 0	3.0	5.1	54.9	53.0	0.86
20043	20DEC.71	3:38 AN	27.1	5.1 / 41	3.0 / 165	1.7 / 283	0.0 / 0	0.0 / 0	1.8	-37.2	39.1	48.0	0.59
20043	20DEC.71	4:38 AS	31.6	6.8 / 48	5.5 / 182	3.8 / 287	0.0 / 0	0.0 / 0	2.6	1.1	32.4	49.3	0.94
20051	20DEC.71	5:9 AN	25.3	4.9 / 203	3.8 / 172	2.2 / -51	0.0 / 0	0.0 / 0	1.6	-33.2	51.2	44.5	0.60
20051	20DEC.71	5:8 AS	36.2	5.4 / 220	5.8 / 167	2.9 / 33	0.0 / 0	0.0 / 0	2.6	-0.6	18.8	68.4	0.78

Table F-2 (continued)

CRAB NEBULA PULSAR FLUX FOR LONG BASELINES AT 111 MHZ

RUN NUMBER	DATE	TIME BASE (UT)	TOTAL FLUX(JY) N=0	FOURIER COMPONENTS AMP(JY) AND PHASE (DEG. REL. TO N=0) ±1	±2	±3	±4	±5	3 SIG LEVEL (JY)	PHASE DEV (DEGREES)	PHASE RMS (DEGREES)	PULSE PEAK (JY)	FRACTION PULSING
20052	20DEC.71	5:14 AN	28.8	5.9 / 60	5.7 / -139	3.3 / 15	0.0 / 0	0.0 / 0	1.7	-37.9	48.0	46.5	0.51
				6.9 / 105	5.3 / 18	4.2 / 39	0.0 / 0	0.0 / 0					
20053	20DEC.71	5:20 AN	27.6	5.7 / 193	4.6 / 93	3.5 / 168	0.0 / 0	0.0 / 0	2.4	-39.3	57.7	63.8	0.45
				8.1 / 292	6.8 / 264	3.5 / 135	0.0 / 0	0.0 / 0					
20054	20DEC.71	5:26 AN	27.4	5.8 / 6	4.5 / 92	3.1 / 142	0.0 / 0	0.0 / 0	1.7	-23.0	25.9	51.1	0.68
				6.8 / 21	6.0 / 140	3.0 / 216	0.0 / 0	0.0 / 0					
23021	23JAN.72	2:17 AN	32.2	6.4 / 35	4.6 / 191	1.2 / 300	0.0 / 0	0.0 / 0	2.3	31.6	34.8	54.1	0.64
				7.0 / 6	7.3 / 132	3.4 / 199	0.0 / 0	0.0 / 0					
23024	23JAN.72	2:35 AN	27.6	5.5 / 135	4.2 / 348	2.5 / 70	0.0 / 0	0.0 / 0	1.5	-14.7	28.0	50.6	0.59
				6.1 / 122	6.1 / 354	3.7 / 166	0.0 / 0	0.0 / 0					
23025	23JAN.72	2:41 AN	22.3	5.0 / 347	3.8 / 283	1.5 / 15	0.0 / 0	0.0 / 0	2.0	32.2	37.4	36.6	0.57
				4.7 / 249	3.6 / 277	2.4 / -67	0.0 / 0	0.0 / 0					
23028	23JAN.72	2:59 AN	31.9	6.0 / 12	4.6 / 117	2.6 / 150	0.0 / 0	0.0 / 0	1.6	-2.5	6.7	59.8	0.63
				6.9 / 16	6.6 / 107	4.0 / 170	0.0 / 0	0.0 / 0					
23030	23JAN.72	3:5 AN	27.1	6.0 / 174	2.8 / 238	9.2 / 62	0.0 / 0	0.0 / 0	2.2	-35.1	41.1	54.5	0.62
				6.6 / 185	7.2 / 332	4.0 / 169	0.0 / 0	0.0 / 0					
24023	24JAN.72	2:19 AN	31.6	6.1 / 264	4.9 / 299	2.5 / 264	0.0 / 0	0.0 / 0	1.6	8.9	11.4	58.6	0.59
				6.8 / 205	6.1 / 278	3.5 / 231	0.0 / 0	0.0 / 0					
24026	24JAN.72	2:25 AN	32.5	6.2 / 84	5.6 / 229	2.4 / 45	0.0 / 0	0.0 / 0	2.2	30.7	43.7	56.7	0.60
				7.3 / 68	6.7 / 170	3.6 / -93	0.0 / 0	0.0 / 0					
24027	24JAN.72	2:43 AN	26.5	5.3 / 107	3.9 / 384	1.9 / 93	0.0 / 0	0.0 / 0	1.5	-9.3	16.8	49.0	0.55
				5.9 / 145	5.9 / 333	3.0 / 132	0.0 / 0	0.0 / 0					
24031	24JAN.72	3:7 AN	28.9	4.6 / 314	5.2 / 25	2.4 / 83	0.0 / 0	0.0 / 0	1.6	13.8	21.4	50.8	0.70
				6.6 / 323	5.2 / 4	2.9 / 12	0.0 / 0	0.0 / 0					
27001	27FEB.72	0: 8 AS	28.1	4.8 / 131	4.1 / 307	2.3 / 46	0.0 / 0	0.0 / 0	1.6	2.4	10.1	48.6	0.47
				6.2 / 117	4.3 / 330	2.0 / 23	0.0 / 0	0.0 / 0					
27001	27FEB.72	0: 8 AS	26.7	0.0 / 0	0.0 / 0	0.0 / 0	0.0 / 0	0.0 / 0	4.4	0.0	0.0	0.0	0.0
27002	27FEB.72	0:14 AN	28.1	6.6 / 324	5.6 / 335	3.2 / 46	0.0 / 0	0.0 / 0	1.6	-5.2	12.2	49.8	0.83
27002	27FEB.72	0:14 AS	28.0	6.5 / 304	5.0 / 353	1.8 / 79	0.0 / 0	0.0 / 0	2.4	31.4	45.9	46.6	0.48
				6.6 / 342	4.1 / 27	1.9 / 60	0.0 / 0	0.0 / 0					
27005	27FEB.72	0:32 AN	32.3	5.7 / 338	2.7 / 0	2.6 / -96	0.0 / 0	0.0 / 0	1.6	3.1	18.3	58.4	0.54
				7.5 / 292	4.9 / 352	2.8 / 245	0.0 / 0	0.0 / 0					
27005	27FEB.72	0:32 AS	28.4	6.0 / 291	6.4 / 299	3.6 / 281	0.0 / 0	0.0 / 0	2.4	7.9	42.0	47.3	0.41
				6.2 / 320	3.6 / -82	2.3 / 327	0.0 / 0	0.0 / 0					
27006	27FEB.72	0:38 AN	28.1	5.7 / 299	4.2 / 5	2.8 / 213	0.0 / 0	0.0 / 0	1.6	-45.3	61.2	45.1	0.52
				5.7 / 193	4.7 / -117	4.7 / 150	0.0 / 0	0.0 / 0					
27008	27FEB.72	0:38 AS	23.2	6.5 / 170	5.3 / 51	3.8 / 277	0.0 / 0	0.0 / 0	2.4	0.0	0.0	0.0	0.0
				0.0 / 0	0.0 / 0	0.0 / 0	0.0 / 0	0.0 / 0					
27009	27FEB.72	0:56 AS	36.2	9.7 / 143	5.9 / 188	6.3 / 95	0.0 / 0	0.0 / 0	2.4	-10.9	23.1	63.0	0.78
				6.2 / 109	5.3 / 248	7.1 / 135	0.0 / 0	0.0 / 0					

Table F-2 (continued)

CRAB NEBULA PULSAR FLUX FOR LONG BASELINES AT 111 MHZ

RUN NUMBER	DATE	TIME (UT)	BASE	TOTAL FLUX(JY) N=0	±1 AMP(JY) / φ	±2 AMP(JY) / φ	±3 AMP(JY) / φ	±4	±5	3 SIG LEVEL (JY)	PHASE DEV (DEGREES)	RMS	PULSE PEAK (JY)	FRACTION PULSING
27236	27FEB.72	23:58	A/N	30.5	6.1 / 346	4.5 / 181, 1.9	27	0.0	0.0	2.0	-10.1	18.6	55.7	0.59
28002	28FEB.72	0:10	AN	26.1	6.8 / 324	6.5 / 70, 4.5	58	0.0	0.0	1.5	9.4	10.9	45.5	0.59
28003	28FEB.72	0:22	AN	24.6	4.7 / 289	3.7 / 334, 2.0	294	0.0	0.0	1.6	2.3	27.9	43.1	0.61
28206	28FEB.72	0:40	AN	24.6	5.0 / 264	4.7 / 302, 2.7	275	0.0	0.0	1.6	32.8	47.3	63.8	0.58
28007	28FEB.72	0:46	AN	26.0	5.5 / 181	3.9 / 56, 2.1	207	0.0	0.0	1.7	-0.1	7.2	40.5	0.76
25220	25MAR.72	22:0	AN	26.0	4.9 / 126	4.7 / 23, 2.0	281	0.0	0.0	1.7	-30.2	50.6	51.7	0.62
26221	25MAR.72	22:6	AN	26.4	6.0 / 99	3.2 / 310, 0.9	208	0.0	0.0	1.6	-13.1	30.1	46.6	0.55
25229	25MAR.72	22:54	AN	26.4	5.4 / 297	5.3 / 285, 2.9	47	0.0	0.0	1.6	-11.6	66.4	25.7	0.48
28230	25MAR.72	23:0	AN	26.1	5.4 / 314	3.7 / -1, 1.7	50	0.0	0.0	1.8	24.3	30.0	37.8	0.50
24222	24FEB.73	22:23	AS	26.1	0.8 / 0	4.4 / 0, 3.2	32	0.0	0.0	2.2	0.0	0.0	0.0	0.0
24223	24FEB.73	22:30	AS	16.0	6.3 / 308	4.3 / 309, 2.4	115	0.0	0.0	2.2	0.0	0.0	0.0	0.0
24224	24FEB.73	22:37	AS	21.2	4.4 / 299	6.7 / 325, 4.9	289	0.0	0.0	2.2	0.0	0.0	0.0	0.0
24237	24FEB.73	23:58	AN	24.9	5.8 / 55	3.6 / 190, 2.2	184	0.0	0.0	3.4	-11.1	16.7	50.0	0.65
24237	24FEB.73	23:58	AS	29.2	4.0 / 29	4.9 / 180, 3.4	299	0.0	0.0	4.2	0.5	7.3	52.7	0.70
25000	25FEB.73	0:4	AN	22.7	4.0 / 109	2.3 / 291, 1.9	123	0.0	0.0	2.0	-15.5	16.7	50.1	0.33
25001	25FEB.73	0:10	AN	34.0	3.8 / 127	2.0 / 206, 1.4	259	0.0	0.0	1.8	26.8	35.0	33.5	0.07
26001	25FEB.73	0:10	AS	33.3	3.4 / 229	3.8 / 235, 4.1	147	0.0	0.0	2.0	-20.8	29.8	27.0	0.45
26001	25FEB.73	0:16	AN	29.3	3.6 / 229	4.1 / 201, 3.3	58	0.0	0.0	1.9	-3.5	8.3	40.6	0.59
25002	25FEB.73	0:16	AN	23.0	0.0 / 0	0.0 / 0, 0.0	0	0.0	0.0	2.3	1.1	66.1	31.3	0.36
25003	25FEB.73	0:22	AN	18.2	0.0 / 0	0.0 / 0, 0.0	0	0.0	0.0	2.2	9.4	18.3	80.4	0.66
25004	25FEB.73	0:28	AN	25.0	0.0 / 0	0.0 / 0, 0.0	2	0.0	0.0	2.1	-3.0	30.5	63.3	0.36

Table F-2 (continued)

CRAB NEBULA PULSAR FLUX FOR LONG BASELINES AT 111 MHZ

RUN NUMBER	DATE	TIME (UT)	BASE	TOTAL FLUX(JY) N=0	±1 AMP(JY)	±1 PHASE	±2 AMP(JY)	±2 PHASE	±3 AMP(JY)	±3 PHASE	±4	±5	3 SIG LEVEL (JY)	PHASE DEV (DEGREES)	RMS	PULSE PEAK (JY)	FRACTION PULSING
25005	25FEB.73	0:34	AS	22.4	0.0	0	0.0	0	0.0	0	0.0 / 0	0.0 / 0	2.7	0.0	0.0	0.0	0.0
25006	25FEB.73	0:40	AM	29.1	4.8	257	3.7	324	1.6	86	0.0 / 0	0.0 / 0	2.2	20.3	35.4	41.7	0.49
25006	25FEB.73	0:40	AS	25.1	5.4	256	4.3	226	1.6	22	0.0 / 0	0.0 / 0	2.9	-43.2	54.3	40.2	0.39
25007	25FEB.73	0:46	AM	27.9	4.9	282	3.6	230	0.9	68	0.0 / 0	0.0 / 0	2.4	37.6	48.7	40.1	0.29
25007	25FEB.73	0:46	AS	26.8	0.0	0	0.0	0	0.0	0	0.0 / 0	0.0 / 0	2.9	0.0	0.0	0.0	0.0
25008	25FEB.73	0:52	AM	30.1	3.5	297	3.2	300	1.9	242	0.0 / 0	0.0 / 0	2.3	10.5	28.3	46.8	0.32
25009	25FEB.73	0:58	AM	26.0	4.4	102	1.3	148	1.3	-162	0.0 / 0	0.0 / 0	2.4	-10.9	16.0	37.6	0.64
25009	25FEB.73	0:58	AS	24.4	4.1	66	3.5	122	0.5	39	0.0 / 0	0.0 / 0	3.1	29.3	80.1	38.1	0.49
28223	25FEB.73	22:41	AS	31.4	0.0	0	0.0	0	0.0	0	0.0 / 0	0.0 / 0	2.3	0.0	0.0	0.0	0.0
28237	25FEB.73	23:54	AM	30.1	5.9	164	3.8	-67	1.9	83	0.0 / 0	0.0 / 0	2.6	-22.6	24.5	45.9	0.65
28237	25FEB.73	23:54	AS	28.3	4.8	137	2.0	342	2.3	295	0.0 / 0	0.0 / 0	3.2	36.8	47.6	41.6	0.40
26000	26FEB.73	0:0	AM	29.1	4.8	61	3.9	339	2.0	349	0.0 / 0	0.0 / 0	2.3	10.6	22.0	46.0	0.40
26001	26FEB.73	0:6	AM	25.9	4.1	76	2.0	174	1.2	276	0.0 / 0	0.0 / 0	2.2	-25.4	37.8	37.0	0.27
26001	26FEB.73	0:6	AS	21.7	5.5	264	2.0	186	1.3	154	0.0 / 0	0.0 / 0	2.7	4.9	6.1	32.3	0.56
26002	26FEB.73	0:12	AM	32.1	6.4	198	3.3	113	1.5	147	0.0 / 0	0.0 / 0	2.4	-29.4	32.5	46.0	0.40
26003	26FEB.73	0:18	AM	33.0	6.4	184	5.0	140	2.2	218	0.0 / 0	0.0 / 0	2.5	18.1	31.2	50.2	0.43
26003	26FEB.73	0:18	AS	30.4	4.8	221	3.1	275	1.2	94	0.0 / 0	0.0 / 0	3.4	-5.6	08.6	48.6	0.53
26004	26FEB.73	0:24	AM	30.1	5.2	208	5.2	148	2.2	-9	0.0 / 0	0.0 / 0	2.3	3.0	17.2	45.7	0.67
26005	26FEB.73	0:30	AM	30.5	4.5	219	3.1	41	1.9	313	0.0 / 0	0.0 / 0	2.3	-17.0	34.7	46.8	0.56
26005	26FEB.73	0:30	AS	25.1	5.7	320	3.7	-4	1.5	263	0.0 / 0	0.0 / 0	1.9	-0.7	18.5	36.0	0.64
26006	26FEB.73	0:36	AM	31.5	2.7	363	2.7	336	2.3	279	0.0 / 0	0.0 / 0	2.4	-7.8	61.0	84.2	0.41

166

Table F-2 (continued)

CRAB NEBULA PULSAR FLUX FOR LONG BASELINES AT 111 MHZ

RUN NUMBER	DATE	TIME BASE (UT)	TOTAL FLUX(JY) N=0	FOURIER COMPONENTS AMP(JY) AND PHASE (DEG. REL. TO N=0) ±1	±2	±3	±4	±5	3 SIG LEVEL (JY)	PHASE DEV (JY)	RMS (DEGREES)	PULSE PEAK (JY)	FRACTION PULSING
26007	26FEB.73	0:42 AN	31.9	235 / 304	3.3 / —	342	0.0	0.0	2.4	26.4	73.2	46.0	0.54
26007	26FEB.73	0:42 AS	28.0	299 / 244	5.2	180	0.0	0.0	2.4	-15.6	41.9	44.7	0.36
2600A	26FEB.73	0:48 AN	29.6	283 / 282	2.3	65	0.0	0.0	2.3	6.0	17.7	40.2	0.62
26009	26FEB.73	0:54 BN	27.1	282 / 237	4.2	203	0.0	0.0	2.4	-29.8	63.5	36.0	0.24
26223	26FEB.73	22:37 AS	29.2	6 / 189	3.2	262	0.0	0.0	2.2	0.0	0.0	0.0	0.0
26236	26FEB.73	23:50 AN	31.0	-1 / 134	3.2	290	0.0	0.0	1.7	29.2	51.9	47.8	0.51
26236	26FEB.73	23:50 AS	29.9	190 / 216	3.0	-143	0.0	0.0	2.2	-12.6	14.3	50.2	0.46
26237	26FEB.73	23:56 AN	29.1	94 / 326	3.5	21	0.0	0.0	1.6	-2.1	34.3	43.5	0.49
26237	2 FEB.73	23:56 AS	30.0	8 / 0	0.0	0	0.0	0.0	2.2	-3.9	17.3	50.3	0.55
27000	27FEB.73	0: 2 AN	26.2	99 / 273	3.9	207	0.0	0.0	1.6	0.5	15.3	40.6	0.44
27000	27FEB.73	0: 2 AS	29.3	79 / 258	3.8	29	0.0	0.0	2.3	-12.5	19.8	47.3	0.56
27001	27FEB.73	0: 8 AN	31.8	107 / 265	4.2	20	0.0	0.0	2.5	5.2	8.0	41.2	0.76
27001	27FEB.73	0: 8 AS	29.9	176 / 305	4.0	27	0.0	0.0	3.3	-31.4	46.3	44.4	0.44
27002	27FEB.73	0:14 AN	32.9	179 / 162	4.0	-65	0.0	0.0	2.4	15.5	33.8	55.2	0.51
27002	27FEB.73	0:14 AS	27.2	192 / 63	4.2	23	0.0	0.0	2.4	9.9	15.2	46.1	0.52
27003	27FEB.	0:20 AN	35.1	171 / 87	3.6	295	0.0	0.0	2.4	-22.5	26.9	55.4	0.46
27003	27FEB.73	0:20 AS	29.0	278 / 76	3.8	350	0.0	0.0	2.2	-5.2	19.2	60.2	0.54
27004	27FEB.73	0:26 AN	32.?	260 / 311	2.6	184	0.0	0.0	2.5	6.8	66.9	46.3	0.41
27004	27FEB.73	0:26 AS	27.2	272 / 284	3.7	226	0.0	0.0	2.4	8.7	28.0	42.8	0.44
27005	27FEB.73	0:32 AN	31.9	347 / 289	4.1	134	0.0	0.0	2.4	-15.7	32.4	48.8	0.67

Table F-2 (continued)

CRAB NEBULA PULSAR FLUX FOR LONG BASELINES AT 111 MHZ

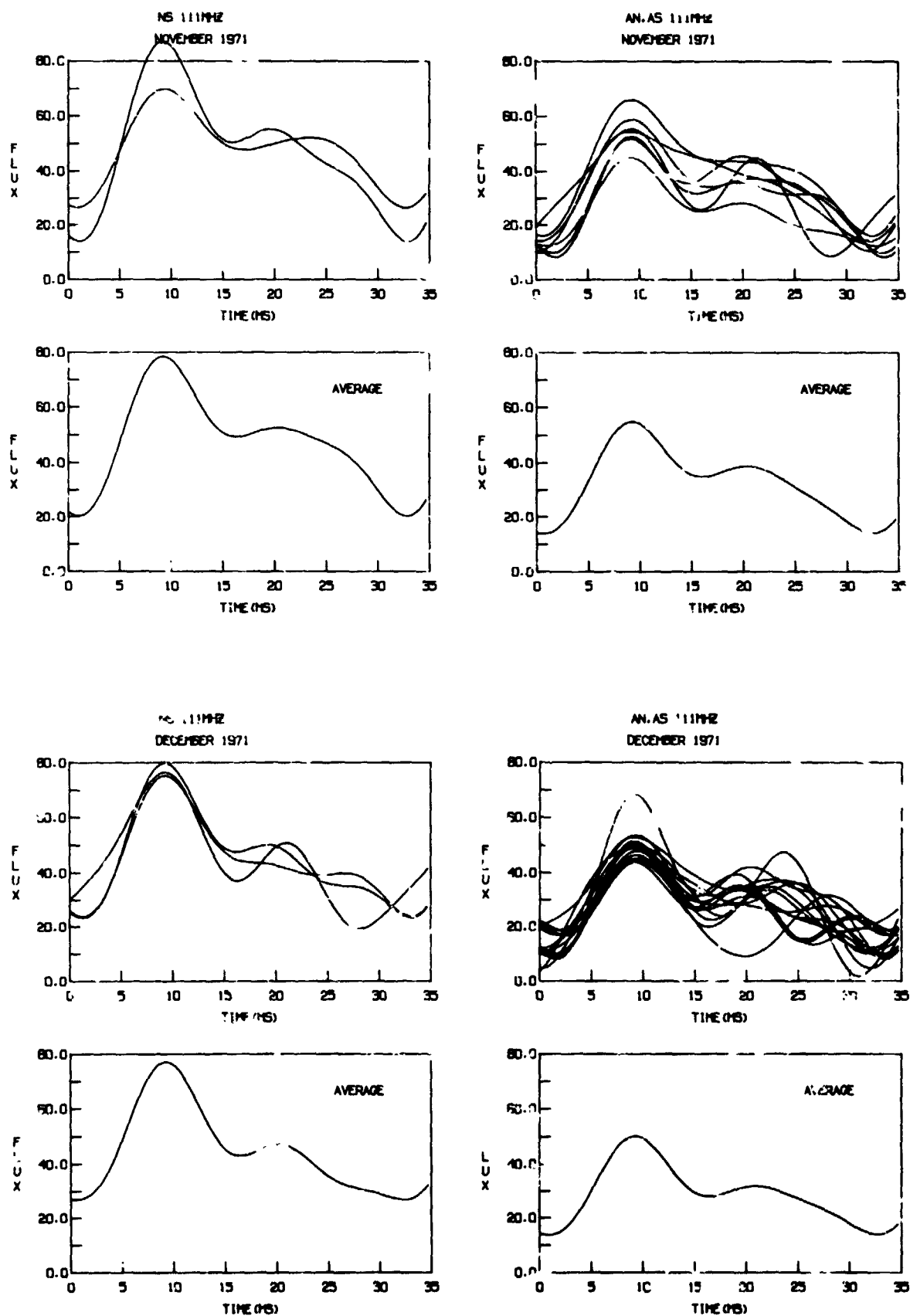| RUN NUMBER	DATE	TIME BASE (UT)	TOTAL FLUX(JY) N=0	FOURIER COMPONENTS AMP(JY) AND PHASE (DEG. REL. TO N=0) ±1	±2	±3	±4	±5	3 SIG LEVEL (JY)	PHASE DEV (DEGREES)	RMS	PULSE PEAK (JY)	FRACTION PULSING
27005	27FEB.73	0:32 AS	32.1	4.4 / 25	3.6 / 182	1.6 / 156	0.0 / 0	0.0 / 0	3.3	34.6	46.0	46.1	0.42
				5.1 / 33	4.3 / 106	2.0 / 17	0.0 / 0	0.0 / 0	2.4	-0.2	23.4	49.9	0.43
27006	27FEB.73	0:36 AN	31.9	4.6 / 97	3.6 / 251	0.9 / -1	0.0 / 0	0.0 / 0					
27006	27FEB.73	0:38 AS	28.6	6.5 / 109	4.6 / 239	3.7 / 49	0.0 / 0	0.0 / 0	2.2	10.4	11.0	44.4	0.56
				4.8 / 120	2.9 / 303	1.3 / 319	0.0 / 0	0.0 / 0					
27007	27FEB.73	0:40 AN	33.1	5.7 / 99	4.2 / 291	2.1 / 289	0.0 / 0	0.0 / 0	2.5	-8.2	40.6	48.7	0.48
				5.8 / 204	3.5 / 94	1.0 / -15	0.0 / 0	0.0 / 0					
27007	27FEB.73	0:44 AS	27.9	5.1 / 146	4.8 / 74	0.5 / 110	0.0 / 0	0.0 / 0	2.3	8.6	20.2	39.6	0.63
				5.5 / 171	3.1 / 154	1.6 / 82	0.0 / 0	0.0 / 0					
27008	27FEB.73	0:50 AN	33.1	4.8 / 164	4.6 / 175	2.6 / 15	0.0 / 0	0.0 / 0	2.5	6.8	42.7	49.4	0.44
				5.8 / 266	3.1 / 359	0.5 / 268	0.0 / 0	0.0 / 0					
27008	27FEB.73	0:50 AS	26.9	7.8 / 289	5.5 / 235	1.4 / 349	0.0 / 0	0.0 / 0	2.4	-39.1	57.9	37.6	0.44
				4.7 / 310	3.0 / -54	1.6 / 62	0.0 / 0	0.0 / 0					
				4.7 / 273	2.0 / 111	2.3 / 168	0.0 / 0	0.0 / 0					

169

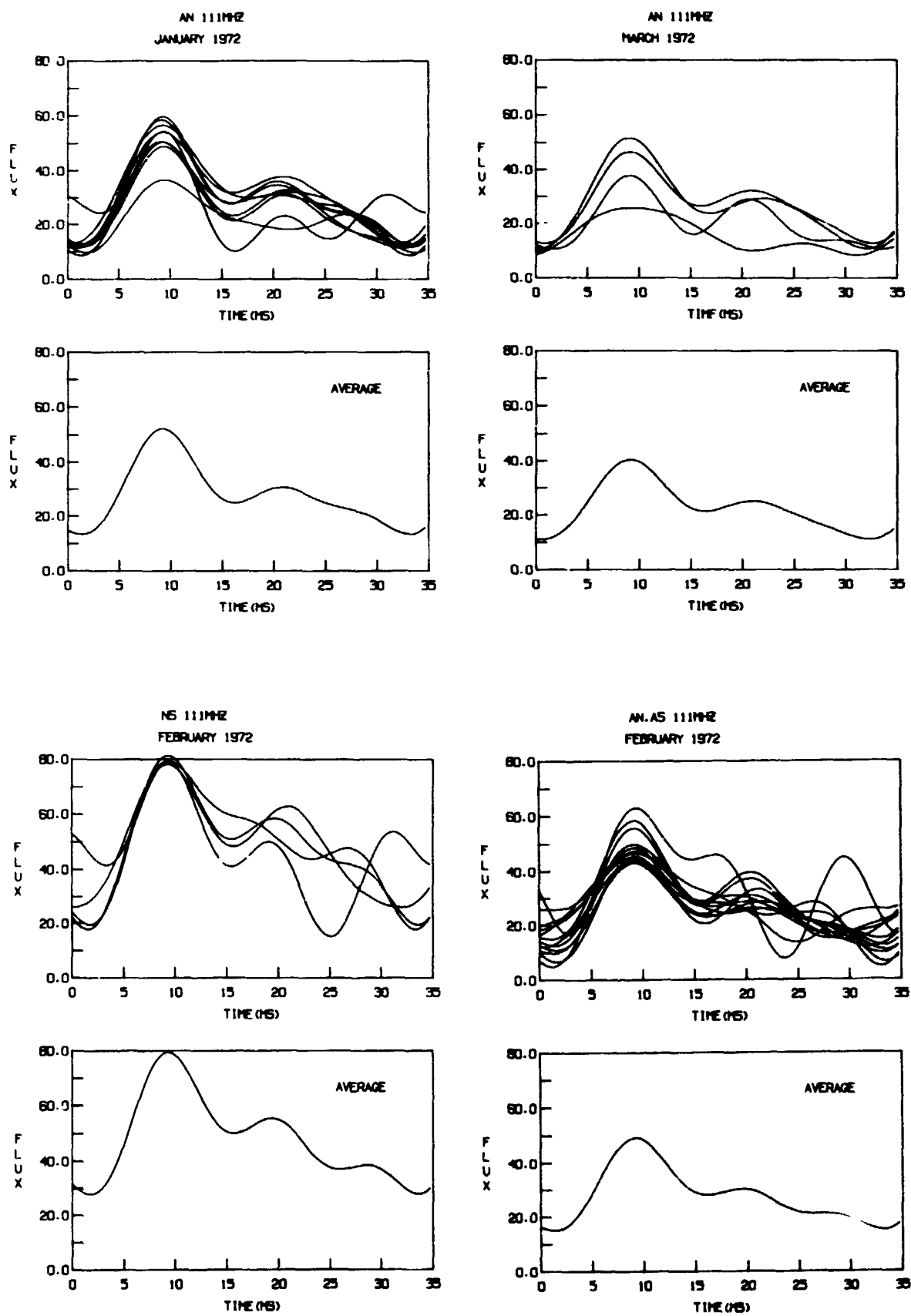Figure F-1. Individual and average pulse shapes at 111 MHz.
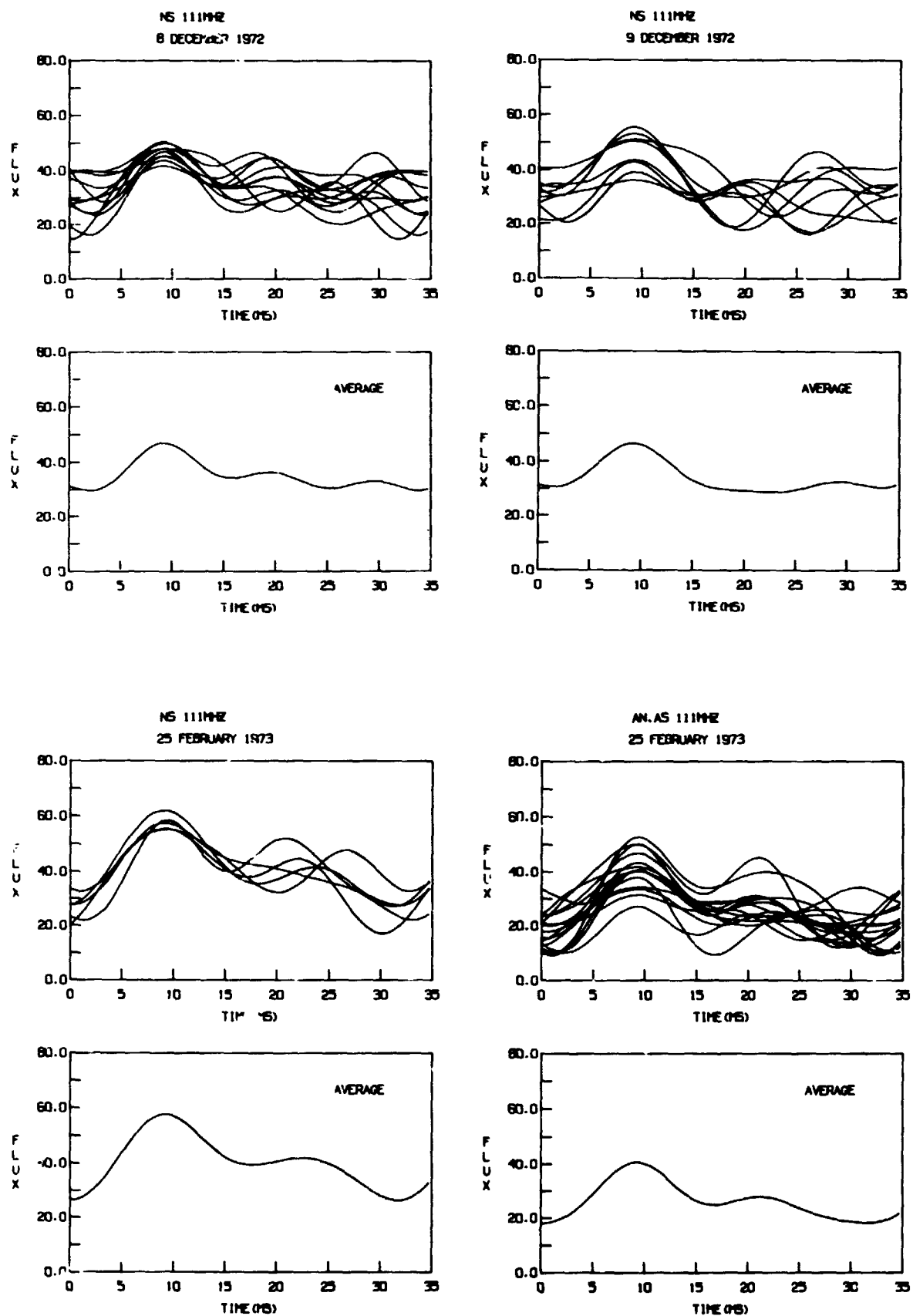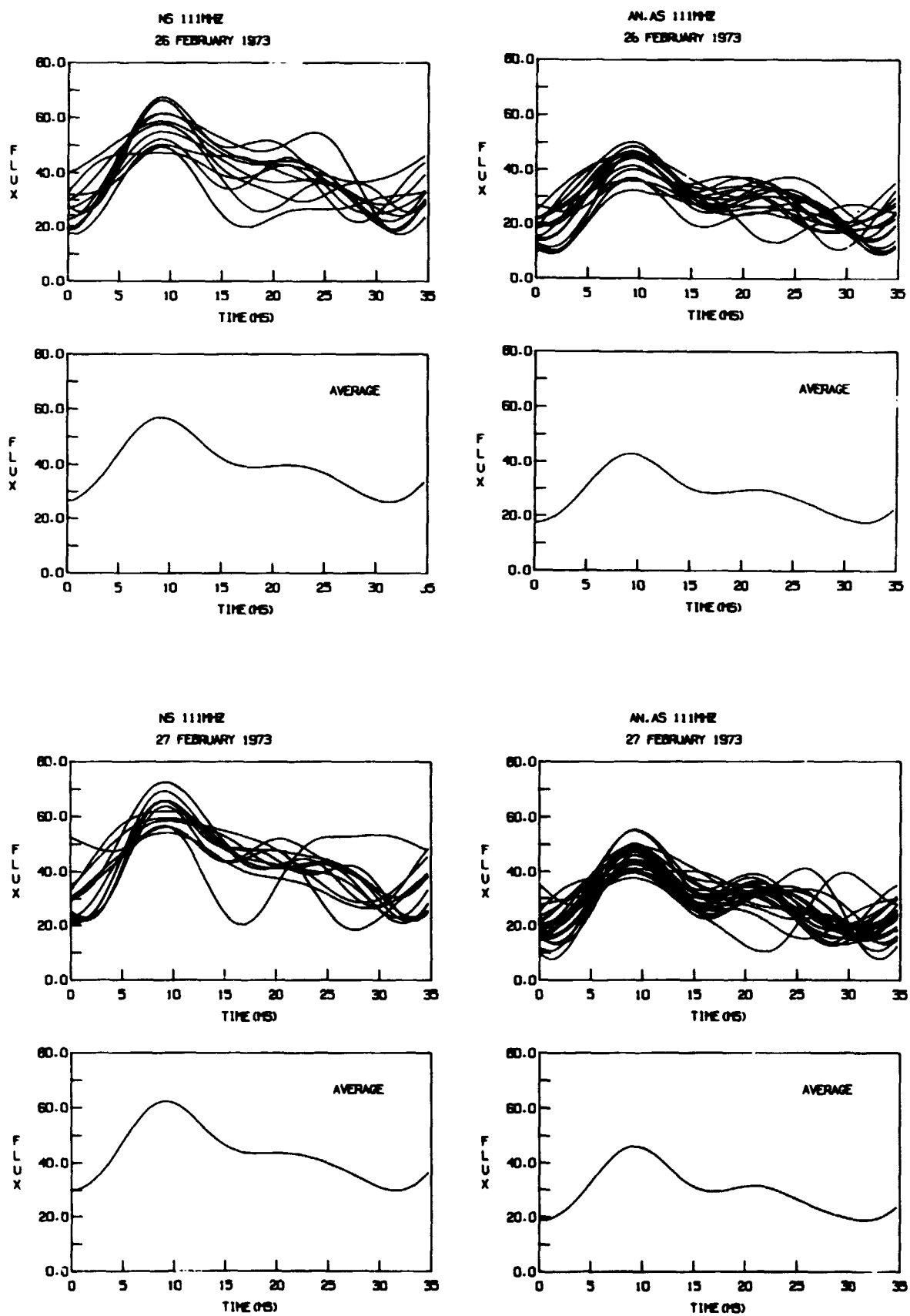
Figure F-1. (continued)

Figure F-1. (continued)

Figure F-1. (continued)

REFERENCES CITED

Armstrong, J. W., Coles, W. A., Kaufman, J. J., Rickett, B. J., "Obser-
    vations of the Crab nebula at 73.8 MHz" 1973, Astrophys. J. 186, L141.

Backer, D. C., "Interstellar Scattering of the Vela pulsar" 1974, Astro-
    phys. J. 190, 567.

Bell, S. J., Hewish, A., "Angular size and flux density of the small
    source in the Crab nebula at 81.5 Mc/s" 1967, Nature 213, 1214.

Bracewell, R. N., The Fourier Transform and its Applications (New York:
    McGraw Hill, Inc., 1965).

Clark, B. G., "The NRAO tape-recorder interferometer system" 1973, Proc.
    I.E.E.E. 61, 1242.

Clark, T. A., Erickson, W. C., "Long wavelength VLBI" 1973, Proc. I.E.E.E.
    61, 1230.

Cohen, M. H., Cronyn, W. M., "Scintillation and apparent angular diameter"
    1974, Astrophys. J. 192 (in press).

Coles, W. A., Rickett, B. J., Rumsey, V. H., "Interplanetary scintilla-
    tions" 1974, paper presented at Asilomar conference.

Counselman, C. C., "Can thin-screen scattering explain the pulse broaden-
    ing of JP 1858 and JP 1933?" 1974, Paper presented at meeting on
    interstellar scattering of radio waves, Jet Propulsion Laboratory,
    Pasadena, California

Counselman, C. C., Rankin, J. M., "Multipath delay distortion of radio
    pulses from NP 0532" 1972, Astrophys. J. 166, 513.

Cronyn, W. M., "Radio scattering in the interplanetary medium" 1970a,
    University of Maryland (Ph.D. thesis).

Cronyn, W. M., "Interstellar scattering of pulsar radiation and its
    effect on the spectrum of NP 0532" 1970b, Science 168, 1453.

Cronyn, W. M., "Interferometer visibility scintillation" 1972, Astrophys.
    J. 174, 181.

Cronyn, W. M., "Power law irregularity structure for the interstellar
    medium" 1973, Bull. Am. Astron. Soc. 5, 407 (abstract).

Cronyn, W. M., "Interferometer visibility function for scattered pulsar
    radiation" 1974 (in preparation).

Drake, F. D., 1969, paper presented at meeting on pulsars, Rome.

Erickson, W. C., Kuiper, T. B. H., Clark, T. A., Knowles, S. H., Broderick, J. J., "Very long baseline interferometer observations of Taurus A and other sources at 121.6 MHz" 1972, Astrophys. J. 177, 101.

Ewing, M. S. Batchelor, R. A., Friefeld, R. D., Price, R. M., Staelin, D. H., "Observations of pulsar spectra" 1970, Astrophys. J. 162, L169.

Galt, J. A., Broten, N. W., Legg, T. H., Locke, J. L., Yen, J. L., "Long baseline interferometer measurements of CP 0329" 1970, Nature 225, 530.

Galt, J. A., Lyne, A. G., "The interstellar scintillation pattern of PSR 0329+54" 1972, Monthly Notices Roy. Astr. Soc. 158, 281.

Harris, D. E., "A low-frequency search for compact radio sources in supernova remnants" 1973, Astron. J. 78, 231.

Hewish, A., Okoye, S. E., "Evidence for an unusual source of high radio brightness temperature in the Crab nebula" 1965, Nature 207, 59.

Hinteregger, H. F., "Geodetic and astrometric applications of very long baseline interferometery" 1972, Massachusetts Institute of Technology (Ph.D. thesis).

Huguenin, G. R., Taylor, J. H., Jura, M., "Dynamic spectra of pulsars in the frequency range 110-420 MHz" 1969, Astrophys. Letters 4, 71.

Huguenin, G. R., Taylor, J. H., Helfand, D. J., "Slow variations of pulsar intensities" 1973, Astrophys. J. 181, L139.

Hutton, L. K., "Total power calibration of the 300-foot radio telescope" 1972, University of Maryland (unpublished research report).

Hutton, L. K., Clark, T. A., Erickson, W. C., Resch, G. M., Vandenberg, N. R., Knowles, S. H., Youmans, A. B., "Meter-wavelength VLBI - I. Cassiopeia A" 1974, Astron. J. (submitted).

Jokippi, J. R., "Turbulence and scintillations in the interplanetary plasma" 1973, Ann. Rev. Astron. Astrophys. 11, 1.

Knight, C. A., Robertson, D. S., Rogers, A. E. E., Shapiro, I. I., Whitney, A. R., Clark, T. A., Goldstein, R. M., Marandino, G. E., Vandenberg, N. R., "Quasars: Millisecond-of-arc structure revealed by very-long-baseline interferometry" 1971, Science 172, 52.

Lang, K. R., "Interstellar scintillation of pulsar radiation" 1971a, Astrophys. J. 164, 249.

Lang, K. R., "The relation of the low frequency source to the Crab pulsar" 1971b, in The Crab Nebula, I.A.U. Symposium No. 46, p. 91.

Lang, K. R., "Pulse broadening due to angular scattering in the interstellar medium" 1971c, Astrophys. Letters 7, 175.

Lang, K. R., Rickett, B. J., "Size and motion of the interstellar scintillation pattern from observations of CP 1133" 1970, Nature 225, 528.

Lovelace, R. V. E., "Theory and analysis of interplanetary scintillations" 1970, Cornell University (Ph.D. thesis).

Manchester, I. N., "Rotation measure and intrinsic angle of the Crab pulsar radio emission" 1971, Nature 231, 189.

Manchester, R. N., Huguenin, G. R., Taylor, J. H., "Polarization of the Crab pulsar radiation at low radio frequencies" 1972, Astrophys. J. 174, L19.

Manchester, R. N., Taylor, J. H., Huguenin, G. R., "Frequency dependence of pulsar polarization " 1973, Astrophys. J. 179, L7.

Manchester, R. N., Taylor, J. H., Van, Y. Y., "Detection of pulsar proper motion" 1974, Astrophys. J. 189, L119.

Matveenko, L. I., "Position of a source of small angular size in the Crab nebula" 1968, Sov. Astr. - AJ 12, 552.

McLean, A. I. O., "Pulsar flux density variations and spectra" 1973, Monthly Notices Roy. Astr. Soc. 165, 133.

Moran, J. M., "Spectral-line analysis of very-long-baseline interferometric data" 1973, Proc. I.E.E.E. 61, 1236.

Mutel, R. L., Broderick, J. J., Carr, T. D., Lynch, M., Desch, M., Warnock, W. W., Klemperer, W. K., "VLB observations of the Crab nebula and the wavelength dependence of interstellar scattering" 1974, Astrophys. J. 192 (in press).

Prentice, A. J. R., Haar, D. ter, "On HII regions and pulsar distances" 1969, Monthly Notices Roy. Astr. Soc. 146, 423.

Rankin, J. M., Comella, J. M., Craft, H. D., Richards, D. W., Campbell, D. B., Counselman, C. C., "Radio pulse shapes, flux densities, and dispersion of pulsar NP 0532" 1970, Astrophys. J. 162, 707.

Rankin, J. M., Roberts, J. A., "Time variability of the dispersion of the Crab nebula pulsar" 1971, in The Crab Nebula, I.A.U. Symposium No. 46, p. 114.

Rankin, J. M., Counselman, C. C., "Pulsar NP 0532: Variability of dispersion and scattering" 1973, Astrophys. J. 181, 875.

Rankin, J. M., Payne, R. R., Campbell, D. R., "The Crab nebula pulsar: Radio frequency spectral variability" 1974, Astrophys. J. Letters (submitted).

Resch, G. M., "Low-frequency spectra of compact radio sources" 1974, Florida State University (Ph.D. thesis).

Readhead, A. C. S., Hewish, A., "Fine structure in radio sources at
    81.5 MHz - III. The survey" 1974, Mem. Roy. Astron. Soc. 78, 1.

Rickett, B. J., "Interstellar scintillation and pulsar intensity varia-
    tions" 1970, Monthly Notices Roy. Astr. Soc. 150, 67.

Rickett, B. J., Lang, K. R., "Two-station observations of the inter-
    stellar scintillation from pulsars" 1973, Astrophys. J. 185, 945.

Rogers, A. E. E., "Very long baseline interferometry with large effective
    bandwidth for phase-delay measurements" 1970, Radio Science 5, 1239.

Scargle, J. D., "Activity in the Crab nebula" 1969, Astrophys. J. 156,
    401.

Scargle, J. D., Harlan, E. A., "Activity in the Crab nebula following the
    pulsar spin-up of 1969 September" 1970, Astrophys. J. 159, L143.

Scheuer, P. A. G., Tsytovich, V. N., "Small-scale irregularities in the
    interstellar gas" 1970, Astrophys. Letters 7, 125.

Seiber, W., "Pulsar spectra: A summary" 1973, Astron. Astrophys. 28, 237.

Slee, O. B., Ables, J. G., Batchelor, R. A., Krishna-Mohan, S., Venugopal,
    V. R., Swarup, G., "Simultaneous observations of pulsar intensity
    variations at Parkes and Ootacamund" 1974, Monthly Notices Roy.
    Astr. Soc. 167, 31.

Smith, F. G., "The pulse energy distribution in pulsars" 1973, Monthly
    Notices Roy. Astr. Soc. 161, 9P.

Staelin, D. H., Reifenstein, E. C., "Pulsating radio sources near the
    Crab nebula" 1968, Science 162, 1481.

Trimble, V. L., "Motions and structure of the filamentary envelope of the
    Crab nebula" 1968, Astron. J. 73, 535.

Trimble, V. L., "The distance to the Crab nebula and NP 0532" 1973, Publ.
    Astron. Soc. Pacific 85, 579.

Turtle, A. J., Baldwin, J. E., "A survey of galactic radiation at 178 Mc/s"
    1962, Monthly Notices Roy. Astr. Soc. 124, 459.

Vandenberg, N. R., Clark, T. A., Erickson, W. C., Resch, G. M., Broderick,
    J. J., Payne, R. R., Knowles, S. H., Youmans, A. B., "VLBI observa-
    tions of the Crab nebula pulsar" 1973, Astrophys. J. 180, L27.

Wentzel, D. G., "Pulsar scintillations due to distant streaming cosmic
    rays" 1969, Astrophys. J. 156, L91.

Whitney, A. R., "Precision geodesy and astrometry via very-long-baseline
    interferometry" 1974, Massachusetts Institute of Technology (Ph.D.
    thesis).

Whitney, A. R., Shapiro, I. I., Rogers, A. E. E., Robertson, D. S., Knight, C. A., Clark, T. A., Goldstein, R. M., Marandino, G. E., Vandenberg, N. R., "Quasars revisited: Rapid time variations observed via very-long-baseline interferometry" 1971, Science 173, 225.

Williamson, I. P., "Pulse broadening due to multipath scattering in the interstellar medium" 1972, Monthly Notices Roy. Astr. Soc. 157, 55.

Williamson, I. P., "Pulse broadening due to multiple scattering in the interstellar medium - III" 1974, Monthly Notices Roy. Astr. Soc. 166, 499.

Wilson, A. S., "The structure of the Crab nebula at 2.7 and 5 GHz - I. The observations" 1972, Monthly Notices Roy. Astr. Sco. 157, 229.

Wilson, A. S., "The structure of the Crab nebula - IV. The variation of polarization with wavelength" 1974, Monthly Notices Roy. Astr. Soc. 166, 617.

Zeissig, G. A., Lovelace, R. V. E., "Interplanetary scintillation, interstellar scattering of two pulsars" 1972, Astron. Astrophys. 16, 190.